UNIVERSITÀ DEGLI STUDI DI PADOVA

UNIVERSITÀ DEGLI STUDI DI PADOVA

DIPARTIMENTO DI INGEGNERIA INDUSTRIALE

CORSO DI LAUREA MAGISTRALE IN CHEMICAL AND PROCESS ENGINEERING

Tesi di Laurea Magistrale in

Chemical and Process Engineering

Valorization of 5-Hydroxymethil furfural through thermal and photocatalysis

Relatore: Prof. Roberta Bertani

Correlatore: Prof. Robert Wojcieszak

Laureando: Leonardo Agnolon

ANNO ACCADEMICO 2023-2024

Abstract

Photocatalysis represents a more sustainable alternative to thermal catalysis, enabling reactions to proceed under light irradiation at lower temperature. When visible light is utilized, reactions can be driven by solar energy, reducing both the production costs for companies and the environmental footprint. This work explores the use of photocatalysis for the selective oxidation of 5-hydroxymethylfurfural (HMF), employing various catalysts and various wavelengths trying to find the optimal configuration to maximize the yield of one of the key products, 2,5-furandicarboxylic acid (FDCA). Once the most effective catalysts were identified, the reactions were led in continuous flow reactor system to achieve a steady production of FDCA. This product is a precursor a biobased plastics that can be used as an alternative to classic fossil-based plastics further improving the process sustainability. This work was carried out in collaboration with the Ecole Centrale de Lille in France thanks to Erasmus+ Project, under the supervision of Dr. Robert Wojcieszak.

Table of Contents

Introduction

The fast consumption of the world petrochemical sources and the growing of the world demand leads to the need to produce chemicals from a renewable one. Between the renewable resources, biomass is one of the most interesting from an industrial point of view because it may be utilised both to produce energy and chemicals products. Biomass carbon valorisation is very important to reduce carbon dependence from fossil fuels. In fact, its annual rate of production is 170 billion tons in nature which makes it a widely available resource.[1] At an industrial level, chemical plants that transform biomass into finished products or energy are called biorefineries which are gradually taking the place of traditional refineries all over the world. Furthermore, with photocatalysis biomass valorisation the goal is not only to use renewable resources but also to use more moderate process conditions exploiting in this way one of the principles of the process intensification of the green chemistry. Using moderate process conditions in addition to greater environmental sustainability has the advantage of economic savings for companies. Lignocellulosic biomass is one of the most abundant biomasses in the earth and it has wide geographical distribution. This biomass, includes softwoods, hardwoods, agricultural residues, grasses, and municipal wastes and it contains up to 50% of cellulose, which can be depolymerised to obtain chemicals.[2] [3] 5-hydroxymethyl furfural (HMF) together with levulinic acid, lactic acid, formic acid can be easily obtained from the depolymerization of cellulose contained in the lignocellulosic biomass. Through the selective oxidation of HMF, a cascade reaction is triggered that can lead to the formation of different products, depending on the stage of the oxidation: 5-diformylfuran (DFF), 5-formyl-2-furancarboxylic acid (FFCA), 2,5 furan dicarboxylic acid (FDCA) and 5-hydroxymethyl-2-furancarboxylic acid (HMFCA). HMF is therefore considered as a platform molecule, from which many other products can be obtained, which can easily replace their counterparts derived from fossil fuels. In this way, not only they are products derived from renewable sources generated, but most of the products derived from HMF are also biodegradable, so the environmental benefit is doubled. This oxidation reaction can be carried out in both thermal catalysis and photocatalysis. Light can affect not only the reaction yield but also the selectivity, potentially being able to give better product yields in milder reaction conditions, thus making the reaction more sustainable both in environmental and cost terms.

Aim of the study

The primary goal of this project is to optimize the photocatalytic conversion of HMF to FDCA by investigating the effects of various reaction parameters, including catalyst type, light wavelength, and pH. The aim is to maximize the yield of FDCA while minimizing side reactions and maximizing carbon efficiency. To explore the potential for industrial-scale production, continuous flow reactor experiments were conducted using the most promising catalysts identified in the batch studies. These experiments aimed to evaluate the long-term stability of the catalysts and the feasibility of continuous FDCA production. To gain insights into the underlying mechanisms of the photocatalytic reaction, a series of experiments were conducted under different conditions. These included variation of the wavelength of light, the catalyst composition, the support material, and the reaction pH. Additionally, thermal control experiments were performed to differentiate between photocatalytic and thermal effects. A summary of the reaction conditions that have been investigated is given below:

- *The pH of the reactions*: the oxidation has been carried out under basic conditions (with NaOH) and with uncontrolled pH (without NaOH).
- *The nature of the catalyst*: Various types of catalysts have been tested. The main objective was to study the effect of chemical order in bimetallic Au-Pd catalysts on FDCA production.
- *The support*: the same catalysts with different support have been tested to study the effect of the support on photocatalytic properties.
- *The bimetallic particle ratio*: To investigate the influence of metal composition on catalytic performance, a series of bimetallic catalysts with different metal ratios were synthesized and tested.
- *The light wavelength*: test without irradiation and under irradiation with various wavelengths (523, 450 and 365 nm) have been carried to study the effect of different light energy on the reaction.
- *The reaction time*: the effect of the time on catalytic results were studied.
- *The flow*: by adjusting the flow rate in the continuous reactor, the residence time of the reactants in contact with the catalyst could be controlled. This allowed for the optimization of the reaction conditions to achieve high FDCA selectivity while minimizing overoxidation to undesired product

Chapter 1

Reaction & Products Overview

5-hydroxymethylfurfural (HMF) is a biomass derived molecule utilized for sustainable chemical production. The selective oxidation of this molecule involves intermediates such as are 2,5-diformylfuran (DFF), 5-formyl-2-furancarboxylic acid (FFCA), and 5-hydroxymethyl-2-furancarboxylic acid (HMFCA). The last step of oxidation is 2,5 furan dicarboxylic acid (FDCA) that has significant application in polymers production. The importance of this compound and the reaction overview are described in this chapter.

1.1 HMF Oxidation reaction

HMF, a molecule composed of a furan ring, a hydroxyl group, and a formyl group, is a versatile platform chemical with significant industrial potential. Its unique structure allows it to participate in a variety of reactions, yielding diverse products. With catalytic oxidation of HMF (Figure 1.1) the most important products that can be obtained are 2,5-diformylfuran (DFF), 5-formyl-2-furancarboxylic acid (FFCA), 2,5 furan dicarboxylic acid (FDCA) and 5-hydroxymethyl-2-furancarboxylic acid (HMFCA). These latter are obtained with a cascade reaction, and the choose of the catalyst is important to stop the reaction when desired to obtain only one compound with hight selectivity.

As shown below there are two different paths to reach FFCA, one is through HMFCA by the oxidation of the aldehyde group and the other one is through DFF by the oxidation of the alcohol group. Both HMFCA and DFF can be further oxidized to obtain FFCA. Subsequently, if FFCA is oxidized, FDCA is obtained. The presence of all these products and of HMF can be detected in the reaction mixture with high performance liquid chromatography (HPLC). Both the reaction pathways may occur at the same time but from the literature it is known that there is an effect of pH, in fact if the reaction is led in non-strong alkaline environment (pH<13) HMF tends to be oxidised to DFF, on the contrary in a strong alkaline environment (pH>13) HMFCA path is favoured.[4] [5] Previous studies have shown that the addition of a small amount of base to gold-based catalysts can promote the oxidation of HMF to HMFCA by facilitating the oxidation of the aldehyde group to the carboxylic acid.

However, higher base concentrations are required for subsequent oxidation steps leading to FDCA. In contrast, platinum and palladium-based catalysts exhibit higher reactivity towards alcohol groups, enabling the formation of FDCA even at lower NaOH concentrations.

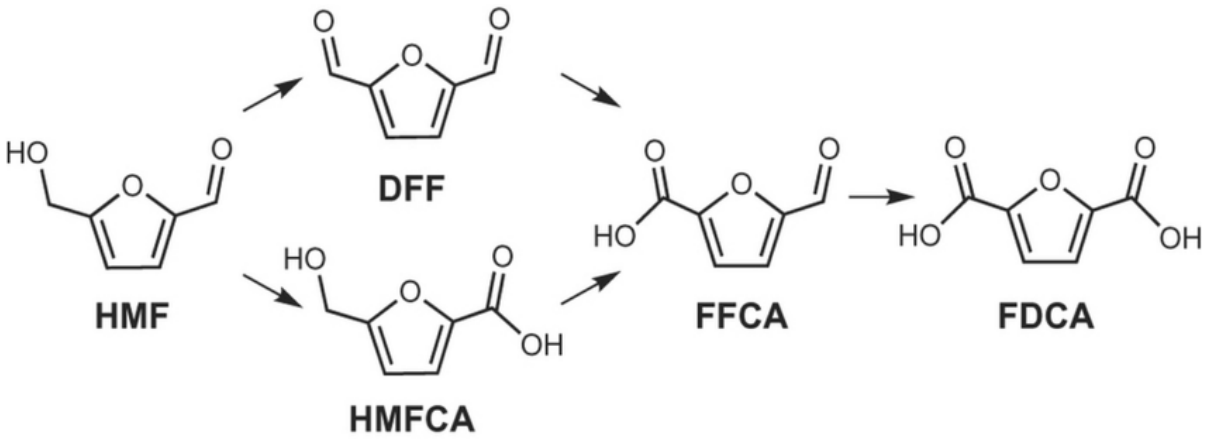

Figure 1.1 . *Reaction pathways in 5-hydroxymethylfurfural (HMF) oxidation. HMFCA pathways is favoured with Au catalysts and DFF pathway is favoured with Pd catalysts.*

The oxidation of HMF is a multi-step process (Figure 1.1) involving two distinct pathways. The initial oxidation can occur either at the aldehyde group, yielding 5-hydroxymethylfurfural-2-carboxylic acid (HMFCA), or at the hydroxyl group, leading to 2,5-diformylfuran (DFF). However, the thermodynamic stability of HMFCA favours its formation as an intermediate. Subsequent oxidation of HMFCA results in 2,5-furandicarboxylic acid (FDCA). The oxidation of the alcohol group is generally more challenging than the oxidation of the aldehyde group. As a result, the formation of DFF and FFCA is often less favoured. Additionally, the deprotonation of carboxylic acids on metal surfaces can hinder their desorption, making alkaline conditions necessary. While alkaline conditions can promote the oxidation process, they also require additional steps for neutralization, which can impact the overall atom economy of the process.

Alkaline conditions can lead to the degradation of furfural and HMF. Douthwaite et al. identified two primary deactivation pathways for furfural oxidation over AuPd/$Mg(OH)_2$ catalysts in basic media.[6] Firstly, the Cannizzaro reaction, catalysed by hydroxide ions, can result in the disproportionation of furfural into furoic acid and furfuryl alcohol. While slower than the desired oxidation reaction, this side reaction can hinder the overall process. Secondly, alkaline conditions and elevated temperatures can promote the self-polymerization of furfural, further reducing the yield of

the desired product. Similar degradation pathways can be expected for HMF oxidation, particularly considering the more challenging oxidation of the alcohol group.

As already stated, HMF oxidation into FDCA poses greater selectivity challenges. However, research continues to focus around the choice of the support and the effect of alloying.[7] Au-supported catalysts have been widely investigated for the oxidation of HMF to FDCA due to their stability and activity in oxidative conditions. Various supports, such as TiO_2 and Al_2O_3, have been explored, often in conjunction with alkaline conditions (e.g. NaOH). While high conversions of HMF can be achieved, the selectivity towards FDCA can be challenging, as the intermediate HMFCA may undergo further oxidation to undesired by-products. It is important to note that the oxidation of the alcohol group in HMFCA is generally more challenging than the oxidation of the aldehyde group. This can lead to incomplete conversion of HMFCA to FDCA, especially if the reaction is terminated prematurely.

The stability of catalysts in aqueous media, particularly during oxidation reactions, is a well-known challenge. This is evident in the case of Au/MgO, where high initial activity and selectivity can be achieved, but long-term stability can be compromised due to leaching and carbon deposition. While Ferraz et al. reported impressive results with this catalyst, achieving 99% conversion and 91% yield of FDCA in just two hours, the catalyst's stability limited its long-term performance.[8] To address this issue, the use of composite supports, such as MgO-MgF_2, has been explored. However, while these composites can improve catalyst stability, they may also negatively impact catalytic activity, leading to lower yields and increased carbon loss.

Platinum-based catalysts have also been extensively studied for HMF oxidation, demonstrating high activity and selectivity towards FDCA. Similarly, to gold-based catalysts, a variety of supports have been explored, with Pt often exhibiting superior catalytic performance. This enhanced activity allows for shorter reaction times, lower temperatures, and the potential for base-free conditions. Numerous studies reported higher FDCA yields (95-100%) and conversions (>95%) using Pt-based catalysts on various supports.[9] [10] [11] This feature highlights the versatility and effectiveness of platinum as a catalyst for HMF oxidation.

Palladium-based catalysts have also been investigated for the oxidation of HMF to FDCA, although they generally exhibit lower activity compared to platinum. To achieve comparable performance, higher oxygen pressures and lower feed-to-metal ratios are often required. While some supports, such as HT, have shown to be promising in base-free conditions, achieving high FDCA yields, other supports, including PVP, KF-Al_2O_3, ZrO_2-La_2O_3, and HAP@Fe_2O_3, have demonstrated high selectivity in the presence of a base. However, the performance of palladium catalysts can vary significantly depending on the support and reaction conditions. In comparison to gold and platinum, palladium catalysts often require more stringent reaction conditions to achieve high yields of FDCA. This highlights the importance of careful catalyst design and optimization of the experimental conditions for maximizing catalytic performance.[12 13 14]

While the support's textural, redox, and electronic properties are essential, they are not the only determinants of catalytic efficiency in HMF oxidation. Reaction conditions, including pH, temperature, and pressure, have a key role in the success of the reaction. Current catalysts can led to side reactions that produce undesired products like complete oxidation or degradation pathways. Further research is needed to understand and reduce these competitive degradation pathways, leading to more selective catalysts for example changing support materials and trying to understand metal-support interactions. In addition, limited research exists on the impact of metal alloying on HMF oxidation. It is difficult to compare metals and supports since Although there are several studies, catalysts are tested under different conditions. The combination of Au with Pd or Pt in bimetallic catalysts can create synergistic effects enhancing catalytic activity and selectivity towards FDCA production achieving also higher conversion of HMF. These synergistic effects can arise from several factors as a change of the electronic properties of the catalyst due to the interaction of Au and Pd of Pt. This change led to a creation of new active sites or enhance the adsorption and activation of the HMF. In addition, the formation of Au-Pd or Au-Pt alloys can introduce new catalytic properties that are not observed in the monometallic catalysts. Bimetallic catalysts can show bifunctional properties, allowing for both oxidation and dehydrogenation reactions to occur simultaneously. It has been proven that bimetallic catalysts tent to be more stable and resistant to deactivation compared to their monometallic counterpart. Further research will be necessary to develop increasingly better and more efficient catalysts for this reaction.[7]

1.2 Importance of HMF and FDCA in the industrial field

As already stated above, HMF is a platform molecule that can be the starting point of a lot of reactions. In addition to the previously discussed oxidation reaction that leads to the formation of FDCA, a very important monomer in the chemical industry, HMF can be used also for the production of fuels, drugs, solvents. HMF is also utilised as quality marker and adulteration indicator in the food industries.

The global industry market for HMF is continuously growing, researcher predict the CAGR of global revenue of 1.5% (Compound annual grow rate) for the next years and an expected market of 69 million of USD in 2029 from 62 million in 2022.

According to the 2004 US department of energy report "Top Value-Added Chemicals from Biomass Volume I" FDCA is one of the top 12 candidates of biomass-derived chemicals for the future chemical production.[15] FDCA is composed by an aromatic furan ring and two carboxyl groups, and it can be used as a monomer for polyester, polyurethane and polyamide. One of the advantages of FDCA is that it can substitute lots of chemicals derived from petroleum such as polyester, polyamides and polyurethanes. FDCA can be used also as a copolymer to produce the bio-based polyethylene furanoate (PEF) which can be a valid substitute for polyethylene terephthalate (PET). [16]In fact, the polycondensation reaction of FDCA with ethylene glycol produces PEF which has better mechanical properties compared to the traditional PET which is often used for food and beverage packaging. For example, PEF oxygen barrier is 10 times better than PET, its carbon dioxide barrier is 6 to 10 time better and the water barrier is twice as good as PET. PEF has also a lower environmental impact respect to PET; studies in fact stated that if all PET bottles were substituted by PEF bottles between $440 \cdot 10^{15}$ and $520 \cdot 10^{15}$ J of non-renewable energy use and 20 to 35 Mt of CO_2 equivalents could be saved.[17] The industrial production of FDCA from HMF has not reached its full potential because of the low yields and the hight price due to hight cost of production. The best way to produce FDCA is from HMF oxidation that is obtained from fructose. Production costs for FDCA synthesis are at an average of \$2300/kg instead; to have an economically viable synthesis the cost should be below \$1000/ton (\$1/Kg).[16] The FDCA production is around 3.5-5 tons but if FDCA would be used at all as an alternative to petrochemical compounds it would reach a production of 50 million of tons. For these reasons is important to find other synthesis methods, more sustainable both from an economic and environmental point of view. Given that one of the main processing costs is associated to HMF

formation stage, costs can significantly decrease by replacing simple sugars necessary for the HMF production with sugars that come from food wastes. It is possible in fact to obtain HMF from food wastes such as bread, cocked rice, and fruit peels.

Despite the strong interest in using FDCA, no large-scale industrial production has been undertaken to date. Avantium and BASF have developed a pilot plant in Netherlands, active since 2016 for an economical production FDCA ($1000/ton) based on new separation technologies and catalyst. However, BASF has announced its exit from the plant in 2019 due to a disagreement on marketing of YXY technology developed by Avantium.[18] The utilization of FDCA as a building block of biopolymers remains constrained due to the multiple steps from raw biomass to plastics production (Figure 1.2)[19], but due to the limited efficiency of FDCA production.

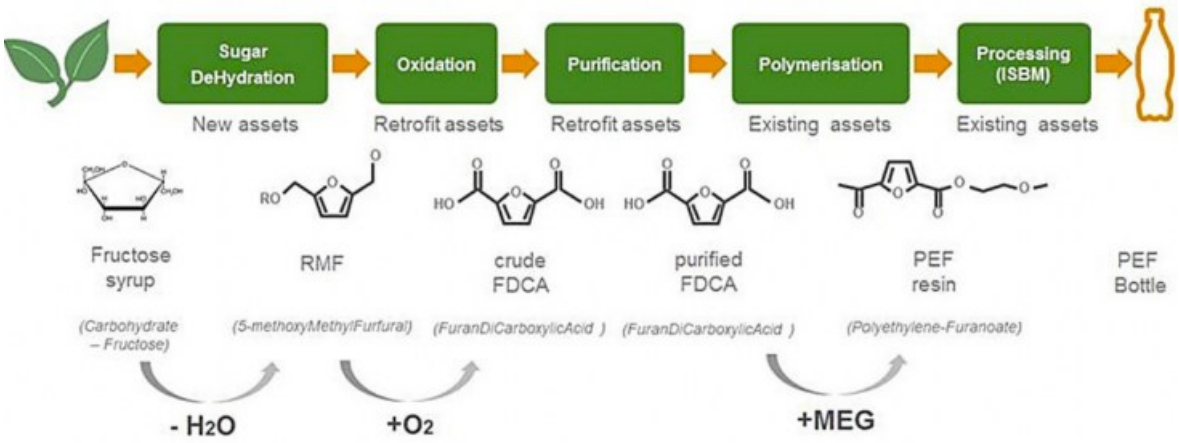

Figure 1.2 *Conversion steps from fructose to plastic PET bottles. Reproduced from ref. 13 with permission from MDPI, copyright 2022.*

To date, the most promising outcomes in FDCA production have been achieved through the oxidation of HMF, despite its vulnerability to acidic conditions. The increase in research interest in HMF and FDCA production is illustrated in Figure 1.3.

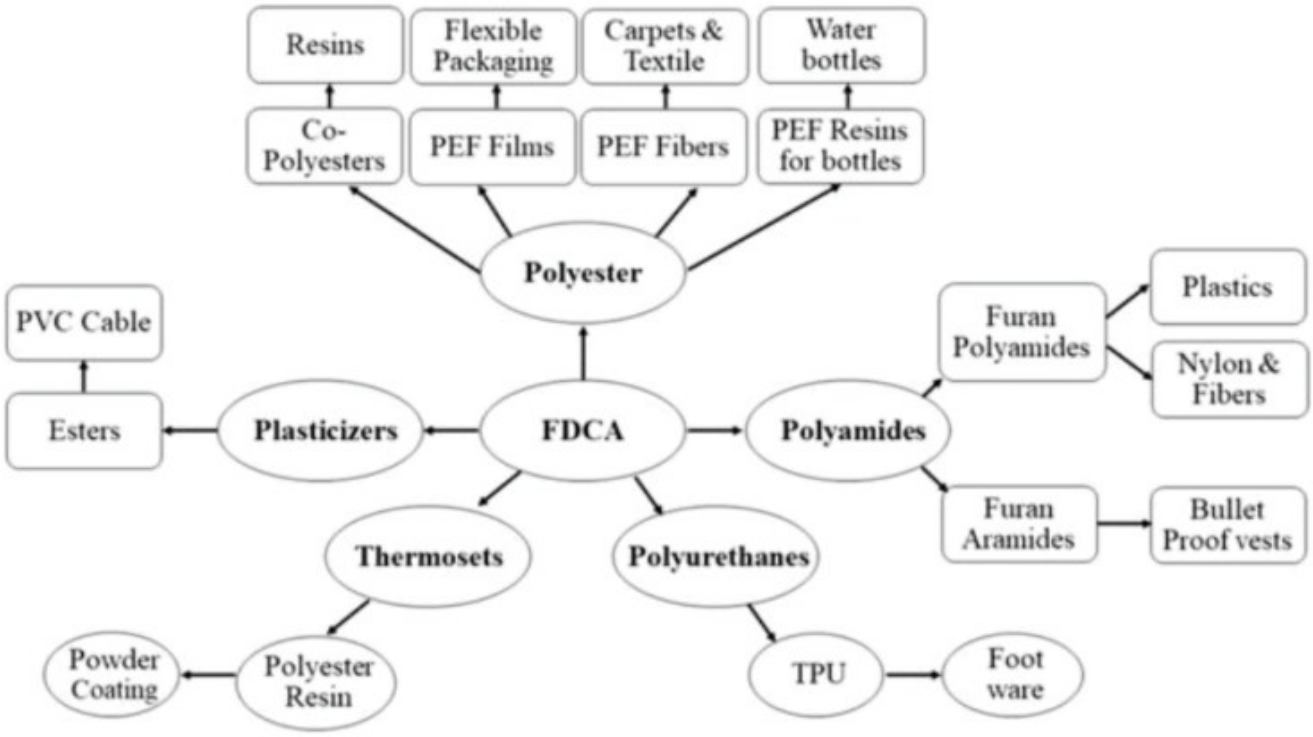

Figure 1.3 *Main FDCA's application. Reproduced from S. Singhal, S. Agarwal, M. P. Mudoi, N. Singhal and R. Singh, Biomass Conversion and Biorefinery 2021 13:17, 2021, 13, 15619–15636 with permission from SPRINGER NATURE, copyright, 2024*[7]

Chapter 2

Equipment and reactant

To carry out the reaction, various instruments were used. This chapter provides a detailed description of the reagents, analytical instruments and different reactors employed in the study.

2.1 Reactant and compounds

All the reactant and the compounds used for the tests are listed below with their degree of purity, their provider and the pictograms.

COMPOUNDS	CHEMICAL NAME	PROVIDER	PURITY	PICTOGRAMS AND HAZARD STATEMENTS
HMF	5-(Hydroxymethyl)furfural	Sigma-Aldrich	≥99%, FG	 Causes Eye Irritation. Causes Skin Irritation
HMFCA	5-hydroxymethyl-2-furan carboxylic acid	APOLLO SCIENTIFIC Supporting Discovery	95%	 May cause respiratory irritation. Causes skin irritation. Causes serious eye irritation.
DFF	Furan-2,5-dicarbaldehyde	APOLLO SCIENTIFIC Supporting Discovery	98%	 May cause respiratory irritation. Causes skin

				irritation. Causes serious eye irritation.
FFCA	5-Formyl-2-furancarboxylic acid	APOLLO SCIENTIFIC Supporting Discovery	≥98%	 Causes Eye Irritation
FDCA	2,5-Furandicarboxylic acid	Sigma-Aldrich.	97%	 May cause respiratory irritation. Causes skin irritation. Causes serious eye irritation.
SODIUM HYDROXIDE	NaOH	fisher scientific	≥97%	 Combustible, corrosive hazardous materials

Table 2.1 *Reactant and compounds list with the name of the provider, purity and pictograms*

2.2 HPLC

HPLC (High-Pressure Liquid Chromatography) is a technique utilized to analyse liquid mixtures. The separations of the compounds contained in the mixture take places thanks to the different speeds with which they cross the column. The equipment utilised is called Thermo scientific Vanquish, and the column is interchangeable. For the experiment the column used was BioRAD ANIMEX HPX 87H (300 x 7.8mm) that is specific for organic solutions. The machine is equipped with a diode array detector DAD. The stationary phase is a styrene-divinylbenzene resin that thanks to its porous structure can separate the molecules based on their hydrodynamic structure. The stationary phase is also functionalized with 8% H^+ links to obtain a better separation of the molecules thanks to an ionic exchange mechanism. The elution has been carried on with H_2SO_4 0.005 mol/L and the injection has been made with an autosampler. The volume taken from the vial for each injection was of 10 µl. One analysis takes 65 minutes, and the elution rate is 0.6ml/min. The detector analyses the mobile phases

when it leaves the column, and it gives in the monitor the chromatograms at different wavelengths. Each component has a different retention time in the column according to the table reported below.

COMPONENT	*RETENTION TIME [min]*
FDCA	25,3
HMFCA	29,7
FFCA	32,9
HMF	40,5
DFF	53,5

Table 2.2 *Retention times of the different HMF oxidation compounds obtained on HPLC used in this study*

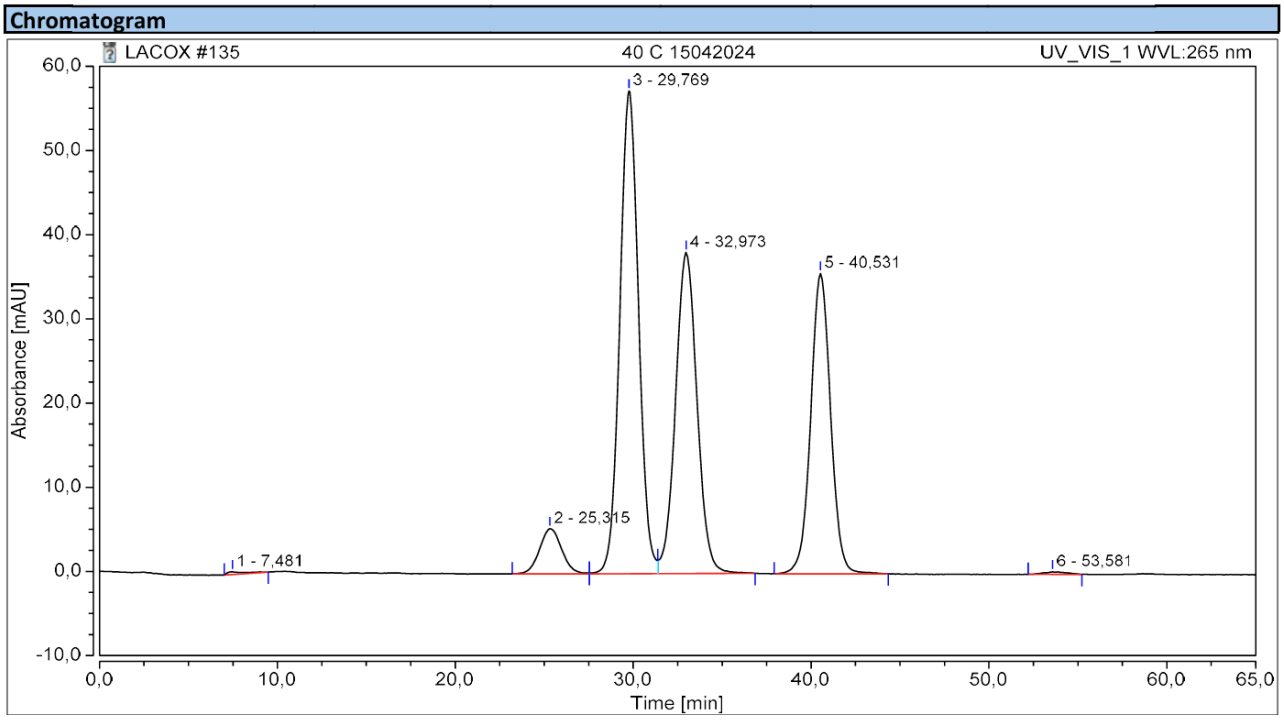

Figure 2.1 *Example of a chromatogram obtained during the calibration of the HMF and different oxidation products of HMF oxidation using the conditions described in the text*

Before each set of analysis, an injection with only pure water was performed to clean the column and to avoid contamination of the following analysis by the previous one. At the end of each set of analysis an arrest injection with pure water was also performed.

Figure 2.2 *HPLC Thermo scientific Vanquish used in this study*

2.3 DrySyn Illumin8

Two DrySyn Illumin 8 reactors are utilised for carry out the photocatalytic reaction in batch conditions. One reactor was equipped with the 450 nm wavelength lamp, and another one with a 365 nm wavelength module. Each reactor can contain up to a maximum of 8 tube tests, thus 8 different catalysts can be tested at the same time under the same conditions. The tests without illumination were also performed in order to study the effect of the temperature. A sensor can be connected to the reactor to have instant measurement of the temperature inside the reactor. The reactor can be heated using a magnetic hotplate to a fixed temperature, and it is useful, for example, to perform thermal catalytic reaction without the illumination. The intensity of stirring can also be fixed and changed.

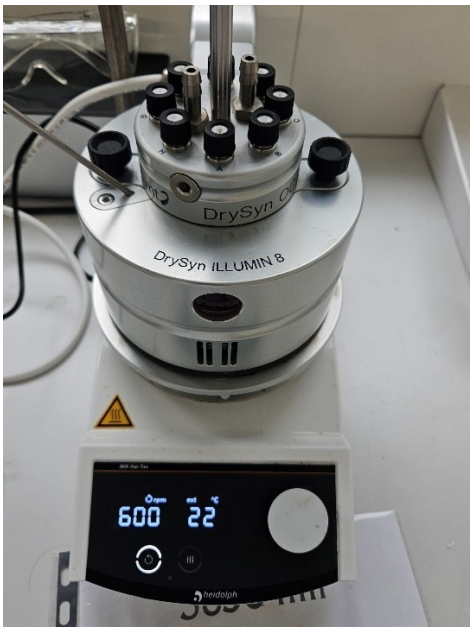

Figure 2.3 *DrySyn Illumin8 reactor above the magnetic hotplate*

2.4 *f*Reactor

Another reactor called *f*Reactor (flow reactor) was also used for catalytic tests. This reactor can work both in continuous and in batch modes. The reactor is made by a set of continuous stirred tank reactors connected in series (from 1 to 5 reactors). Each reactor has the minimum working capacity of 2 ml. The minimum working volume refers to the volume that the solution actually occupies before reaching the height level of the exit hole from which the tube connects it to the next reactor, or the final beaker used for sampling. This reactor system offers the advantage of a removable lamp, mounted on the top rather than fixed within the reactor. This versatility allows for easy lamp swapping. For instance, testing can be conducted with a 460 nm lamp in the first reactor and with a 523 nm lamp in the second, followed by a second test with the lamps reversed, placing the 523 nm lamp in the first reactor and the 460 nm lamp in the second. The flow rate can be regulated throught a pump and the starting mixture is injected in the first reactor using a syringe. In each reactor a magnetic treble bar can be put to ensure mixing. The reactor can be connected to another one using a tube or can be closed to have a closed reactor. If the reactors are connected each other, a cotton filter is necessary to avoid the transfer of the catalyst from one reactor to another and then go out from the

reactor chain. The reactor set is mounted on a support positioned above a magnetic hot plate, enabling stirring. The hotplate also allows for temperature control and monitoring. Each reactor is equipped with a top-mounted lamp. This setup offers considerable flexibility, as each reactor can accommodate a different catalyst or lamp. Furthermore, the reactors can be connected in series or used individually as closed systems.

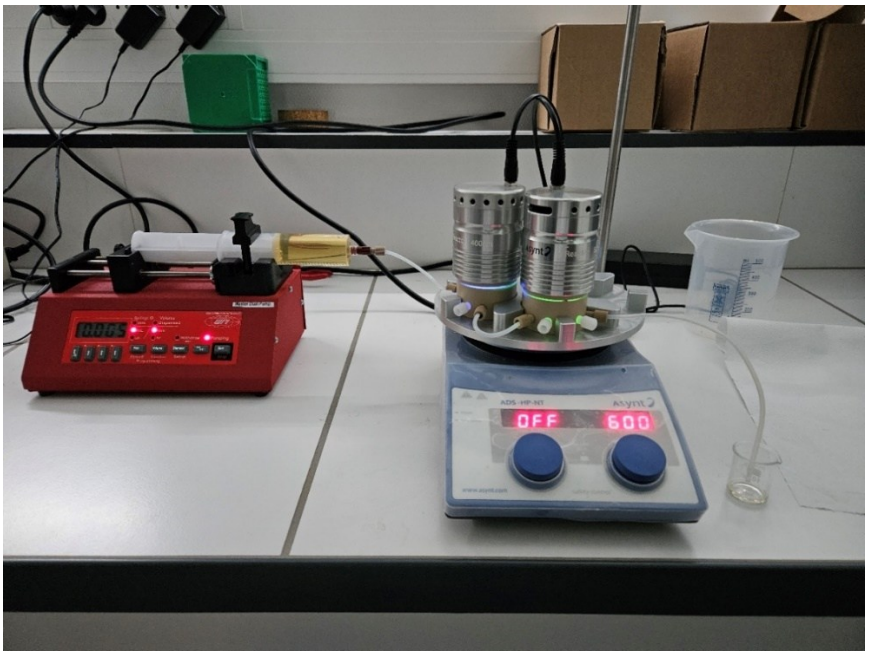

Figure 2.4 *fReactor in continuous flow with a syringe that provide the reactant to the reactor*

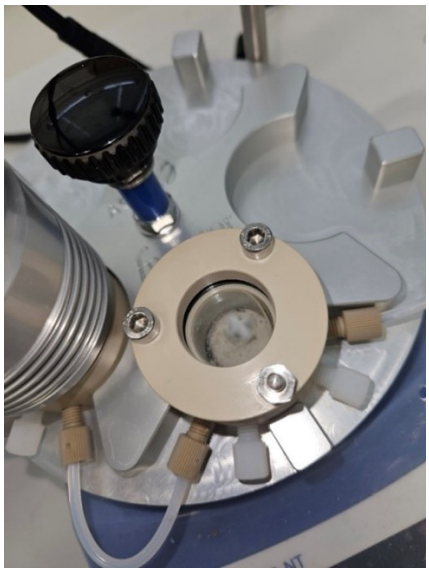

Figure 2.5 *Single reactor with the magnetic treble*

Chapter 3

Methods

3.1 Calibration

To correlate peak area with precise concentration, a calibration was performed. Five standard solutions were prepared, each containing known concentrations of HMF, DFF, FFCA, FDCA, and HMFCA. Each component was weighed using an analytical balance and dissolved in ultra-pure water in a 25 mL flask. A 1 mL aliquot from each of the five solutions was then transferred to a vial for analysis. The weights and molarities of each component in each standard solution are detailed in the tables below.

COMPONENT	*SAMPLE 1*	*SAMPLE 2*	*SAMPLE 3*	*SAMPLE 4*	*SAMPLE 5*
HMF	1,5 mg	3,4 mg	7,2 mg	9,3 mg	13,9 mg
DFF	1,8 mg	3,4 mg	6,1 mg	9,7 mg	12,6 mg
FFCA	1,8 mg	3,4 mg	7,2 mg	10,4 mg	14,6 mg
FDCA	1,8 mg	3,9 mg	8,1 mg	11,5 mg	15,5 mg
HMFCA	1,7 mg	3,3 mg	7,4 mg	10,7 mg	14,1 mg

Table 3.1 *weight of each component used for the calibration*

COMPONENT	*SAMPLE 1*	*SAMPLE 2*	*SAMPLE 3*	*SAMPLE 4*	*SAMPLE 5*
HMF	0,000476 M	0,001078M	0,002284M	0,00295 M	0,004409 M
DFF	0,00058 M	0,001096M	0,001966M	0,003127 M	0,004062 M
FFCA	0,000514 M	0,000971 M	0,002066 M	0,00297 M	0,004169 M
FDCA	0,000461 M	0,000999 M	0,002076 M	0,002947 M	0,003921 M
HMFCA	0,000479 M	0,000929 M	0,002083 M	0,003012 M	0,0039689 M

Table 3.2 *Molarity of each component used for the calibration*

The objective of the calibration was to establish a relationship between the peak area obtained from HPLC analysis and the corresponding concentration for each compound. This relationship is represented by a calibration curve, enabling the determination of a component's concentration within a sample vial based on its peak area. The calibration curves were constrained to pass through zero (since zero area implies zero concentration). The slope (angular coefficient) and coefficient of determination (R^2) were calculated for each curve. The calibration results are presented below.

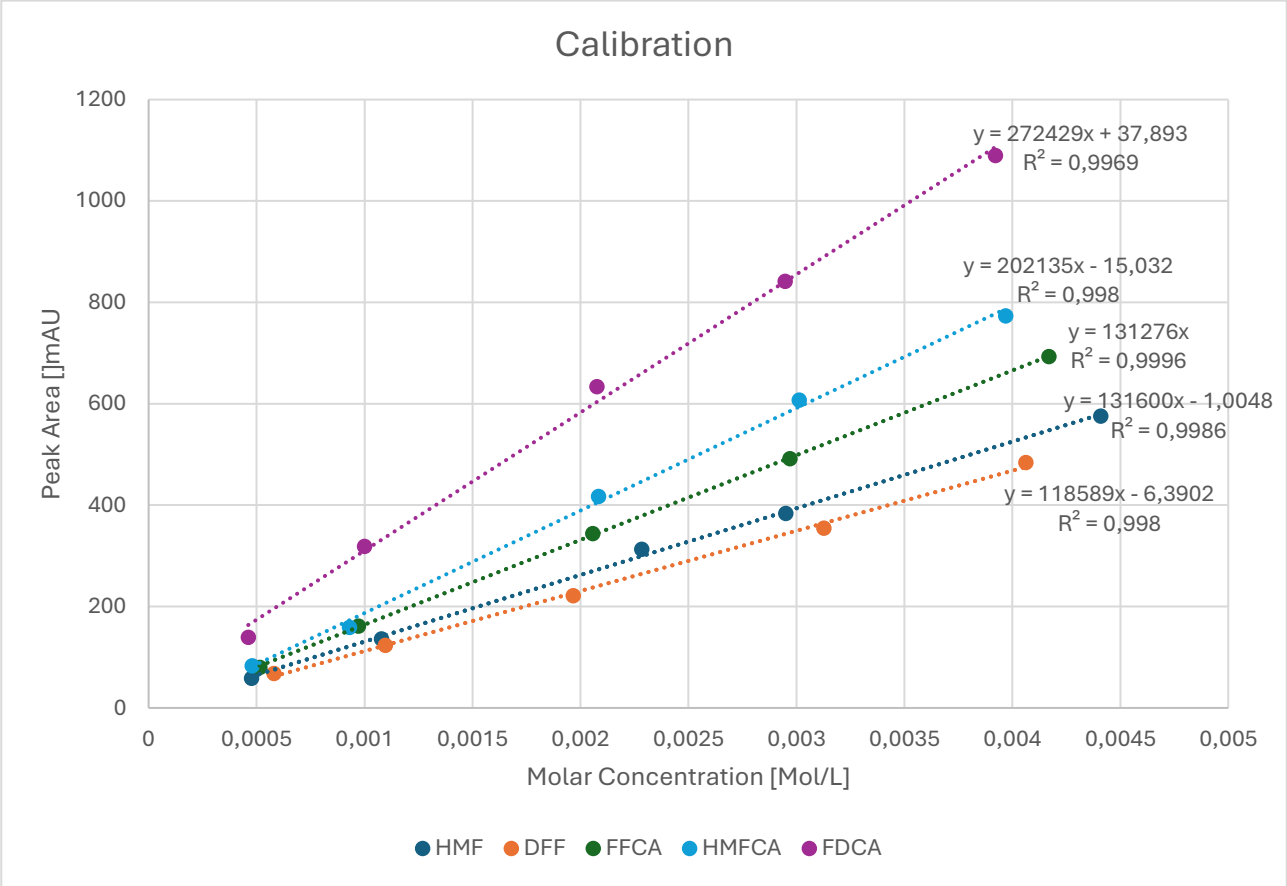

Figure 3.1 *Calibration lines for all the reactants and products*

To verify whether the calibrations are suitable for analysis or if any errors were made during the experimental phase, it is necessary to understand if the regression is acceptable through R^2. R^2 is an index utilised in statistics to understand the goodness of data in a linear regression model. In addition, R^2 is closed to one the stronger is the relationship between the dependent variable (peak area) and the independent variable (molar concentration). All the R^2 coefficients are close to one, it means that the regression model is good.

3.2 Reactions Set-Up

5 mg of catalyst are weighed on an analytical balance and put in the test tube. A water solution of HMF 25mM has been prepared by weighing 78,75 mg of HMF which have been introduced in a 25 ml flask. For basic conditions tests, it was necessary to add 3 equivalents in moles of NaOH (in respect to HMF), so 75 mg of NaOH have been weighted and added to the solution. The flask was brought to volume with ultra-pure water. 3 ml of this solution have been picked up with a micropipette and added to each test tubes containing the catalyst. A magnetic stirrer bar has been introduced into each reactor to ensure optimal stirring of the reaction mixture. Each test tube has been put in the reactor. Two reactors were available, one operating at 365nm wavelength and the second one at 450 nm. Each reactor can contain 8 test tube at the same time. The reactions have been carried at atmospheric pressure. Usually, temperature was not set except in one experiment performed in order to evaluate the difference between thermal and photocatalysis. In this case the temperature was set at 40°C for a reactor and 80°C for the other one. Each experiment was performed with mixing at a speed of 600 rpm. In all the others experiments the reaction starts at ambient temperature but due to the heat generated by the lamps, the reactor reached a temperature of about 40°C. At the end of the reactions, the reactors are switched off, the test tubes are removed, and the magnetic treble bar has been removed from the tube test. The solution has been filtered using PTFE filter and put in a container. To avoid the problem of exceeding the detection limit of the HPLC, the final solutions have been diluted. For the experiments carried out without using NaOH a 1:10 dilution has been made taking 0.1ml of final solution and 0.9ml of ultra-pure water with a micropipette and put it in a vial, while for the experiments carried out with NaOH a 1:20 dilution has been made taking 0.05ml of solutions and 0.95ml of ultra-pure water with a micropipette and put it in a vial. Each vial was put inside the HPLC to carry on the analysis. Before to start each injection of sample an injection with ultra-pure water is has been made to clean the column from the impurities. Other tests have been performed maintaining the same procedure but carrying on the reaction for longer periods of time.

Key metrics for evaluating reaction performance include conversion, yield, selectivity, and carbon balance. The conversion of HMF has been calculated as follow:

$$X = \frac{(Initial\ moles\ of\ HMF) - (final\ moles\ of\ HMF)}{(Initial\ moles\ of\ HMF)}$$

(2.1)

The selectivity has been calculated as follows:

$$S = \frac{(final\ moles\ of\ the\ desired\ product)}{(initial\ moles\ of\ HMF) - (final\ moles\ of\ HMF)} = \frac{(final\ moles\ of\ the\ desired\ product)}{(Reacted\ moles\ of\ HMF)}$$

(2.2)

Note that this formula has been calculated for each of the desired products because the stoichiometry coefficients ratio between the reactant (HMF) and each product is one.

The yield has been calculated as the products between the HMF conversion and the selectivity:

$$Y = X * S = \frac{(final\ moles\ of\ the\ desired\ product)}{(Initial\ moles\ of\ HMF)}$$

(2.3)

3.3 Catalysts Preparation

Alloy catalysts: The sol-immobilization method was employed to synthesize Au/ZrO_2 catalysts (Figure 3.2). First, the gold precursor solutions were prepared ($HAuCl_4x3H_2O$), solubilizing them in a beaker with distilled water, achieving a final metal molar concentration of 0.13 mmol L^{-1} (sum of metal molar concentrations). This solution was kept under stirring at room temperature for all the synthesis. Subsequently, a solution of stabilizing agent, in this case, polyvinyl alcohol (PVA) (0.0505 g of PVA dissolved in 5 mL of distilled water) was added to achieve a PVA: metal weight ratio of 1.2:1. After three minutes from the addition of PVA, a fresh aqueous solution of the reducing agent sodium borohydride ($NaBH_4$) was added ($NaBH_4$: metal molar ratio of 5:1). The reduction process

typically resulted in an immediate change in the solution's colour due to the phenomenon of plasmon resonance of nanoparticle structures.[20] Specifically, for Au, a shift from yellow to red was observed, indicating the successful formation of metal nanoparticles. After an additional period of 30 minutes, support powder was added, keeping the system under stirring, and the solution was acidified, adjusting the pH under the isoelectric point of the specific support to maximize the interactions between the support and the colloidal nanoparticles. After that, the solution was kept under stirring for an additional hour and filtered with a Büchner filter. The catalyst was washed with distilled water (about 1L) to remove impurities and until the filtrated solution reached neutral pH. The catalyst was left to dry overnight at room temperature and then dried in an oven for 4 hours at 80 °C. The same synthesis method has been utilised for the other catalyst with different metal and support, modifying the metal precursor according to the selected metal.

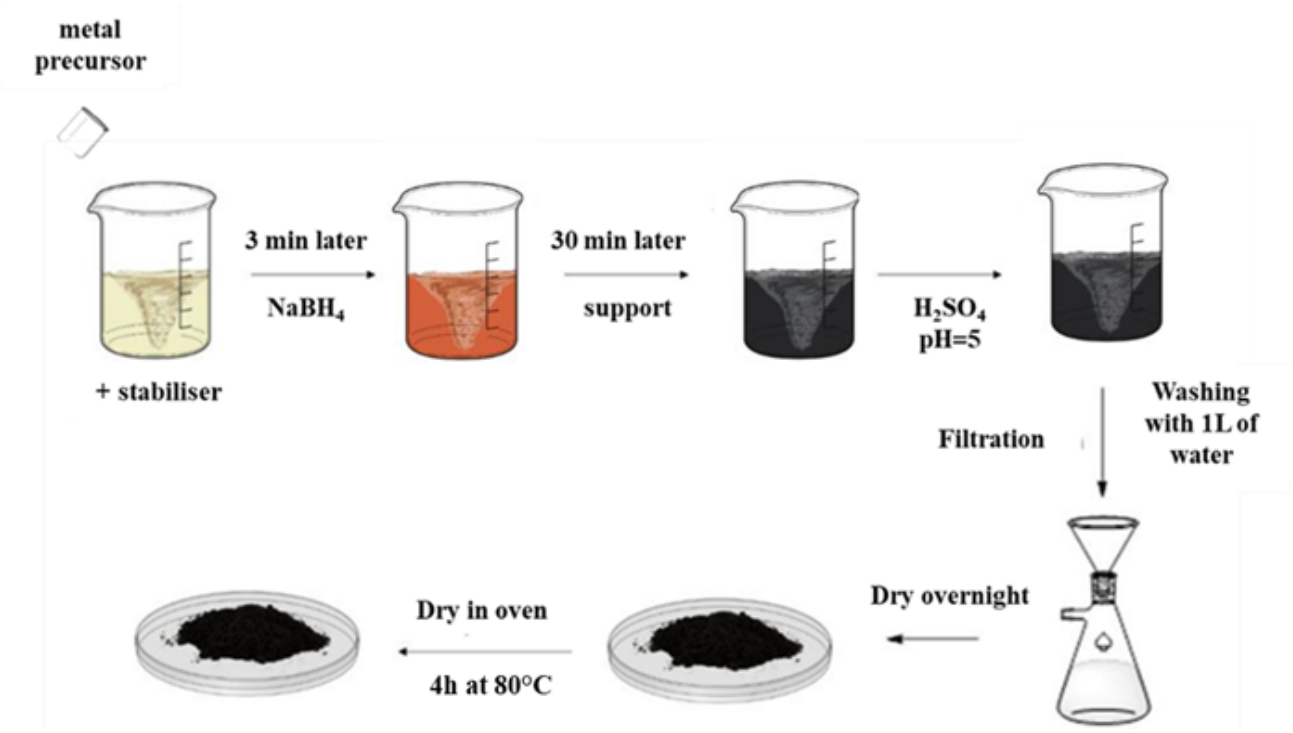

Figure 3.2 *The sol immobilization method, schematically visualised here, was used in the synthesis of the catalysts*

Core-shell catalysts: Bimetallic catalysts were prepared by Turkevich method. 5 mg/mL sodium citrate was added into 95 mL deionized water then put in the oil bath at a temperature of 100 °C. Once the solution starts to boil, 2 mL of 25 mM $HAuCl_4x3H_2O$ Au precursor was added into the reaction mixture and kept the temperature at 100 °C. The solution was boiled for 8 min and then cooled to room temperature. The synthesis of Au-Ag (or Au-Pd and Au-Pt) core-shell NPs is based on the gradual reduction of Ag^+ ion on the as-prepared citrate-stabilized Au NPs through addition of the Ag, Pd or Pt precursors, stepwise. For the first cycle, 150 μL of 0.1 M potassium hydroxide, 120 μL of 0.1 M ascorbic acid and 30 μL of 0.1 M silver nitrate (or $PdCl_2$) were added into 10 mL of the as-prepared Au NPs at room temperature respectively, then reaction was stirred constantly for 30 min, to obtain intermediate (IN)-layer Au-Ag core-shell sample. The cycles were repeated three times with reaction time of 30 min for each cycle, the Thick (TH)-layer Au-Ag core-shell sample was obtained. These bimetallic nanoparticles were then deposited on ZrO_2 support using standard impregnation method.

For the Atomic (AT)-layer of the Au-Ag core-shell NPs, 10 mL of the as-prepared Au NPs were added into a round bottom flask which was then placed in a sonication bath under ambient conditions. Typically, 150 μL of 0.1 M potassium hydroxide and 120 μL of 0.1M ascorbic acid were added into the flask followed by sonication (120 s). 30 μL of 0.01 M silver nitrate was then added into the flask and sonicated for another 120 s to obtain a well sonochemical dispersion of Ag. This method ensured the reduction of Ag^+ onto the Au cores while inhibited the formation of free Ag nuclei. After that the mixture was stirred constantly for 30 min at room temperature.

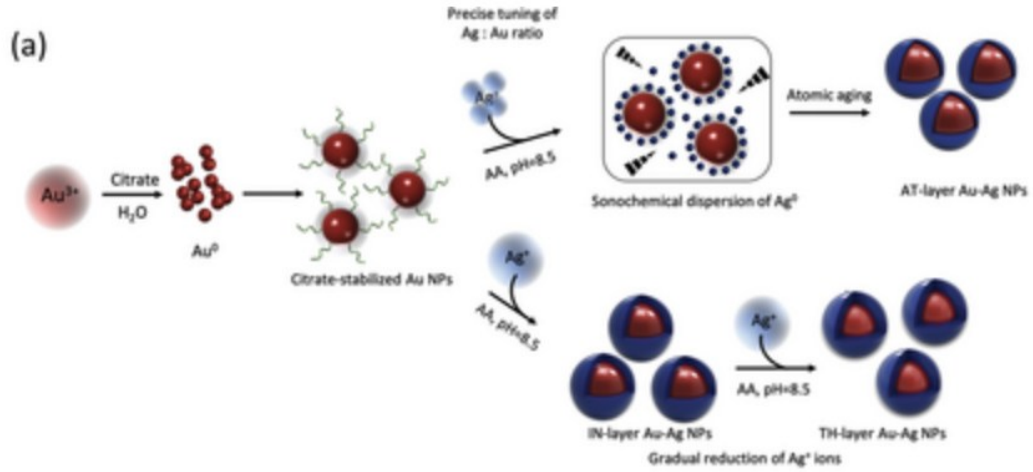

Figure 3.3 *Schematic illustration of sonochemical dispersion and gradual reduction process used to synthesize the Au–Ag core–shell nanoparticles*.

3.4 Characterization of the catalysts

The metal loadings were determined by ICP-OES (Inductively Coupled Plasma Optical Emission Spectrometry) analysis, performed using Agilent 720-ES ICP-OES equipment combined with Vulcan 42S automated digestion system.

Transmission Electron Microscopy (TEM) images were recorded by placing a drop of the particle's dispersion in isopropanol over a carbon film supported on a copper grid. FEI Tecnai microscope was used to record the images. More than 600 particles were used for the distribution size studies. It was performed using Image J software. For the analysis of individual nanoparticles, high resolution Scanning Transmission Electron Microscopy (STEM) was performed on a TITAN Themis 300 S/TEM microscope equipped with (1) a probe aberration corrector and monochromator, allowing spatial resolution of 70 pm and energy resolution of 150 meV; (2) a super-X windowless 4 quadrant SDD (silicon drift detector) detection system for STEM-EDX mapping and several annual dark field detectors; (3) a high-resolution post column GIF, the GATAN's Quantum ERS/966 with 2kx2k Ultrascan camera with 994G sensor, for the acquisition of electron energy loss spectra. In order to investigate the elemental distribution within bimetallic particles, high-angle annular dark field

(HAADF) imaging and high-resolution electron energy loss spectroscopy (HR-EELS) were carried out in the STEM mode. Measurements were performed with a spot size of about 500 pm, a semi-convergence angle between 16 and 21 mrad, and a probe current of approximately 100 pA. For HAADF images, collection angles between 50 and 200 mrad were chosen. Dual EELS acquisition was performed in the spectral imaging mode with a collection angle of 49 mrad, a 0.25 eV/ch dispersion, a step between 150 and 700 pm, and a dwell time between 50 and 200 ms. Alignment of the energy drift was done on the zero-loss peak. When possible, noise reduction by PCA was performed on the spectrum images using HyperSpy.

X-ray Photoelectron Spectroscopy (XPS) analysis was performed on an XPS Kratos, Axis UltraDLD “2009” with monochromatic Al Kα ($h\upsilon$=1486.6 eV) radiation as the excitation source and equipped with high-performance hemispheric analyser. The binding energies were calibrated using the carbon C 1s reference at 284.8 eV

Chapter 4

Results

A comprehensive screening of various catalysts and light sources was performed to optimize the reaction conditions for FDCA production. By systematically evaluating different combinations, the most efficient catalyst-light pair was identified, maximizing selectivity and yield.

4.1 Analysis without catalyst (blank tests)

Control experiments were performed to establish a baseline for HMF degradation. These experiments involved irradiating HMF solutions in the absence of a catalyst and in the presence of NaOH, respectively. By comparing these results to those obtained with catalytic systems, the specific contributions of the catalyst to the reaction can be evaluated.

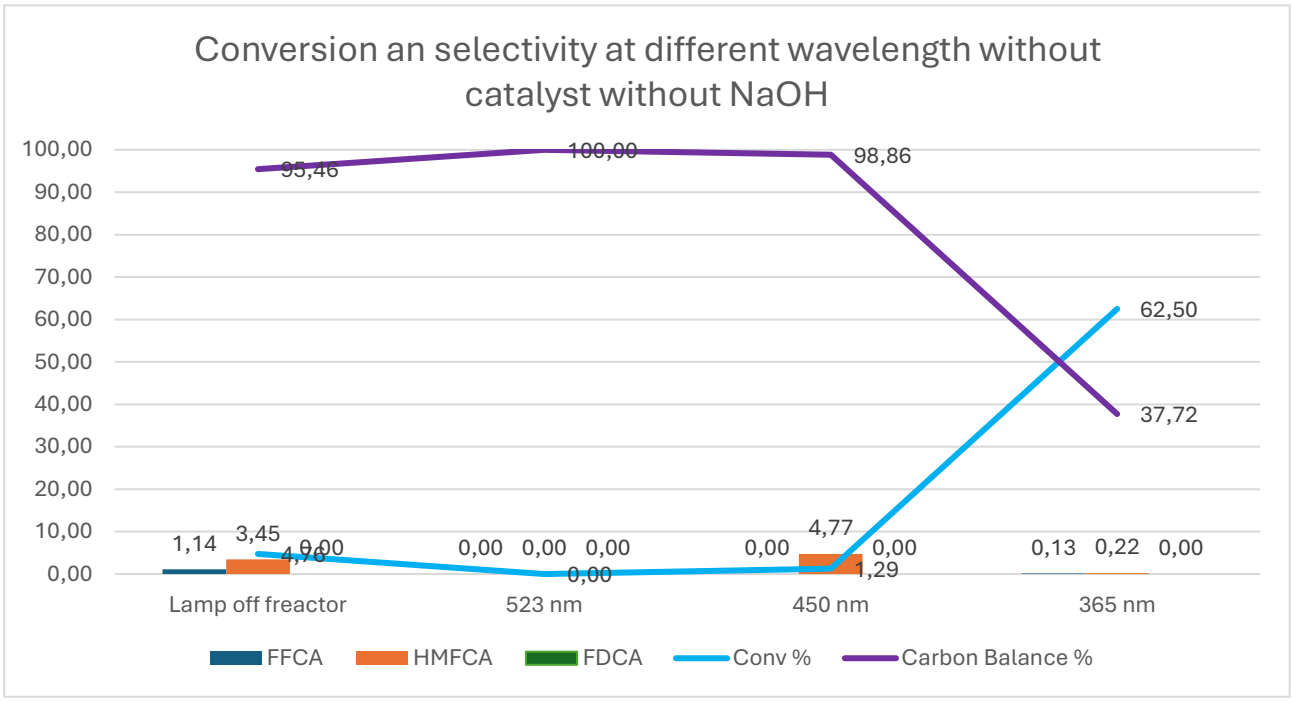

Figure 4.1 *Blank tests results. HMF conversion and selectivity at different wavelengths without catalyst and without NaOH*

Without NaOH (Figure 4.1) the only significant conversion is obtained at 365 nm wavelength (62,5%) but with very low carbon balance (37,72%). It clearly shows that the HMF is not stable under this irradiation and easily degrades to produces humins or it was overoxidized to CO_2 as any other products were detected by HPLC. On the contrary, at the wavelength of 523 nm and without light, no conversion was observed. Intermediate conversion was observed at the wavelength of 450 nm.

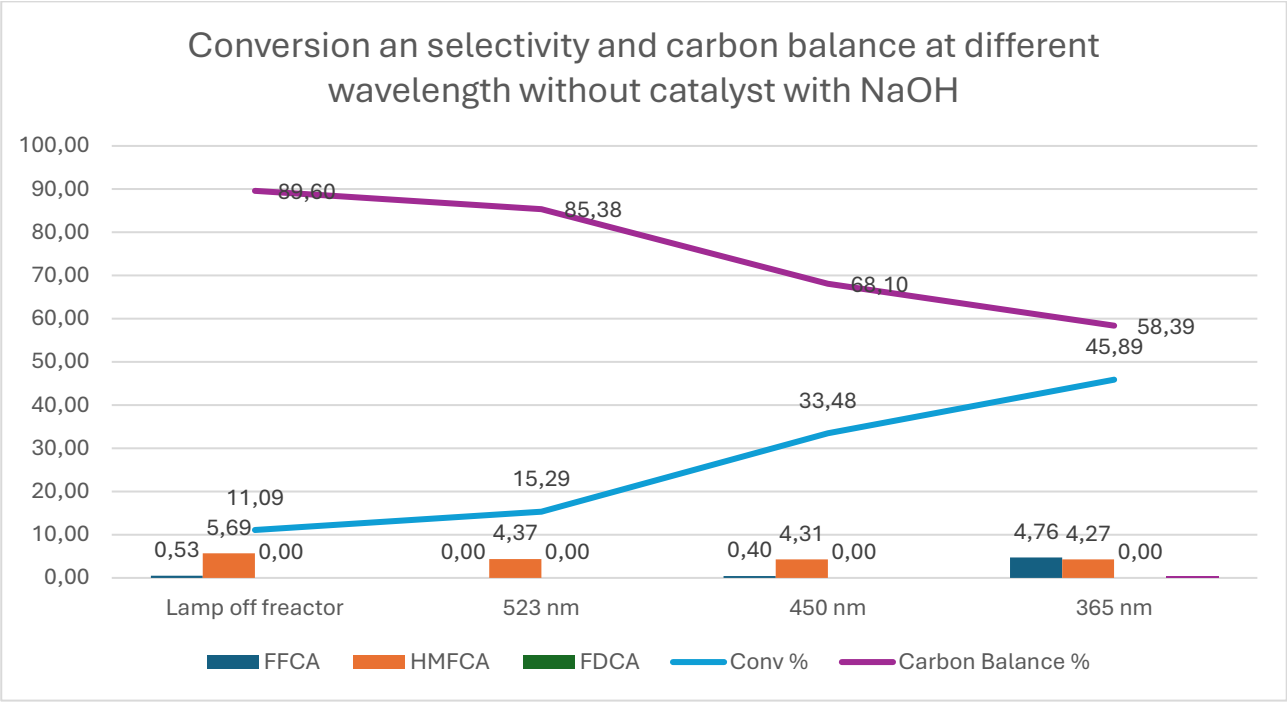

Figure 4.2 *Blank tests results. HMF conversion and carbon balance at different wavelength without catalyst and without NaOH*

The addition of NaOH promoted the conversion of HMF even in the absence of light, yielding a 11% of conversion. As the irradiation wavelength decreased, the conversion increased, reaching a maximum of 45.89% at 365 nm. These results suggest that the basic environment favours the initial step of the reaction, the conversion of HMF to HMFCA. However, the observed decrease in carbon balance at shorter wavelengths indicates the occurrence of side reactions and potential degradation of the reactant (as represented in Figure below).

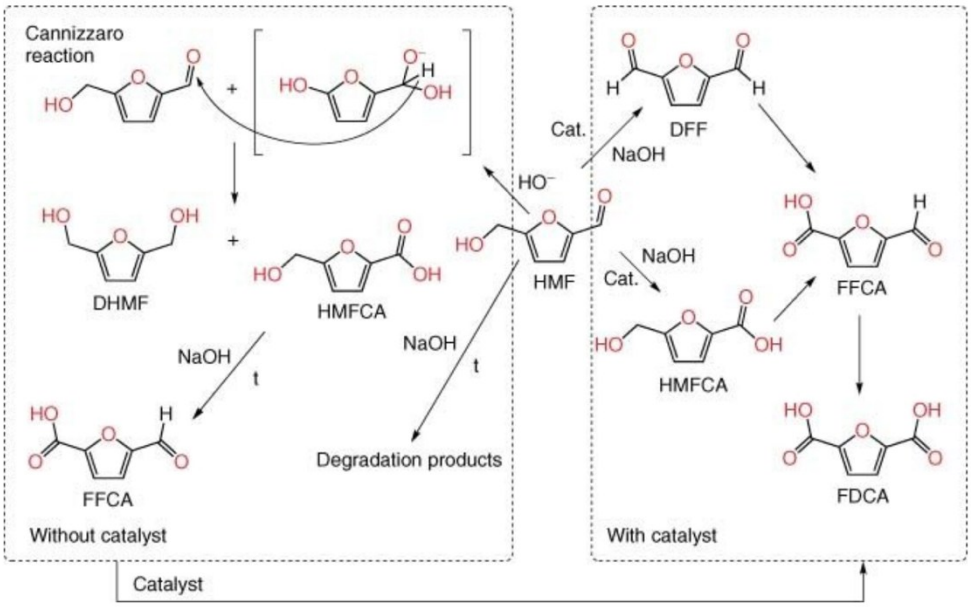

Figure 4.3: *Reaction pathways for the oxidation of HMF in the presence of NaOH with and without a catalyst.[ref: F. Neat, R. S. Marin, M. Florea, N. Petrea, O. D. Pavel,and V. I. Pârvulescu, Appl. Catal. B Environ., 2016, 180, 751.*

4.2 Core-shell gold palladium catalysts

The first set of catalysts tested was the core shell gold palladium catalyst supported with ZrO_2 with different concentration of palladium on gold (Figures 4.4 and 4.5). Also test with not supported gold palladium core shell catalysts has been made to study the effect of zirconia support. The tests were performed at two different wavelengths: at 365 and 450 nm.

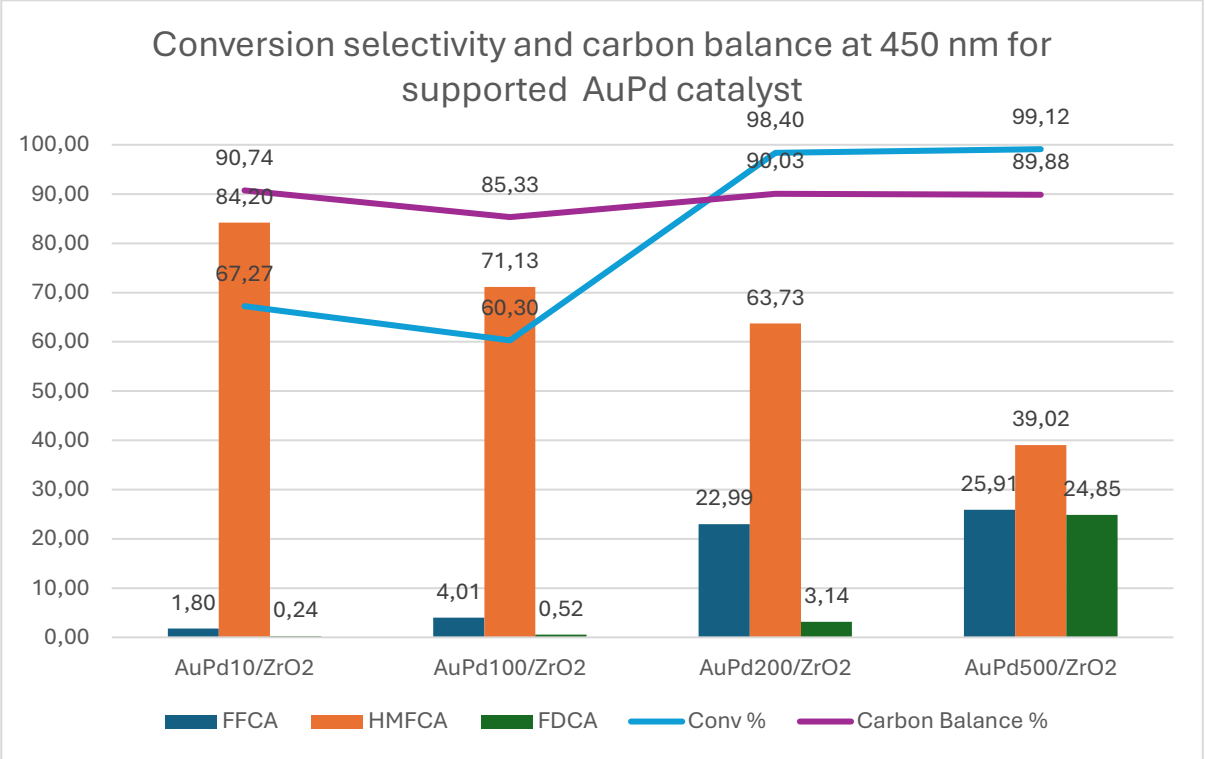

Figure 4.4 *Catalytic tests: HMF conversion, selectivity and carbon balance for AuPd core-shell supported catalysts at 450 nm.*

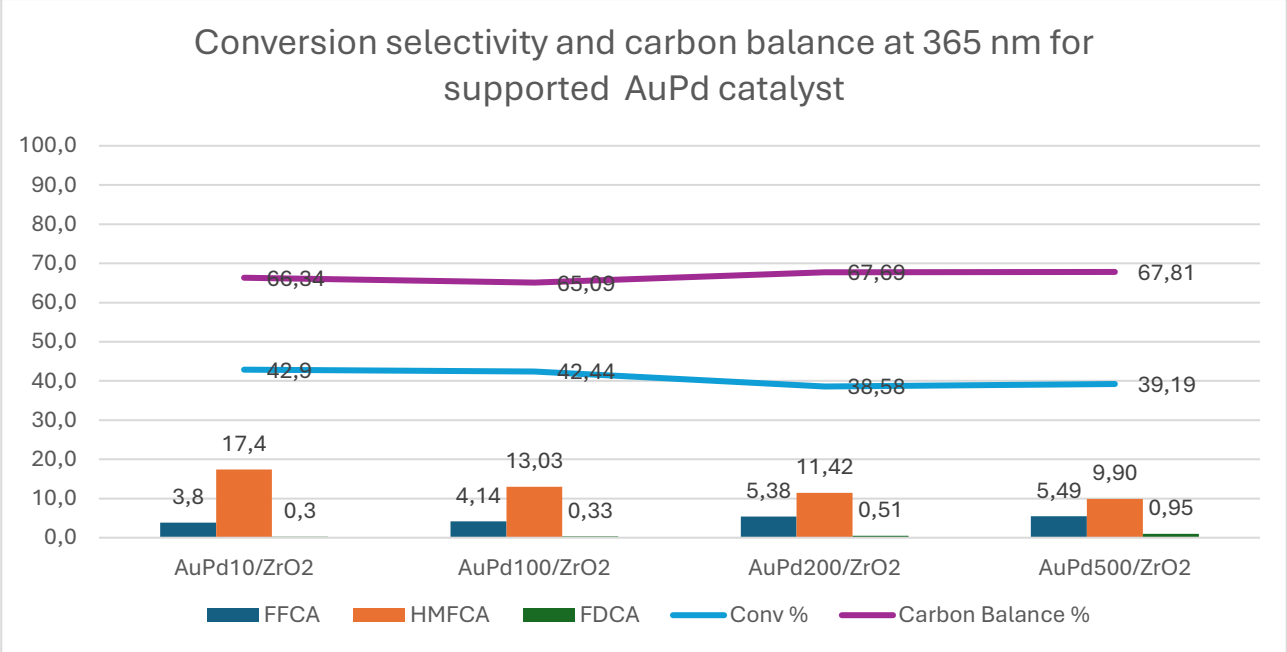

Figure 4.5 *Catalytic tests: HMF conversion, selectivity and carbon balance for AuPd core-shell supported catalysts at 365 nm.*

At 450 nm the carbon balance remained relatively stable around 90% for all catalysts. However, the conversion varied significantly. While the first two catalysts achieved conversions between 60% and 70%, the AuPd200/ZrO_2 and AuPd500/ZrO_2 catalysts exhibited nearly complete conversion (Figure 4.4). Interestingly, the reaction pathway shifted towards the final product, FDCA, as the palladium content increased. For instance, AuPd10/ZrO_2 favoured the formation of HMFCA, whereas AuPd500/ZrO_2 promoted the further oxidation to FDCA. This suggests that the higher palladium content facilitated the subsequent oxidation steps.

At 365 nm, the conversion stabilized at 40%, with HMFCA as the primary product (Figure 4.5). However, the low carbon balance of around 68% indicates that a significant portion of the HMF undergoes degradation or mineralization to CO_2, likely due to the high energy of the 365 nm light.

To evaluate the influence of the support, similar reactions were conducted with unsupported AuPd catalysts (AuPd10, AuPd100, and AuPd200) and pure Au nanoparticles. These catalysts were tested under both 365 nm and 450 nm irradiation (Figures 4.6 and 4.7).

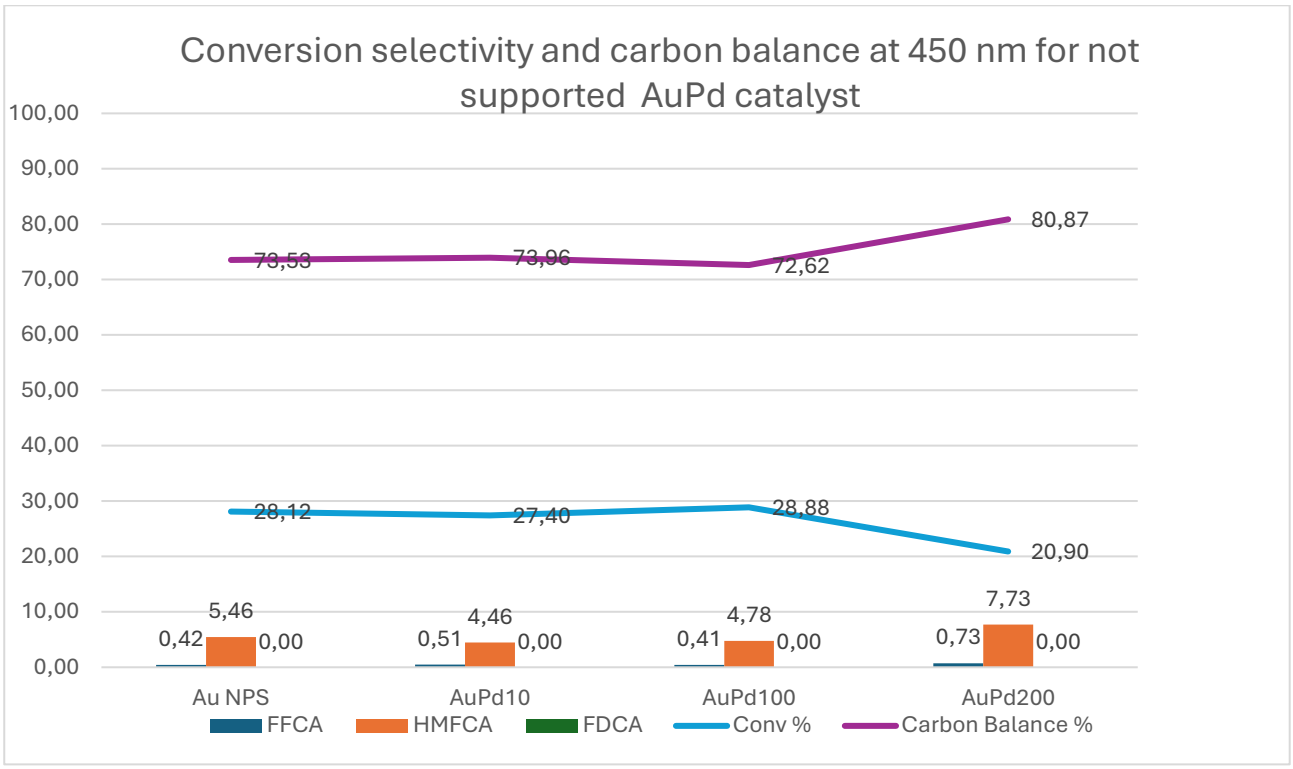

Figure 4.6 *Catalytic tests: HMF conversion, selectivity and carbon balance for AuPd core-shell unsupported catalysts at 450 nm.*

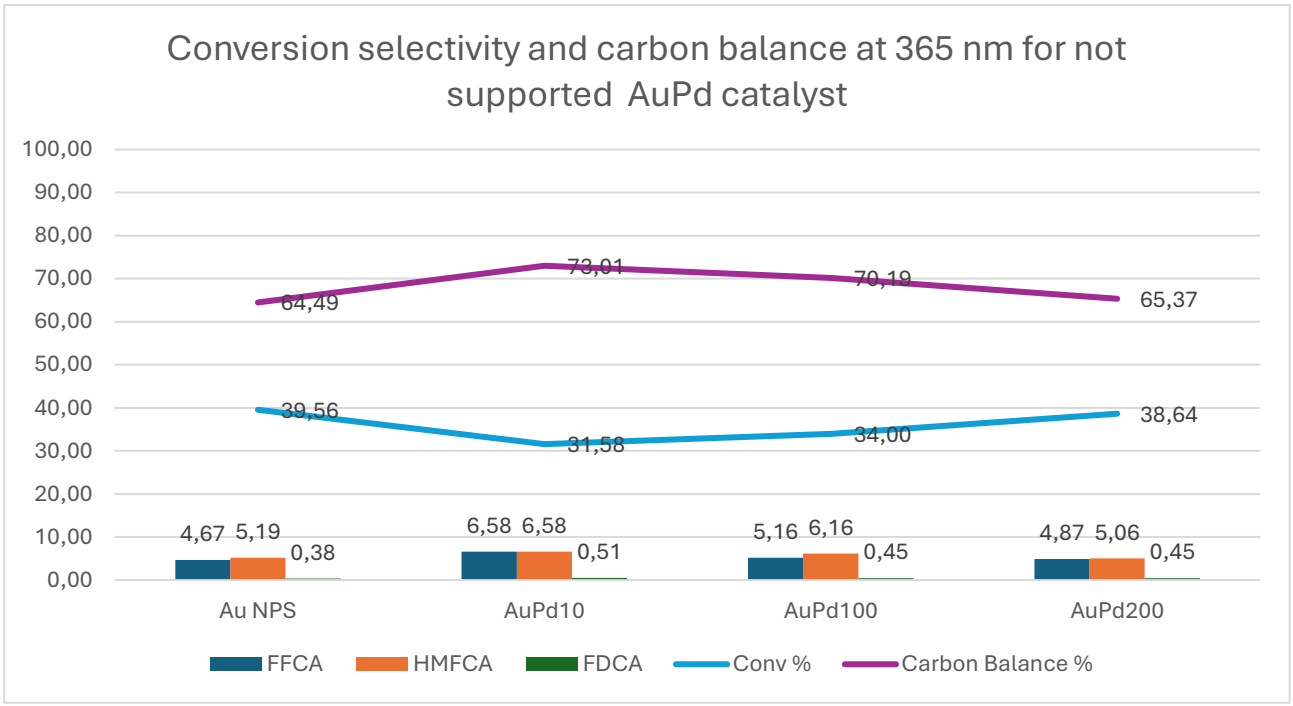

Figure 4.7 *Catalytic tests: HMF conversion, selectivity and carbon balance for AuPd core-shell unsupported catalysts at 365 nm.*

The unsupported catalysts exhibited lower conversion rates compared to their supported counterparts, both at 450 nm and 365 nm. Additionally, the product distribution was less selective, with a lower carbon balance. These results suggest that the support plays a crucial role in enhancing catalytic activity and selectivity. It can provide the active sites for the adsorption of the substrate and activate the metallic nanoparticles.

Furthermore, no clear trend was observed in the catalytic performance with increasing palladium content for the unsupported catalysts. This indicates that the support is essential for optimizing the catalytic properties of the Pd nanoparticles.

To isolate the effect of light irradiation from thermal effects, a control experiment was conducted by heating the reaction mixture to approximately 40°C using a hotplate, while keeping the light source off. This experiment allowed us to assess the contribution of thermal energy to the reaction. The results are presented on Figure 4.8.

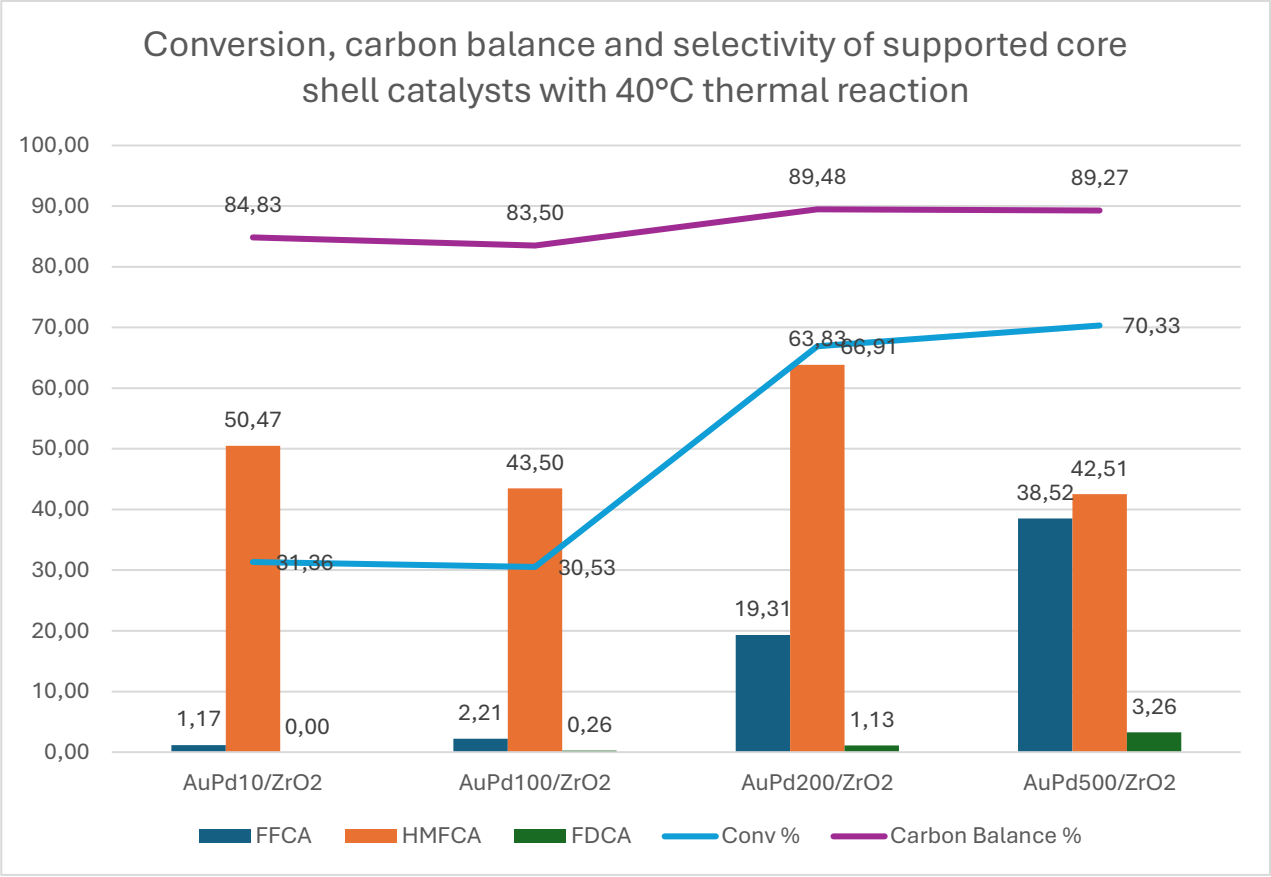

Figure 4.8 *Catalytic tests: HMF conversion, selectivity and carbon balance for AuPd core-shell supported catalysts at 40°C without light.*

Comparing these results (Figure 4.8) with the corresponding obtained with 450 nm wavelength (Figure 4.4) the effect of light can be clearly identified. Firstly, the conversion in absence of light is lower for all catalysts: for the first two catalysts with low Pd content (AuPd10/ZrO_2 and AuPd100/ZrO_2) in the absence of light in fact a 30% conversion was obtained. On the contrary, under the 450 nm irradiation, the conversion exceeded 60%. In the case of the catalysts with high Pd content (AuPd200/ZrO_2 and AuPd500/ZrO2) in the absence of light the conversion increased, reaching the value of 64% and 70% respectively, confirming the trend already observed before, but the conversion was still lower when compared to that observed under light (near to 100%). In addition, the selectivity to main products was also different. In fact, it can be observed that under irradiation, the reaction can go further to the oxidation (with the AuPd500/ZrO_2) but without light the selectivity of FDCA was lower proving that the light strongly impacts the kinetics of the oxidation process. However, increasing the amount of palladium in the catalyst the selectivity towards the final products of the reaction (FDCA and FFCA) increased confirming the trend already observed in the presence of light. This comparison between photo and thermal catalysis proved the effect of the light in the reaction and shows that the products were obtained not only because of the heat but also with the light itself.

4.3 Alloy gold palladium catalyst

4.3.1 Gold Palladium nanoparticles supported on ZrO_2 oxide

Gold palladium alloy catalyst supported on zirconia were synthetised using sol-immobilization method. Different molar ratios between both metals were studied: AuPd/ZrO_2 3:1, AuPd/ZrO_2 2:1, AuPd/ZrO_2 1:1, AuPd/ZrO_2 1:2. For comparison two monometallic catalysts Pd/ZrO_2 and the Au/ZrO_2 were also synthetised and tested under the same conditions. Three different commercial zirconia were used denoted as 61192, 61143 and 61156. The number corresponds to the commercial nomenclature and describes the zirconia with different composition and acidity: ZrO_2-61192: 90% of ZrO_2, 4.7% of SO_3, 1.1% SiO_2 and 0.46% of HfO_2 ZrO_2 -61143: 90% of ZrO_2, 15.3% of WO_3 and 1.5% of HfO_2, ZrO_2-61156: 90% of ZrO_2, 7.96% of La_2O_3, 0.23% of Al_2O and 1.75% of HfO_2. The photocatalytic tests were led both at 365 nm and at 450 nm.

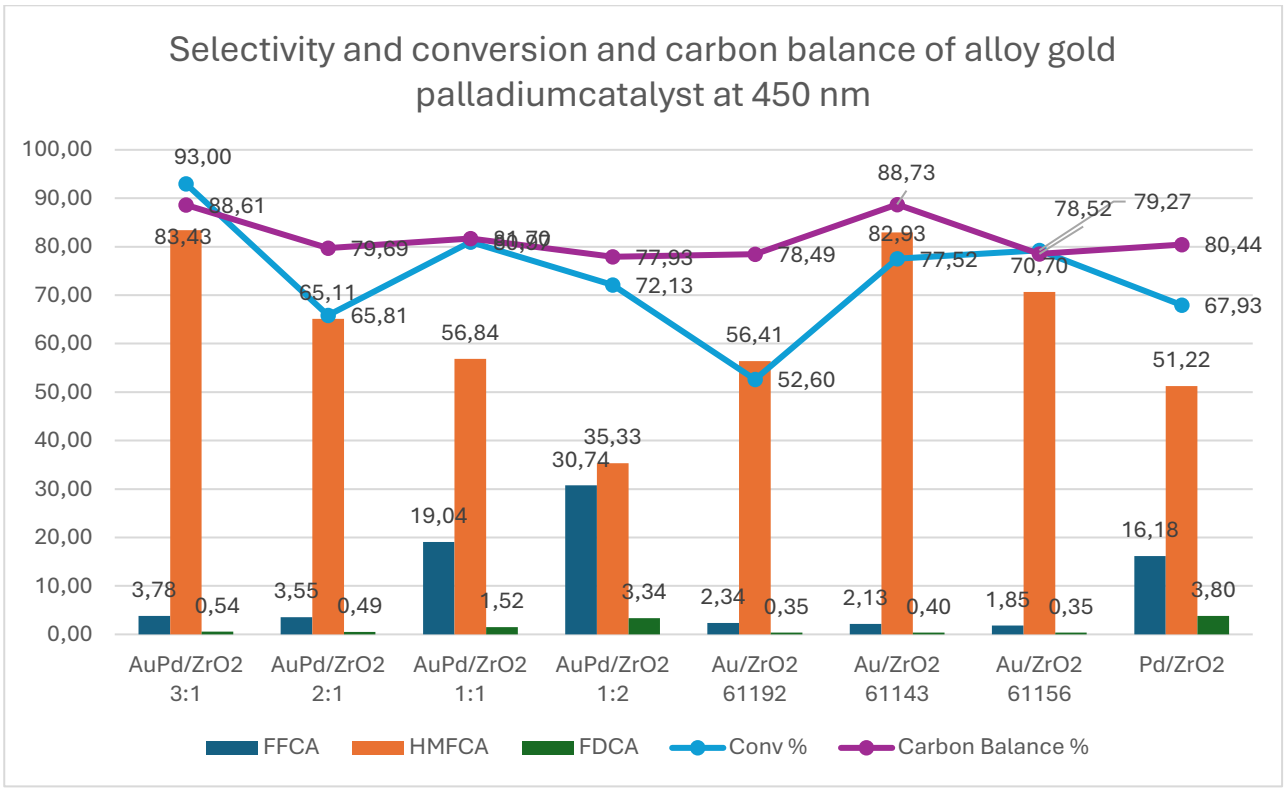

Figure 4.9 *Catalytic tests: HMF conversion, selectivity and carbon balance for AuPd alloy supported catalysts at 450 nm.*

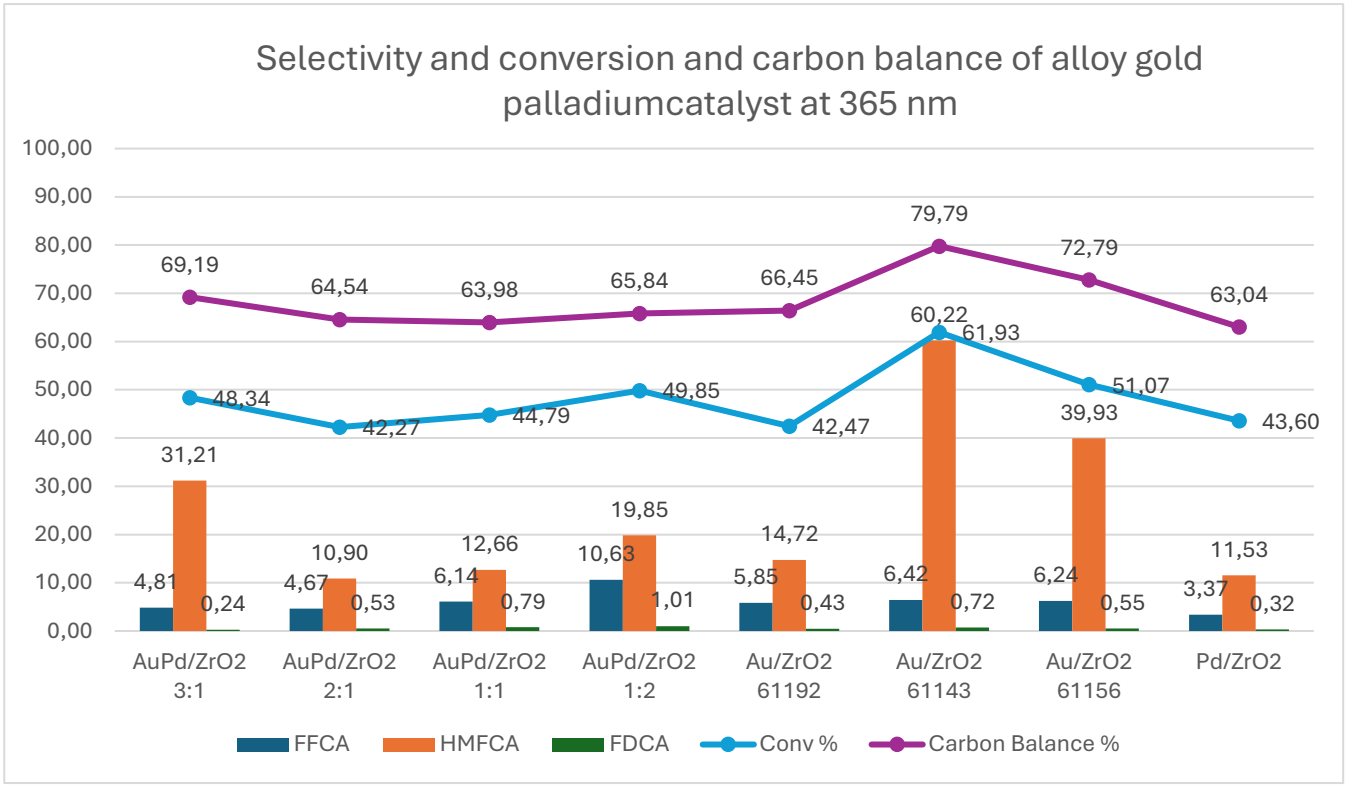

Figure 4.*10* *Catalytic tests: HMF conversion, selectivity and carbon balance for AuPd alloy supported catalysts at 365 nm*

Bimetallic catalysts demonstrated consistently high carbon balances, regardless of the Pd/Au ratio, particularly at 450 nm. At 365 nm, however, carbon balances were lower due to increased degradation pathways. This trend aligns with expectations, as shorter wavelengths corresponding to higher energy photons, which can promote undesired side reactions. For zirconia-supported catalysts, a slight decrease in conversion was observed with increasing Pd content. However, the trend towards deeper oxidation, favouring the formation of FDCA, was more pronounced at 450 nm. At 365 nm, the lower selectivity and carbon balance made it more challenging to identify clear trends.

Among the monometallic Au catalysts, Au/ZrO_2 61143 consistently exhibited the best performance in terms of both conversion and selectivity, particularly at 450 nm. This catalyst achieved a remarkable 82% selectivity towards HMFCA at 77.52% conversion, highlighting the potential of ZrO_2 as a support for Au-based catalysts.

To assess the cost-effectiveness of palladium-based catalysts, a plot of FDCA production rate per gram of palladium was generated (Figure 4.11). This analysis allows us to evaluate the impact of palladium loading on catalytic performance. The mass of FDCA produced was normalized by the mass of palladium in the catalyst and the reaction time (240 minutes). The plot was generated using a logarithmic scale to visualize the trend more effectively

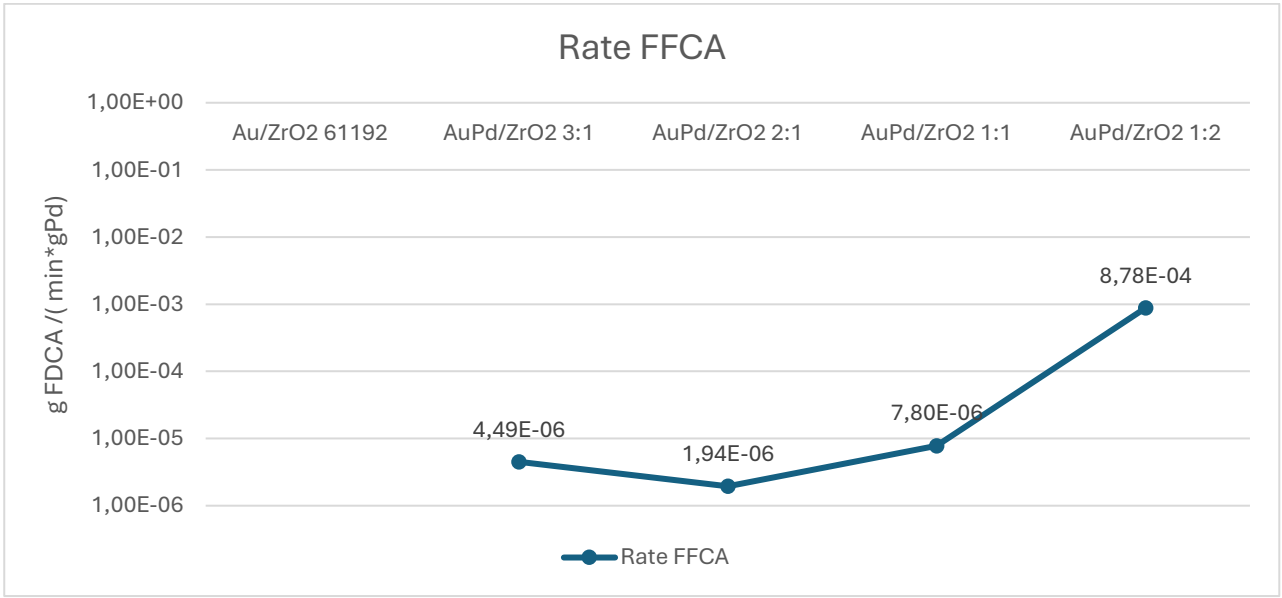

Figure 4.11 *Catalytic tests: FDCA production rate on AuPd alloy supported catalysts at 450 nm.*

The plot indicates that increasing the palladium-to-gold ratio from 2:1 to 1:1 did not lead to a significant increase in FDCA production rate per gram of palladium. In fact, a further increase in the palladium content to a 1:2 ratio resulted in a substantial improvement in the rate, suggesting that this composition is optimal. While this catalyst contains more palladium, its higher activity compensates for the increased metal loading.

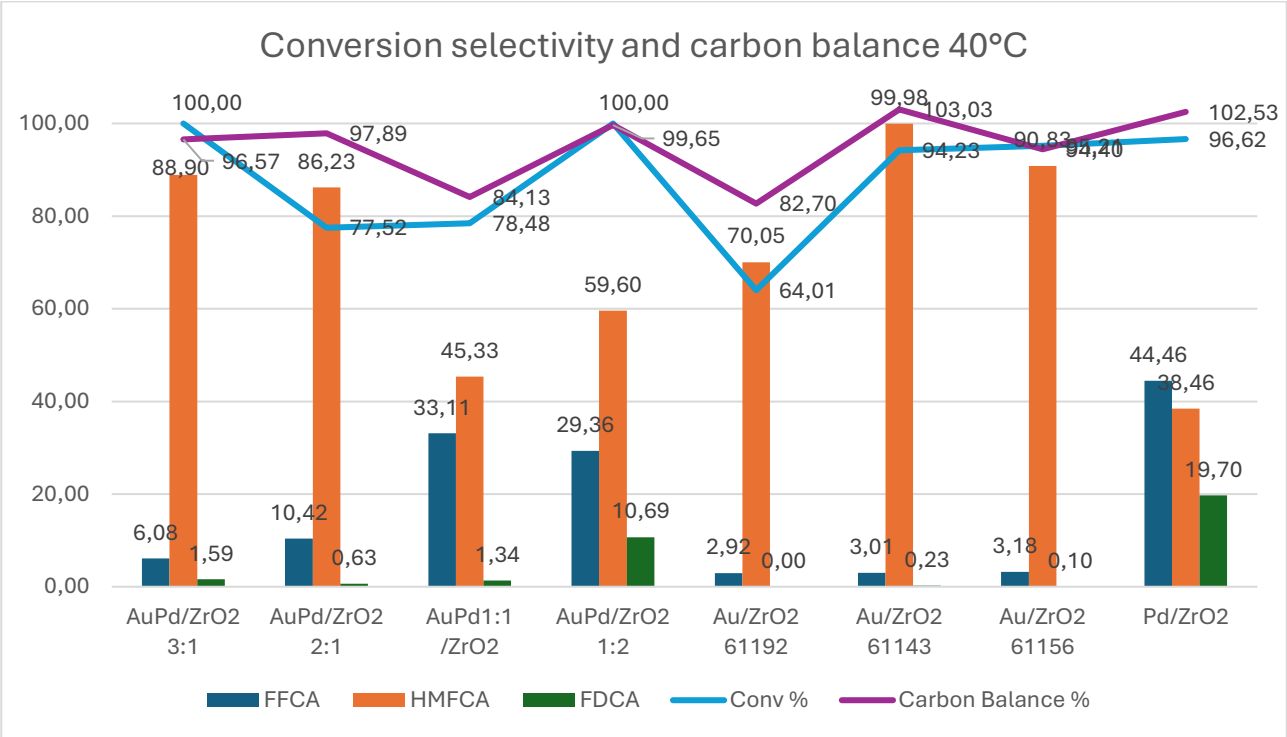

Figure 4.12 *Catalytic tests: HMF thermal oxidation at 40°C using monometallic and bimetallic Au-Pd catalysts.*

Interesting results were observed during thermal oxidation of HMF using Au, Pd and Au-Pd bimetallic alloy catalysts (Figure 4.12). The best results were observed for Pd monometallic catalyst with the FDCA yield of 20%. In case of bimetallic Au-Pd catalysts the conversion is comparable for all cases (about 80%), while the yield to FFCA increased with increasing Pd content. However, the efficiency of the AuPD/ZrO_2 1:2 catalyst was slightly better with the FDCA selectivity of about 10%. No visible differences were observed for Au supported on different zirconia which suggests that the mechanism of the photooxidation does not depend on ZrO_2 composition.

4.3.2 Gold Palladium alloy catalyst with Silica support

To investigate the influence of support material on catalytic performance, a series of experiments were conducted using SiO_2 as a support for gold-palladium catalysts. Unlike ZrO_2, silica is an insulator. Four different catalysts were prepared with varied Pd/Au ratios: Au/SiO_2 (no Pd), $Au99.5Pd0.5/SiO_2$, $Au97.5Pd2.5/SiO_2$, and $Au95Pd5/SiO_2$

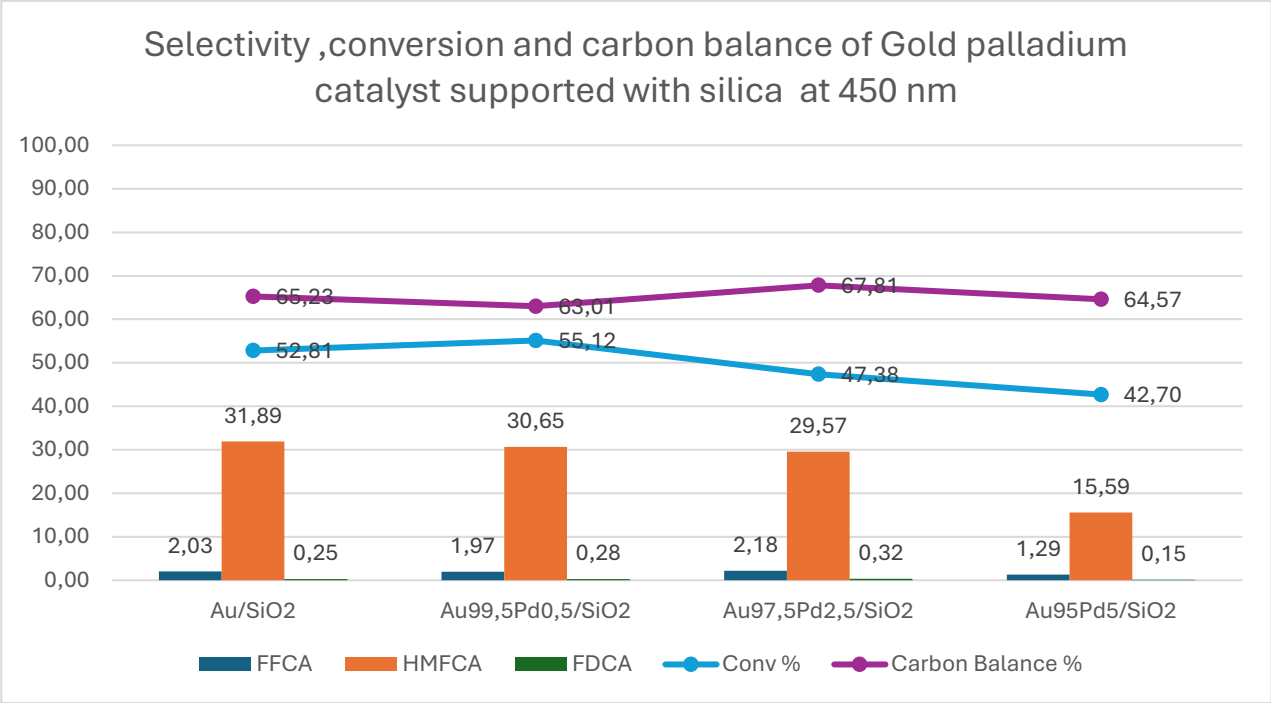

Figure 4.13 *Catalytic tests: HMF conversion, selectivity and carbon balance for AuPd alloy supported on SiO_2 at 450 nm.*

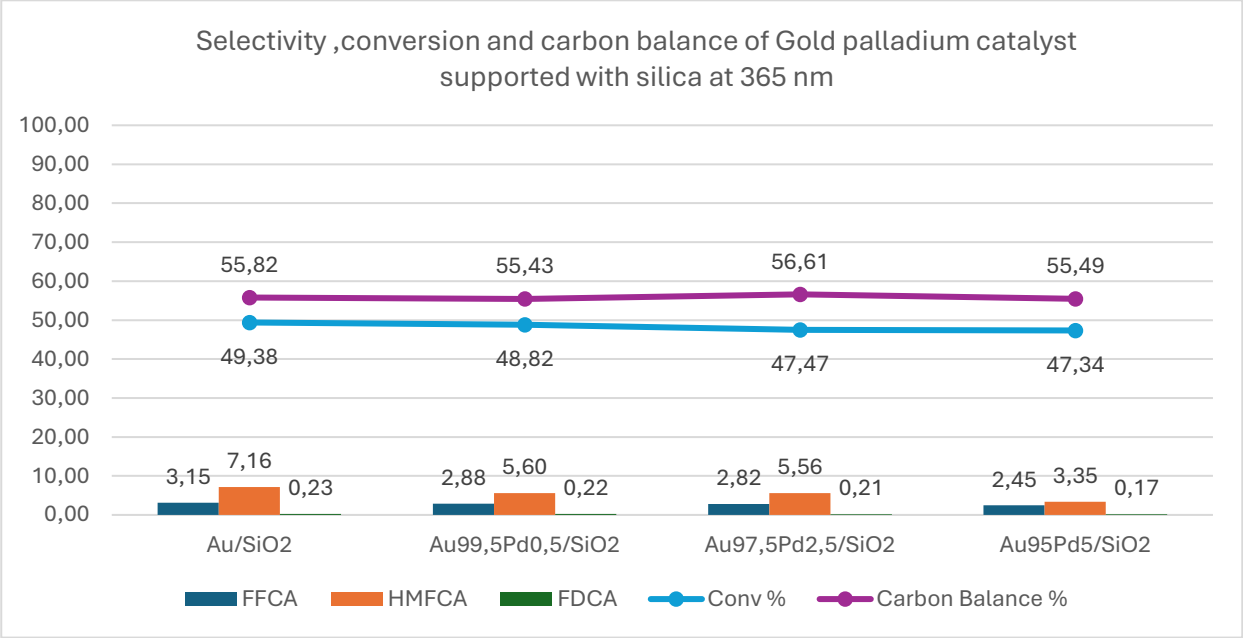

Figure 4.14 *Catalytic tests: HMF conversion, selectivity and carbon balance for AuPd alloy supported on SiO_2 at 365 nm.*

For both 365 nm and 450 nm irradiation, the silica-supported catalysts exhibited similar performance in terms of conversion, carbon balance, and product selectivity. This is expected, as the palladium content varied only slightly between the different catalysts.

Compared to the zirconia-supported catalysts, particularly those with higher gold content, the silica-supported catalysts demonstrated lower activity and selectivity. The lower carbon balance suggests increased side reactions and degradation pathways. Additionally, the reaction tended to halt at the intermediate HMFCA stage, with limited formation of FFCA and FDCA. This indicates that the silica support may not be as effective as zirconia in promoting the complete oxidation of HMF to FDCA. The difference could be explained by the optical properties of both supports. When UV light shines on the ZrO_2, electrons are excited from the valence band to the conduction band, creating electron-hole pairs. These electron-hole pairs can then migrate to the surface of the ZrO_2. The gold nanoparticles on the ZrO_2 surface can act as "electron sinks," trapping the photogenerated electrons. This enhances charge separation and promotes the generation of reactive oxygen species (ROS). The holes can oxidize adsorbed molecules, while the electrons on the gold can reduce oxygen, leading to the formation of superoxide radicals (O^{2-}) and other ROS. These ROS can then participate in the oxidation of target molecules. In case of an insulator (SiO_2) the charge separation does not occur. The mechanism of the oxidation is only depending on gold. SiO_2 can facilitate plasmon excitation in gold,

leading to hot electron generation and potential interfacial charge transfer. However, the formation of "hot electrons" via plasmon depends on the light wavelengths. It is about 523 nm for Au. These hot electrons, if formed, can then be transferred from the gold to adsorbed molecules or to the SiO_2 support, potentially leading to charge separation and the generation of ROS.

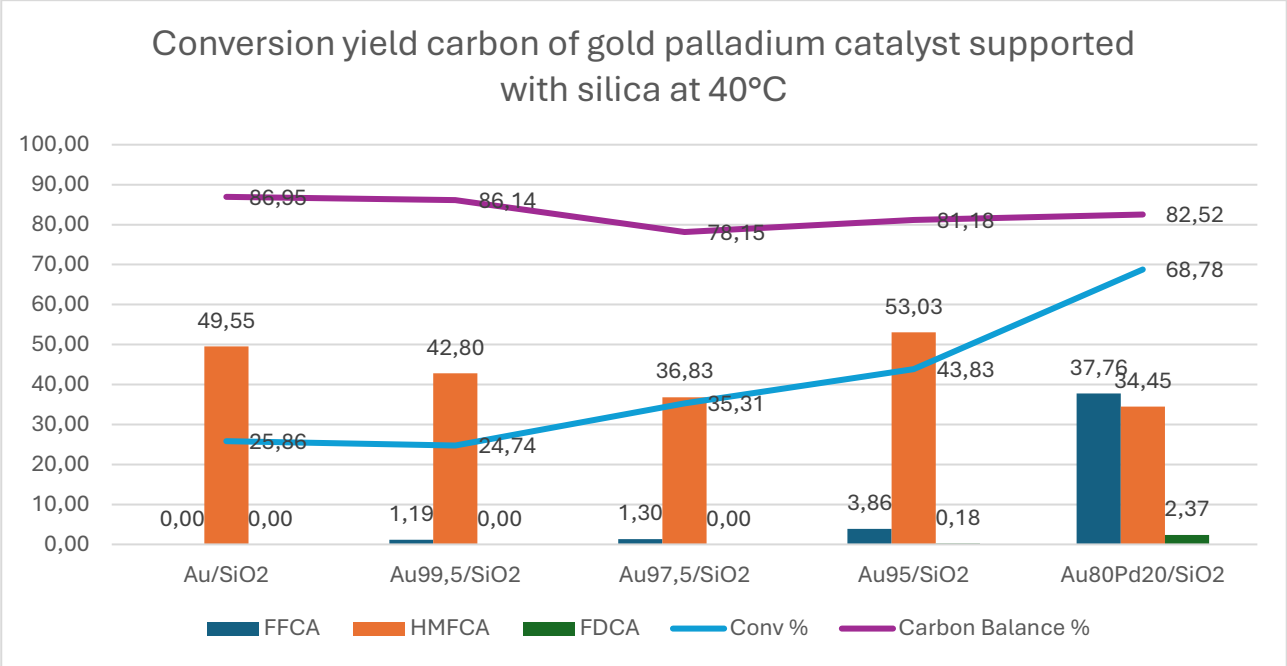

Figure 4.15 *Catalytic tests: HMF conversion, selectivity and carbon balance for AuPd alloy supported on SiO_2 at 40°C.*

As the SiO_2 based catalysts were not efficient for the photo-oxidation reaction, tests at 40°C without light were performed (Figure 4.15). Good results were observed for $Au80Pd20/SiO_2$ catalyst with almost 70% of conversion and correct carbon balance. These results clearly showed that observed activity under illumination are due to the increase of the temperature of the solution during illumination. The oxidation of HMF on $AuPd/SiO_2$ catalysts is considered as a thermal process and not photocatalytic.

4.4 Silver Palladium alloy catalysts supported by silica

To further investigate the influence of support material and metal composition, a series of experiments were conducted using silica-supported silver-palladium alloy catalysts. Four different catalysts were

prepared with varying palladium content: pure silver (0% Pd), Ag99.7Pd0.3/SiO_2, Ag98.3Pd1.7/SiO_2, and Ag96.6Pd3.4/SiO_2.

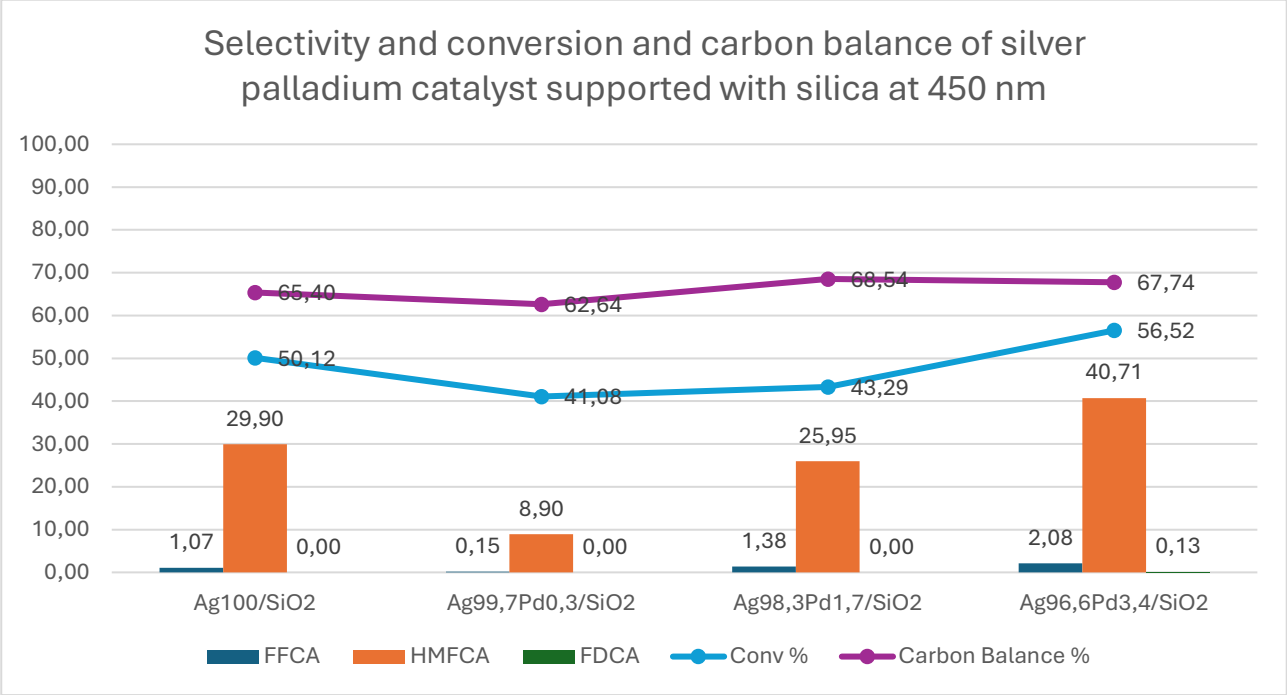

Figure 4.16 *Catalytic tests: HMF conversion, selectivity and carbon balance for AgPd alloy supported on SiO_2 at 450 nm.*

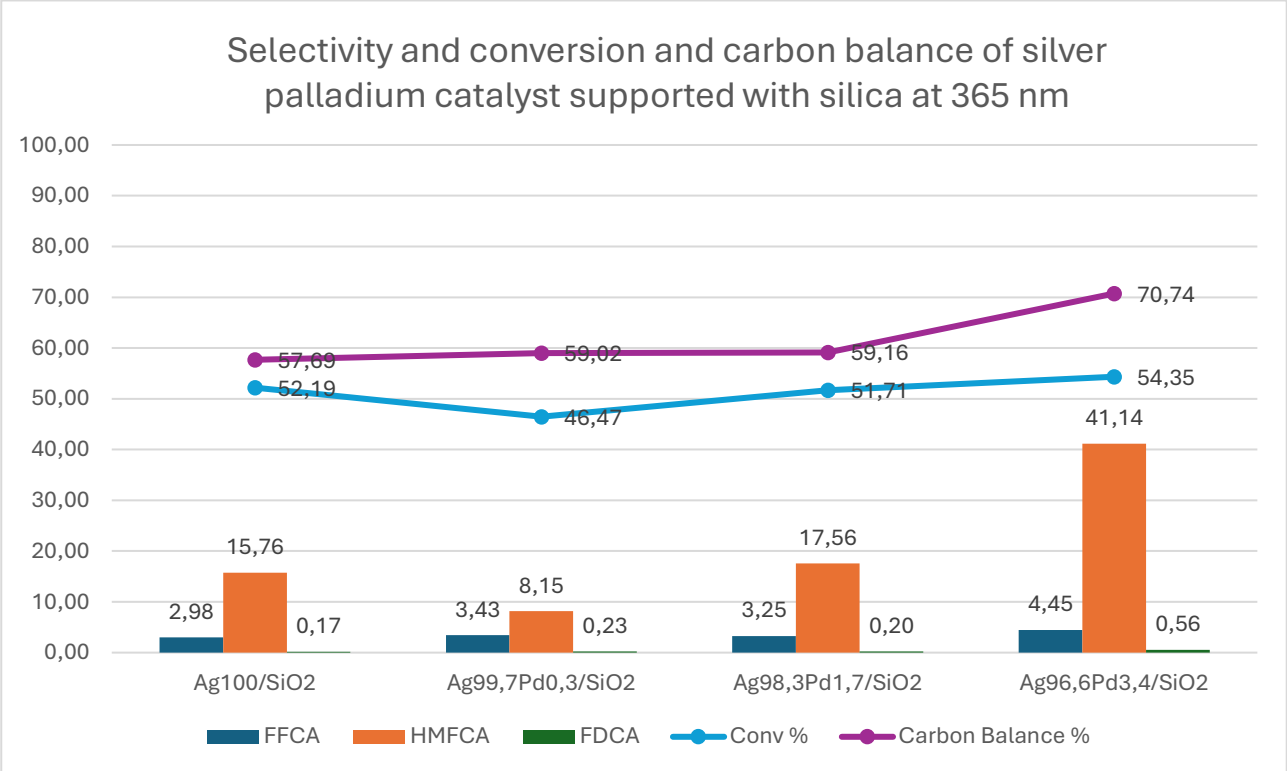

Figure 4.17 *Catalytic tests: HMF conversion, selectivity and carbon balance for AgPd alloy supported on SiO_2 at 365 nm.*

At 450 nm, the conversion initially decreased with increasing palladium content, reaching a minimum for the Ag99.7Pd0.3/SiO2 catalyst. However, further increasing the palladium content to 3.4% led to a slight increase in conversion. In all cases, the reaction primarily yielded HMFCA, with limited formation of FFCA and FDCA.

Comparing the silica-supported silver-palladium catalysts to the gold-palladium catalysts, it was observed that the former exhibited lower conversion but similar selectivity and carbon balance. The lower activity of the silver-palladium catalysts may be attributed to their intrinsic properties or the influence of the support.

At 365 nm, the silver-palladium catalysts showed higher selectivity towards HMFCA compared to the gold-palladium catalysts. However, no significant differences were observed in terms of conversion and carbon balance

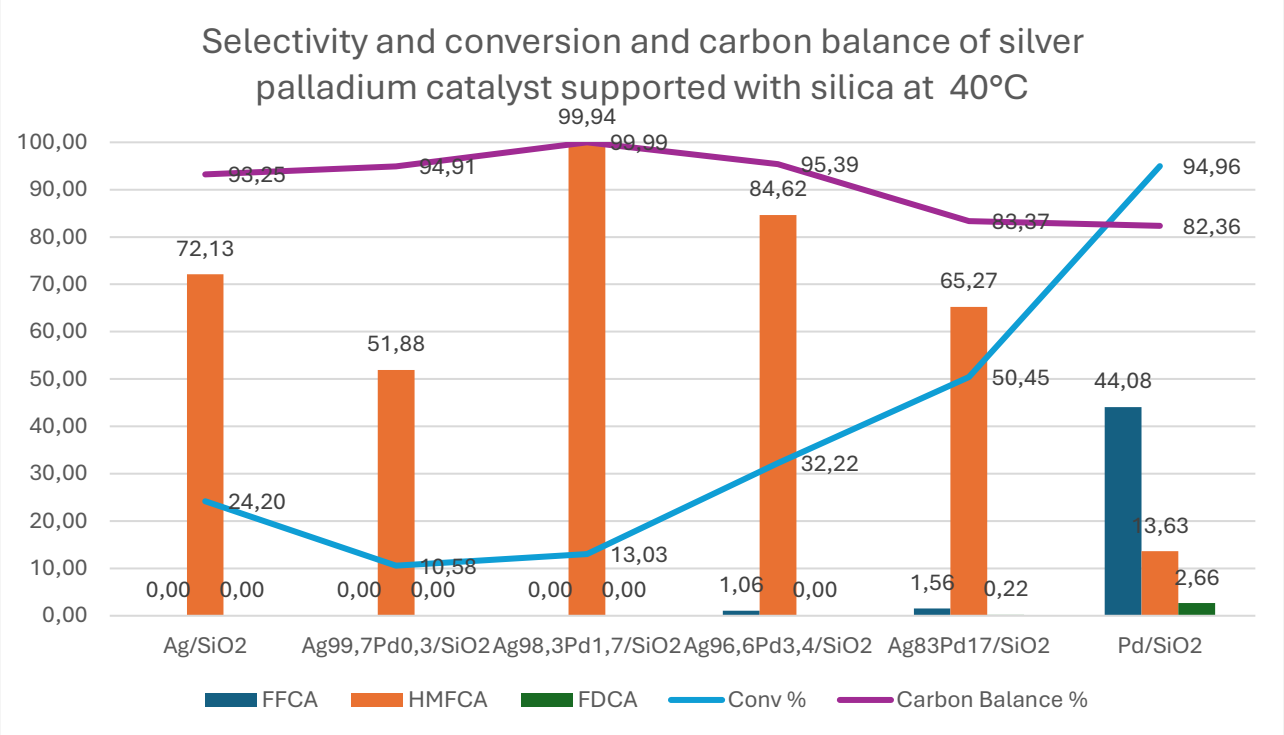

Figure 4.18 *Catalytic tests: HMF conversion, selectivity and carbon balance for AgPd alloy supported on SiO_2 at 40°C.*

As it was already observed for $AuPd/SiO_2$ catalysts the thermal catalysis is involved. Tests performed at 40°C without light (Figure 4.18) clearly showed better catalytic results.

4.5 Copper palladium catalyst on zirconia support

A series of palladium-copper alloy catalysts supported on zirconia were also investigated. These catalysts included pure copper, PdCu alloys with ratios of 1:3, 1:1, and 3:1, as well as a zirconia support without any metal loading. This comprehensive approach allowed for a thorough evaluation of the influence of the metal composition and support material on catalytic performance.

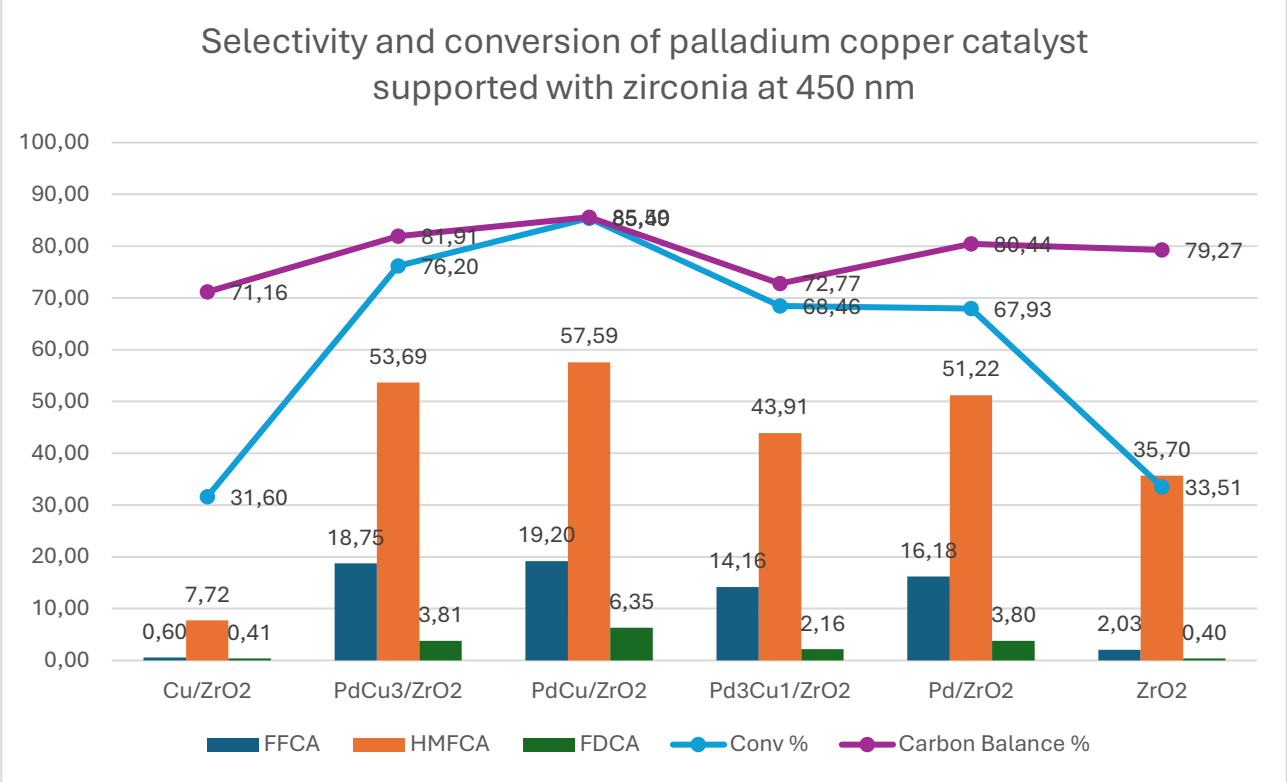

Figure 4.19 *Catalytic tests: HMF conversion, selectivity and carbon balance for CuPd alloy supported on ZrO_2 at 450 nm.*

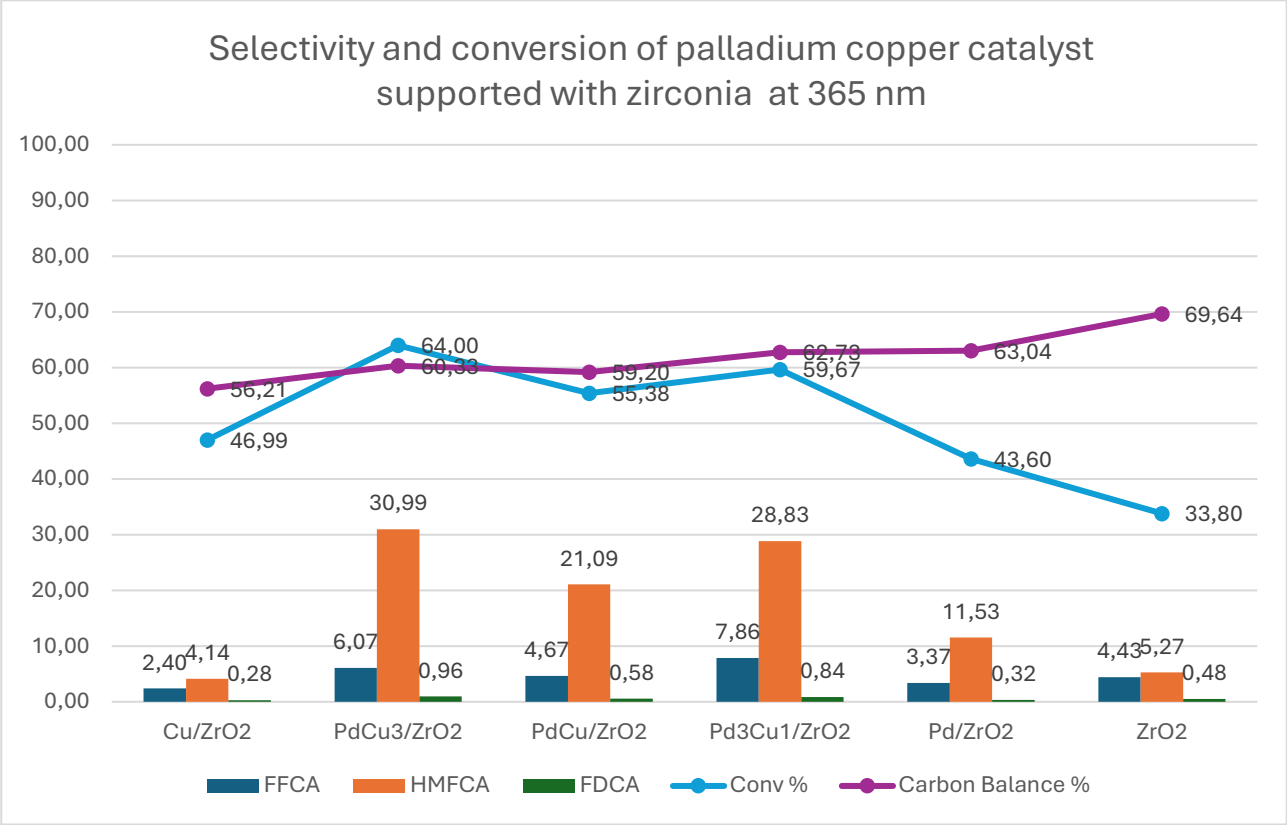

Figure 4.20 *Catalytic tests: HMF conversion, selectivity and carbon balance for CuPd alloy supported on ZrO_2 at 365 nm.*

At 450 nm, a clear trend emerges in the conversion, with the highest conversion observed for the 1:1 Pd/Cu ratio. This suggests that a balanced combination of palladium and copper is optimal for this reaction. All palladium-copper catalysts, except for pure copper, were able to catalyse the oxidation of HMF to FDCA.

At 365 nm, the catalytic performance of the different catalysts was similar, with conversions ranging from 55% to 65%. While the presence of both palladium and copper was necessary for the formation of FFCA and FDCA, the higher energy input at 365 nm limited the extent of the reaction, leading to a higher proportion of intermediate products and lower carbon balance.

To understand if the good results achieved with these catalysts were obtained by the light or by the heat generated by the irradiation a thermal reaction at 40°C with the lamp off has been also performed. The results are given in Figure 4.21.

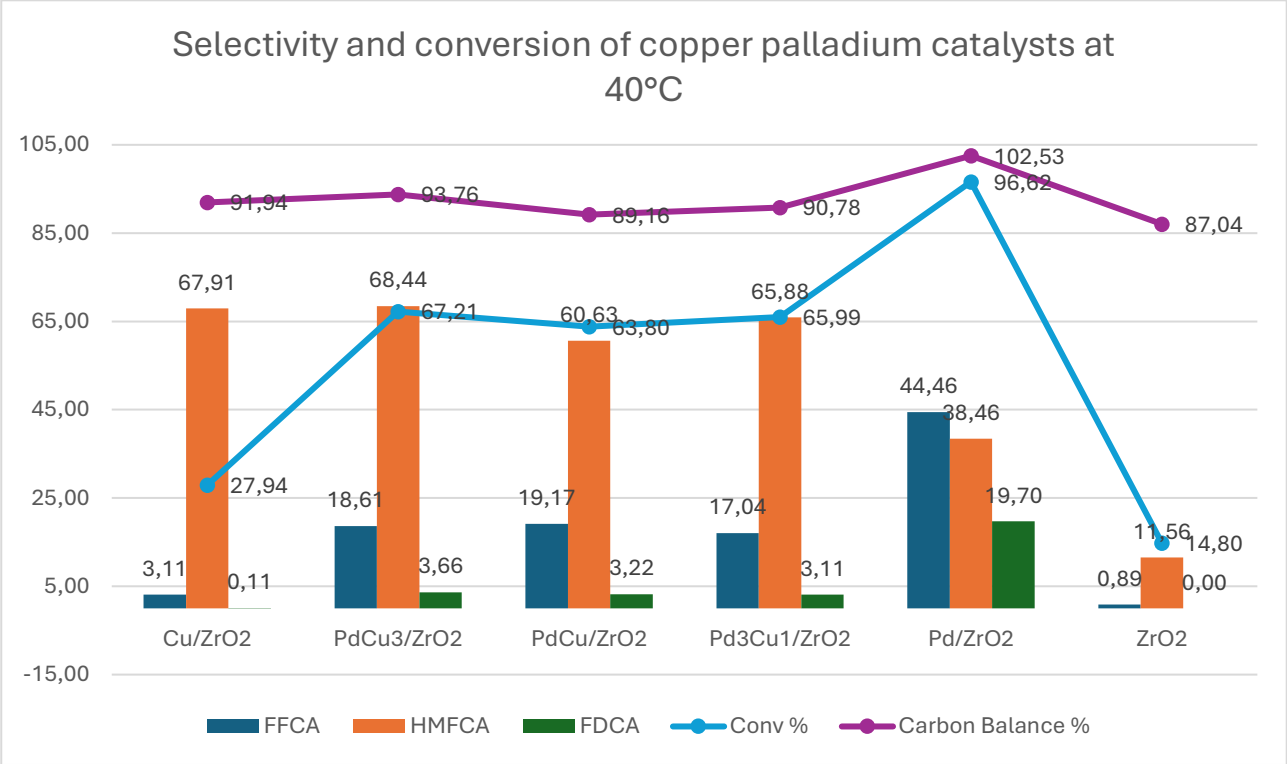

Figure 4.21 *Catalytic tests: HMF conversion, selectivity and carbon balance for CuPd alloy supported on ZrO_2 at 40°C.*

The work continued by exploring the use of different noble metals and comparing their performance with that of Au. This deviation aimed to investigate whether other metals could replace Au in terms of activity and cost-effectiveness, thereby facilitating the scale-up of the process. As depicted in Figure 4.21, the alloy catalysts $CuPd/ZrO_2$ exhibit a volcano plot trend. It is evident that the oxidation progresses deeper (if compared the HMFCA yield) when the molar ratio of the two species, Cu and Pd, approaches 1:1. This trend differs from that observed with alloy $AuPd/ZrO_2$ catalysts, indicating that oxidation towards FFCA and FDCA yields better results when the molar ratio of Cu to Pd is close to 1:1. Nevertheless, in cases where the noble metals is Au, the alloy catalysts demonstrate better activity when the amount of Pd exceeds that of Au.

Figure 4.21 reveals that Pd plays a more dominant role as the active metal in these reactions compared to Cu, because the Cu/ZrO_2 and ZrO_2 catalysts exhibit very low substrate conversions, with selectivity solely towards HMFCA. When the amount of Pd in the catalyst is increased, the catalyst's activity experiences a significant surge compared to that of the pure copper catalyst and demonstrates a much more targeted selectivity towards the FDCA compound.

The best catalyst identified in the obtained results is $CuPd/ZrO_2$, with a conversion of 86 % and a carbon balance of 85 %. These results can be compared to those of the best alloy catalyst Au:Pd 3:1/ZrO_2, which achieved a conversion of 93% and a carbon balance of 88%. As far as selectivity is concerned, catalyst $CuPd/ZrO_2$ exhibits a selectivity towards HMFCA of 58%, FFCA of 19% and FDCA of 6%, similar to $AuPd/ZrO_2$ which demonstrates selectivity towards HMFCA of 57%, FFCA of 19% and FDCA of 1,5%. The results obtained are comparable, but the effective costs of $CuPd/ZrO_2$ are significantly lower compared to $AuPd/ZrO_2$, as it involves costs related to Cu that are not comparable to those related to Au. Furthermore, the selectivity towards FDCA of $CuPd/ZrO_2$ is higher with respect $AuPd/ZrO_2$. This makes $CuPd/ZrO_2$ a very interesting catalyst due to its activity, selectivity and reasonable cost.

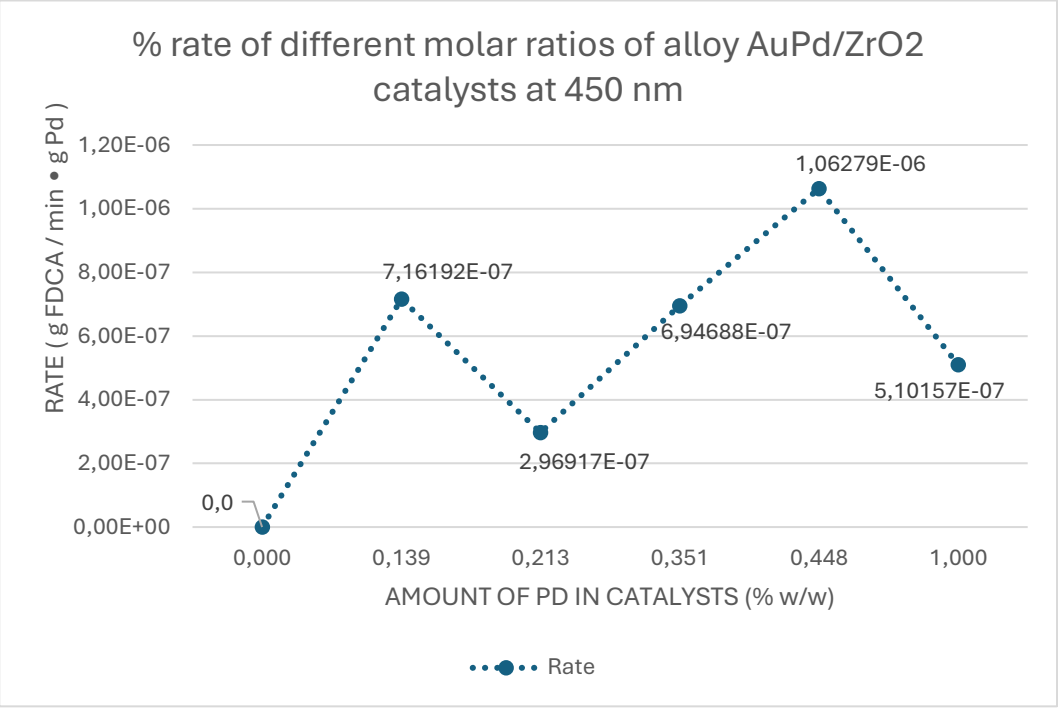

Figure 4.22 *Catalytic tests: FDCA production rate for AuPd alloy supported on ZrO_2 at 450 nm.*

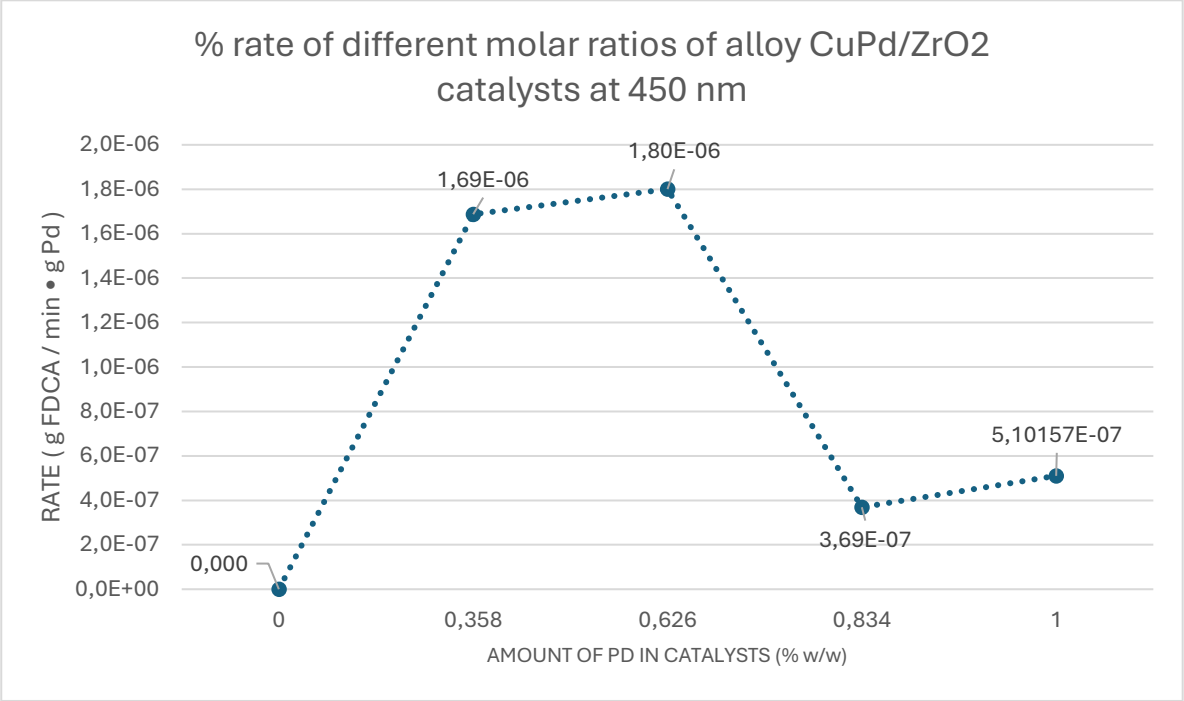

Figure 4.23 *Catalytic tests: FDCA production rate for CuPd alloy supported on ZrO_2 at 450 nm.*

A direct comparison of AuPd and CuPd catalysts, based on FDCA production rates per gram of palladium, reveals interesting insights (Fig 4.22 and Figure 4.23). While both systems exhibit catalytic activity, Cu-based catalysts, particularly Cu3Pd and CuPd, demonstrate significantly higher rates compared to their AuPd counterparts. This suggests that copper, despite its lower cost, can offer comparable or even superior performance.

The influence of support material is also evident. Zirconia-supported catalysts, especially those with optimized metal compositions, show promising results in terms of both activity and selectivity. However, the choice of support and metal loading can significantly impact the overall performance of the catalyst.

It is important to note that while selectivity is a crucial factor, the production rate is equally important for practical applications. By considering both factors, it becomes clear that Cu-based catalysts, particularly Cu3Pd and CuPd, offer a compelling balance of activity, selectivity, and cost-effectiveness. Future research should focus on further optimization of these catalysts to maximize their potential for industrial applications.

4.6 Gold catalyst coated with manganese oxide

Plasmonic effect in the visible spectrum is largely confined to the use of gold, which neglects the numerous properties offered by other elements in the periodic table. Additionally, we have also seen that the LSPR band can be modulated on the basis of the synthesis of the nanoparticles. To further optimize the use of the LSPR effect, it is also possible to combine two or more materials with different properties to create hybrid nanoparticles. This approach allows for the integration of two distinct functionalities into a single nanoparticle, thereby enhancing or modifying their properties. Coating nanoparticles with a thin layer is expected to alter their functions, as well as their optical and electronic properties, chemical reactivity, catalytic activity, thermal stability, dispersibility, and magnetic properties. The development of a shell around the core also helps to stabilize colloidal particles. Additionally, the shells can retain ligands on their surface, preventing particle aggregation and maintaining the integrity of the assembled superstructures. In core-shell structures, the shell acts as a physical barrier between the surrounding environment and the optically active core, making the nanostructures less susceptible to environmental fluctuations, surface chemistry alterations, and photo-oxidation. Silica, titania, and other oxide shells are the most commonly used materials. These oxides are compounds formed by the combination of a metal with oxygen. Each oxide has its advantages and disadvantages, but in our case, MnO_2 is of particular interest. MnO_2 is a semiconductor material that has demonstrated notable catalytic performance while being low-cost, low-toxicity, and abundantly available. The core-shell structure of Au@MnO_2 nanoparticles is utilized to enhance the efficacy of radiotherapy and can have promising role in cancer treatment. MnO_2 is known to improve tumor oxygenation by catalyzing the decomposition of endogenous hydrogen peroxide (H_2O_2) into oxygen. This increasing in the oxygen levels within the tumor microenvironment addresses the common issue of tumor hypoxia, which often limits the effectiveness of radiotherapy.[21] The ability to control the thickness of the MnO_2 shell allows for fine-tuning of the nanoparticle's properties, optimizing their performance for specific applications. The Au@MnO_2 nanoparticles maintain their plasmonic absorption with a red shift proportional to the MnO_2 layer thickness, which can be advantageous for imaging and diagnostic purposes.

Tests has been run on gold catalyst coated with manganese and prepared at the Helsinki University by Arthur Raymond, PhD student of Dr Robert Wojcieszak. The thickness of the MnO_2 was changed in different catalysts, and it was interesting to study if there were some differences in terms of activity. Specifically, catalysts with 4 different MnO_2 thickness layers were taken into consideration, respectively of 3.5, 5, 7,5 and 10 nm.

Au NPs and Au@MnO_2 NPs were characterized by their LSPR position using UV-Vis spectroscopy. Figure 4.24 displays the extinction spectra of AuNPs and the extinction spectra after reaction with varying amounts of $KMnO_4$, which was intended to result in the deposition of ultrathin MnO_2 shells. As shown in Figure 4.24, the red shift of the LSPR band of the AuNPs from around 580 nm to 600 nm indicates the formation of a MnO_2 overlayer, resulting in Au@MnO_2. This shift also demonstrates an increase in the MnO_2 shell thickness as the amount of $KMnO_4$ available for the reaction increases. Furthermore, a peak is observed around 320 nm corresponding to the absorption of MnO_2. UV-Vis spectroscopy served as an effective diagnostic tool for rapid monitoring of LSPR changes in Au@MnO_2.

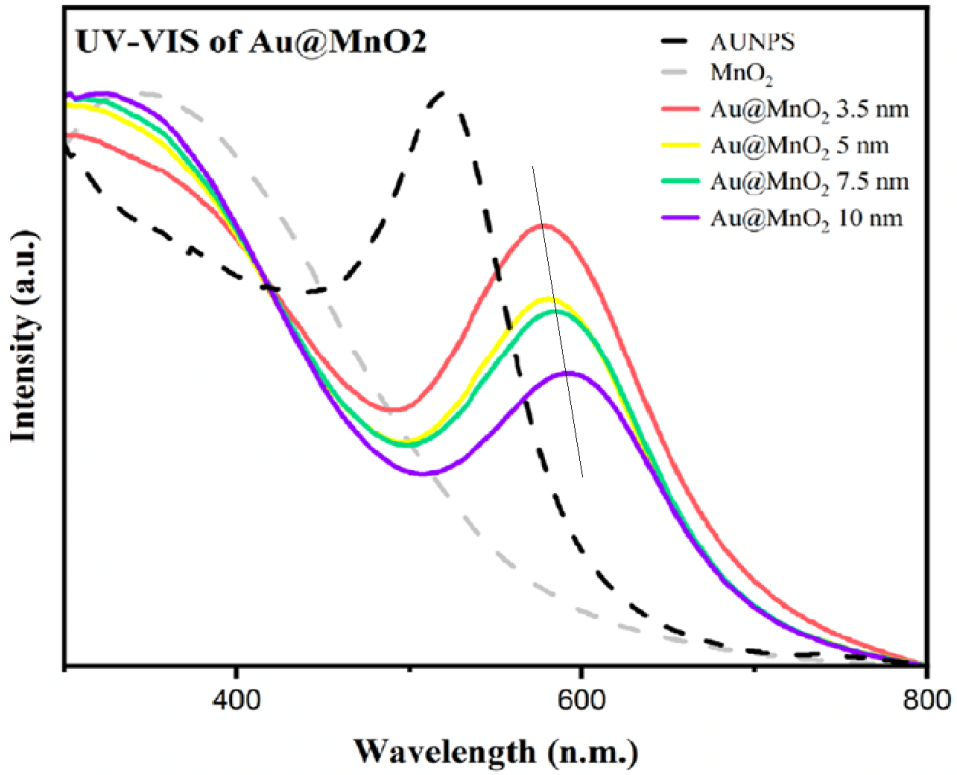

Figure 4.24: *UV-VIS spectra of Au@MnO2 core-shell nanoparticles for different shell thicknesses (3.5 nm, 5 nm, 7.5 nm, 10 nm) and comparaison with AuNPS and MnO2 spectra.*

To provide additional evidence of the core-shell structure, TEM images were obtained for the material and are presented in figures 4.25. The manganese oxide layer, appearing in gray, is seen more precisely covering the gold nanoparticles, which appear in black. The nanoparticles have retained their spherical shape with a diameter of 15 nm, and the manganese layer is observable here, still

exhibiting the spiky features noted in the previous section. The differences in thickness are difficult to discern across the four cases. However, a decrease in the presence of MnO_2 is observed as the concentration decreases from (a) to (d) respectively. It can also be noted, when comparing the images at the 100 nm scale, that the particles tend to come closer together, with a slight agglomeration occurring when there is less MnO_2. This suggests that there may not be enough material to uniformly cover all the particles. In any case, these results confirm the successful synthesis and remain consistent with the previous analyses.

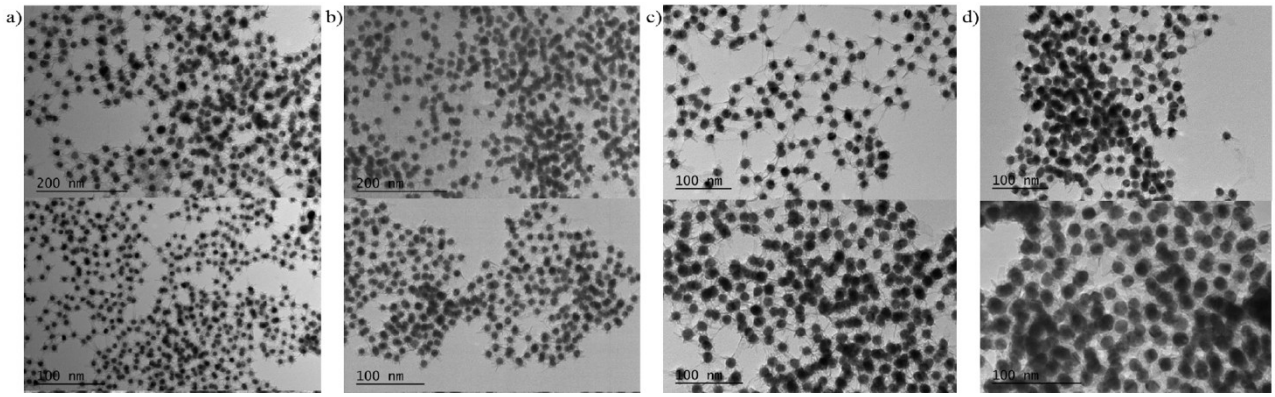

Figure 4.25: *(a) TEM images of Au@MnO_2 with a 10 nm thick layer (b) TEM images of Au@MnO_2 with a 7.5 nm thick layer (c) TEM images of Au@MnO_2 with a 5 nm thick layer (d) TEM images of Au@MnO_2 with a 3.5 nm thick layer*

Catalytic tests were performed on this materials and the results are given below :

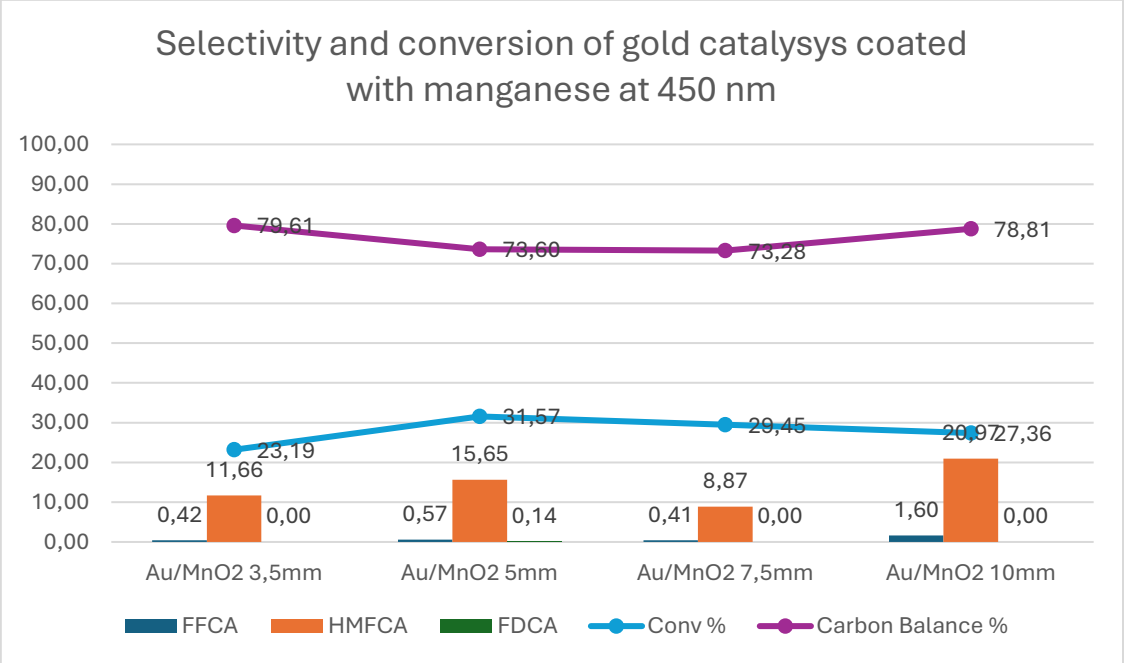

Figure 4.26: *Catalytic tests: HMF conversion, selectivity and carbon balance for Au catalyst coated on MnO_2 at 450 nm.*

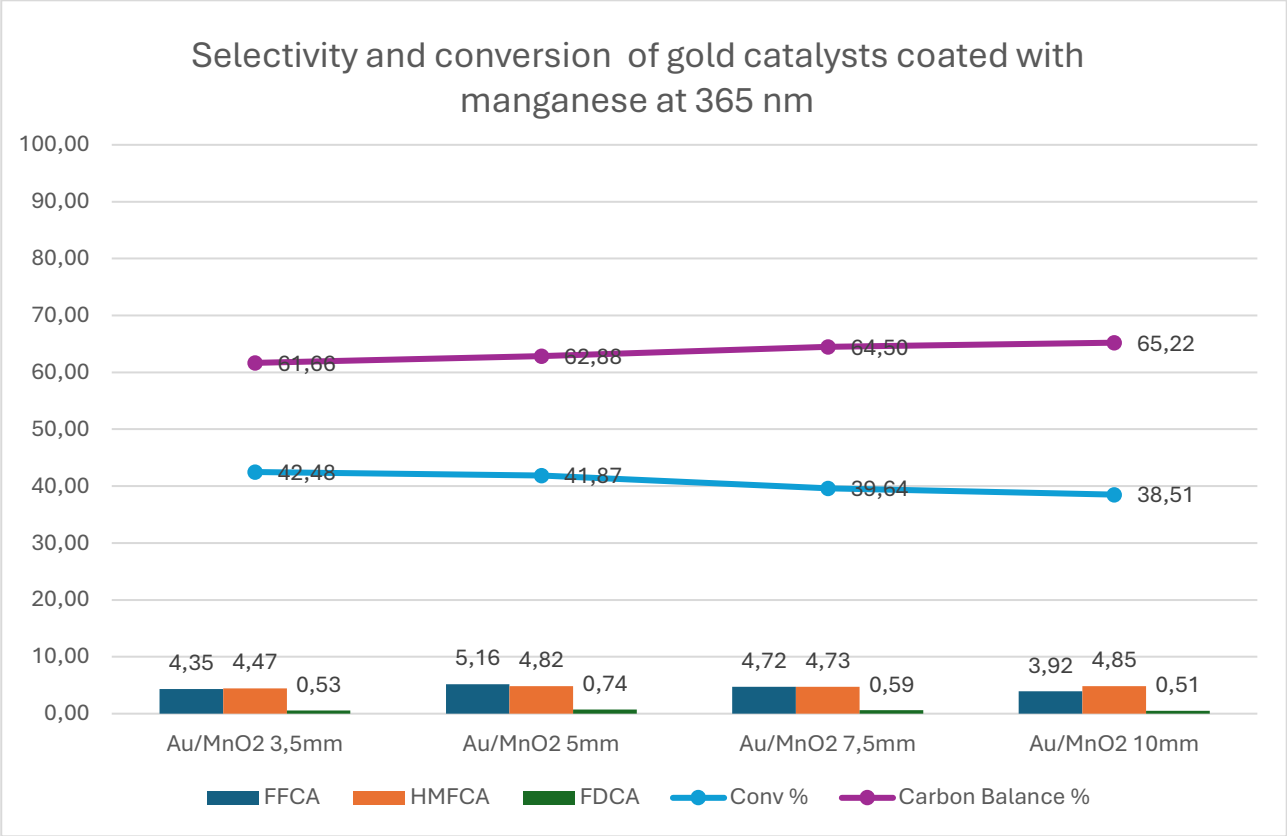

Figure 4.27: *Catalytic tests: HMF conversion, selectivity and carbon balance for Au catalyst coated on MnO_2 at 365 nm.*

These kinds of catalysts are not very active both at 365 nm and a 450 nm and the reaction does not go at the lasts steps as the selectivity in FDCA is close to zero. Only at 365 nm FFCA is obtained in small quantities instead at 450 nm the only product obtained is HMCA. Carbon balance is lower if compared to that of the other catalysts even at 450 nm. More specifically, all values of carbon balance at 450nm are below 80% and at 365 nm they are below 65%. Consequently, we can conclude that part of the reactant goes to complete oxidation. Both a 450 and at 365 nm a trend in terms of conversion or selectivity between the different particles size seems not be present. We can conclude that the particle size of this catalysts does not affect the behaviour of this reaction in the wavelengths used and that the effect of the support is crucial for the development of the reaction: in this case zirconia performs better than manganese regardless of the metal loaded.

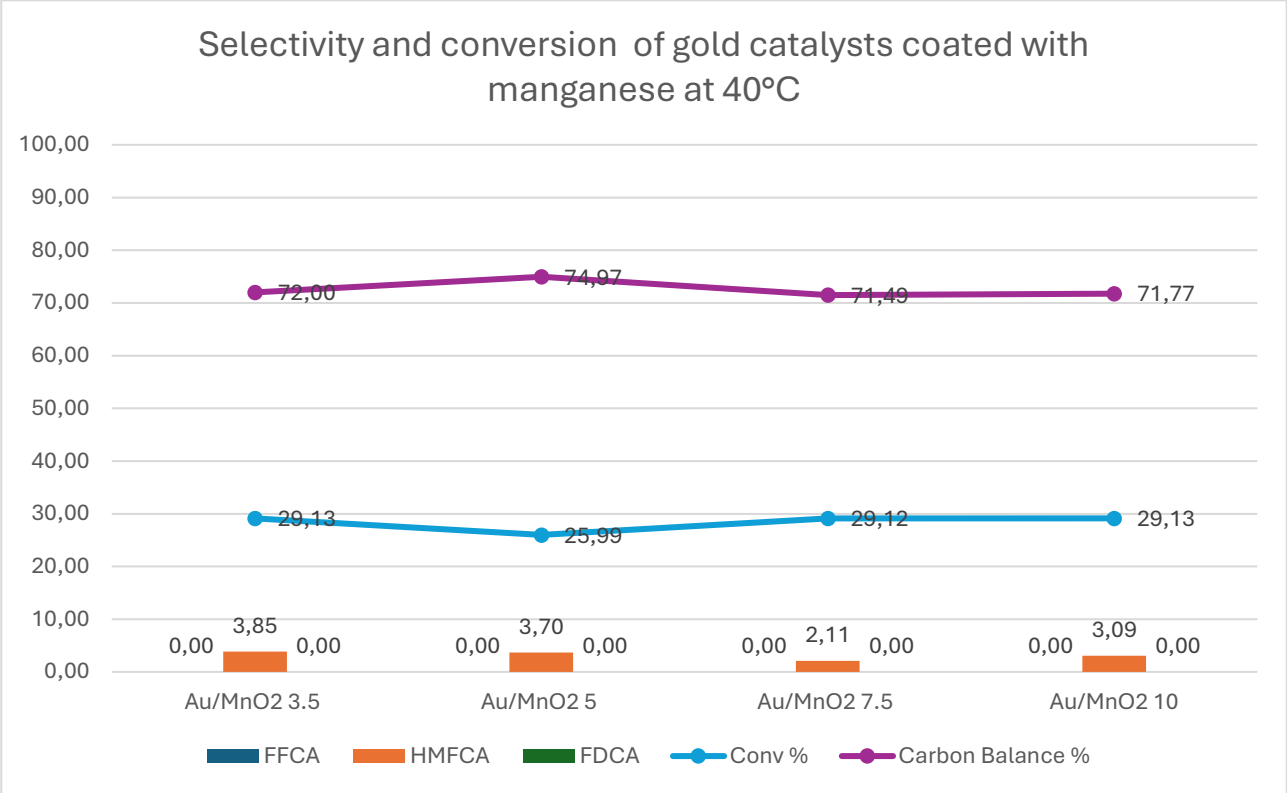

Figure 4.28: *Catalytic tests: HMF conversion, selectivity and carbon balance for Au catalyst coated on MnO_2 at 40°C.*

With the thermal catalysis, results similar to those of photocatalysis have been obtained with a carbon balance around 70% and conversion values between 25% and 30%. It means that with this support the effect of the light is limited. In this case bad results are obtained both with thermal and photocatalysis indicating that the catalyst does not suits with this reaction and does not interact with the light. It follows that the kind of support is important not only for the successful results of the reaction but also for having a successful interaction with the light to have an enhancement of the reaction.

4.7 Nanowire catalysts

Nanowire catalysts are defined as catalysts with structure of the order of nanometers. Usually, they have an anisotropic structure with a diameter that is lower than 100 nm or a length- diameter ratio lower than 1000 nm. Gold and gold-palladium catalysts have been tested with three different supports: titania TiO_2, zirconia ZrO_2 and silica SiO_2. This allows for an understanding of

the performance of this new catalytic structure by varying both the type of metal and the type of support.

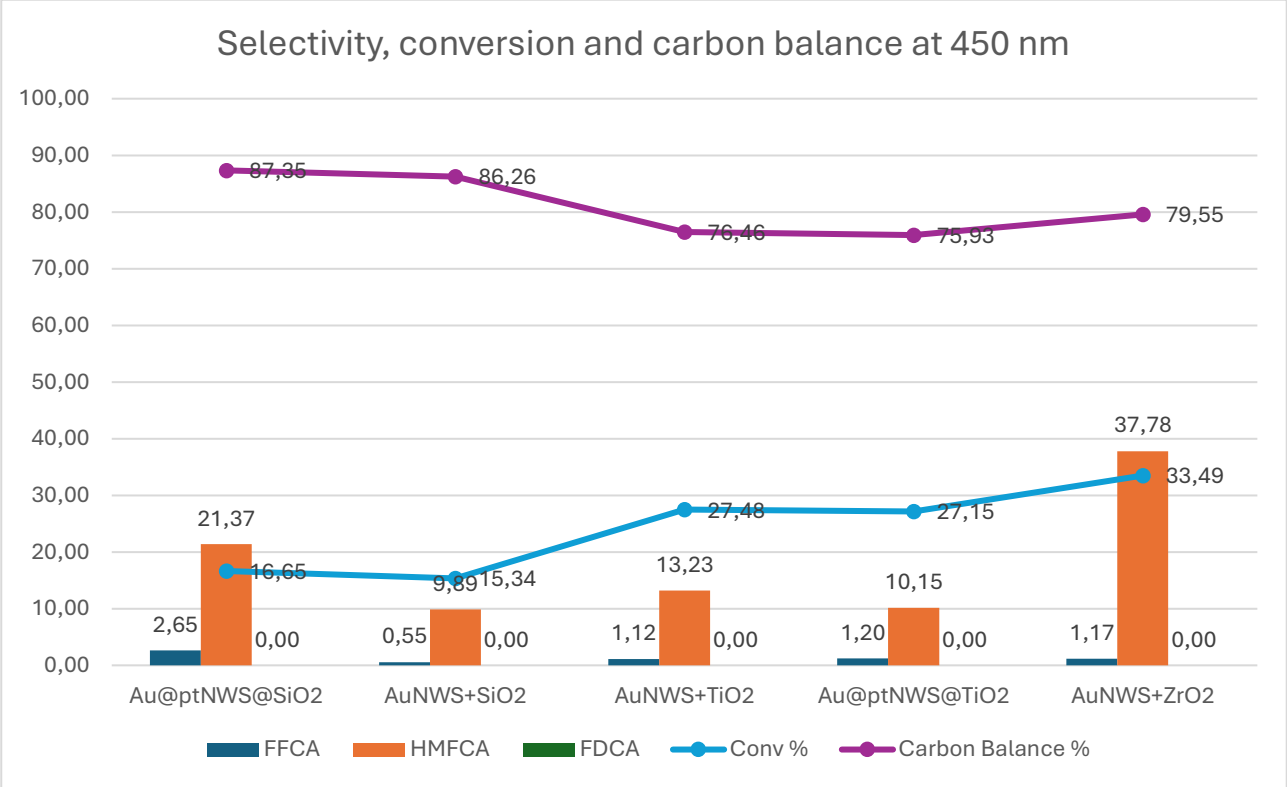

Figure 4.29: *Catalytic tests: HMF conversion, selectivity and carbon balance for NWS catalysts on different supports at 450 nm.*

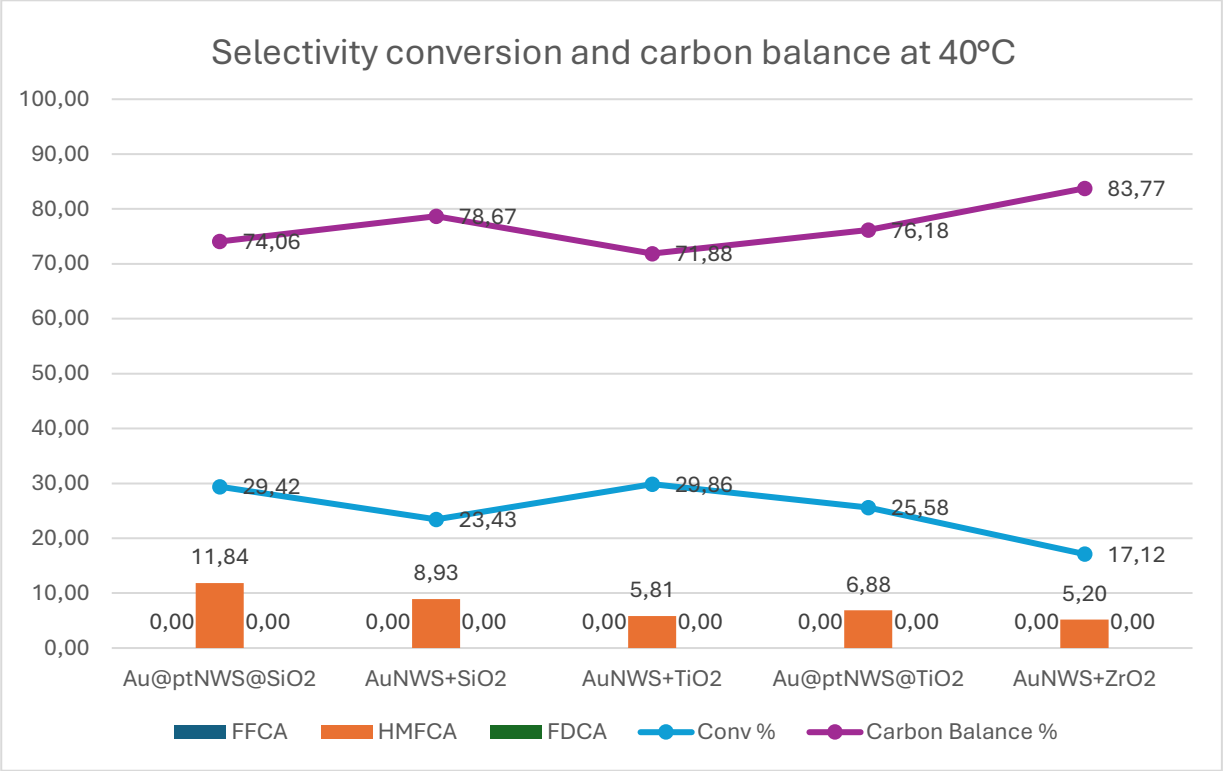

Figure 4.30: *Catalytic tests: HMF conversion, selectivity and carbon balance for NWS catalysts on different supports at 40°C.*

At 450 nm wavelengths none catalyst gives good results both in terms of conversion and selectivity. It seems that the Au NWS supported with zirconia provides slightly better results respect to others catalyst with a conversion of 33,49%. The main product is HMFCA and traces of FFCA have been formed; while FDCA has not been obtained. Carbon balance is at 79,55%, meaning that part of reactant has been completely oxidated.

The worst-performed support is silica, in fact, regardless of the metal loaded it provides conversions lower than 20%, while with the titania support conversion of 27% has been obtained with both Au and AuPt.

Except for the zirconia based catalyst, other catalysts provide similar results with thermal reaction denoting a limited effect of the light. On the contrary, for the zirconia-based catalyst the conversion with thermal catalysis without light is half respect to that carried out at 450 nm.

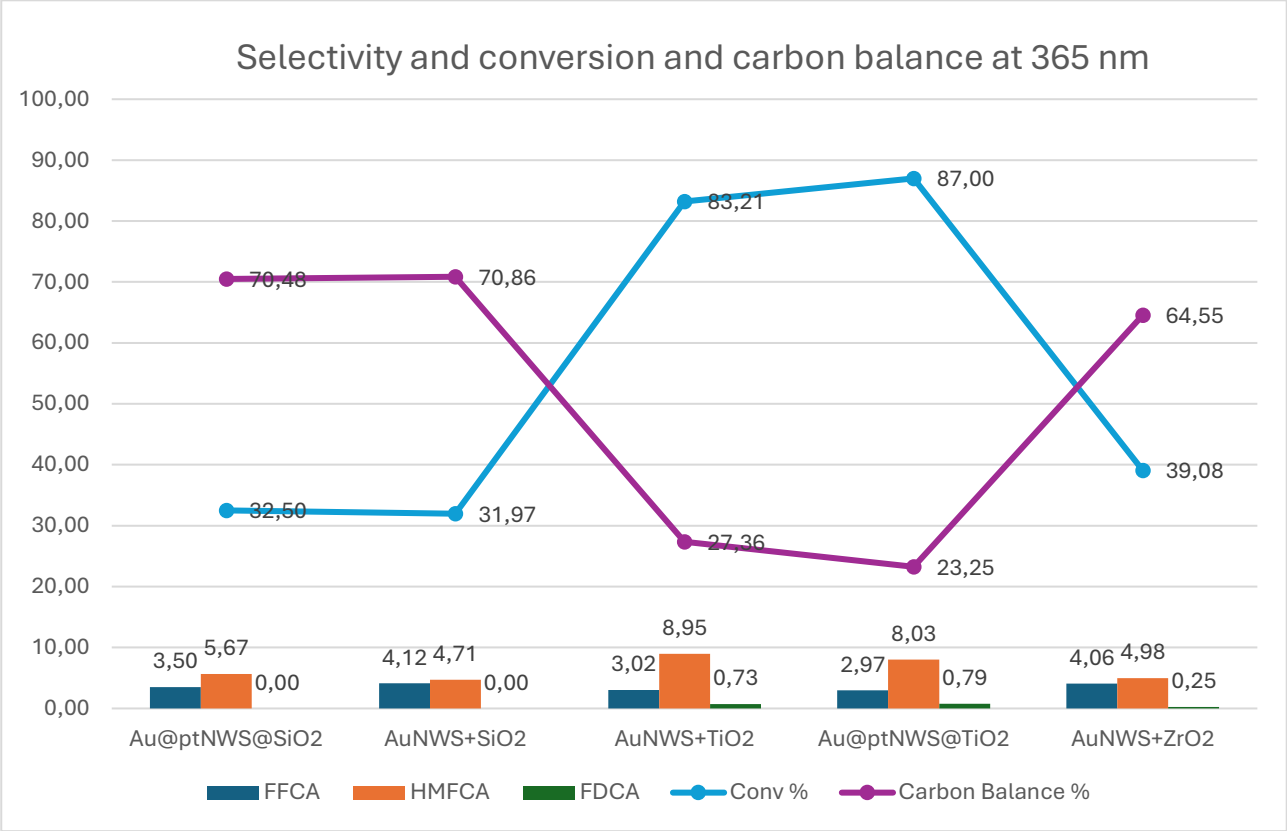

Figure 4.31: *Catalytic tests: HMF conversion, selectivity and carbon balance for NWS catalysts on different supports at 365 nm.*

At 365 nm it can be noticed that Titania support catalysts give the highest value of conversion that reached 87% with the gold/palladium catalyst, however the selectivity is very low for each of the desired product. Looking at the low values of carbon balance it can be stated that most of the reactant goes to complete oxidation. It should be noted that the titania-based catalyst delivers this performance only at 365 nm, while at 450 nm it does not. Therefore, the light wavelength is crucial for this type of metal-support combination. For silica and zirconia-based catalysts the results are similar with conversion between 30% and 40% and carbon balance between 65% and 70%. These catalyst structures have proven to be too active for this reaction, preventing the desired products from being obtained. In fact, even at low conversion the carbon balance drops; that means that the reaction does not go to desired pathways, but it goes to alternative pathways like complete oxidation to form carbon dioxide.

4.8 Green light analysis

Some of the catalysts discussed before have been tested with the 523 nm light (green light). This light is less energetic, but some interesting results can be achieved thanks to the plasmonic effect mainly with gold-based catalysts. When a metal nanoparticle is excited at a well-defined frequency the free electrons in metals made a collective oscillation called localize surface plasmons resonance (LSPR). So plasmons can be described as a charged electron cloud dislocated from its equilibrium position around a lattice of positively charged ions.[22] These phenomena take place when the frequency of incident electromagnetic wave matches the one of the electrons oscillating on the lattice of the nuclei that are charged positively and fixed. For this reason, LSPR occurs at different wavelength for different atoms; for example, for Au the frequency in which plasmonic occurs is 523 nm (green light). Has been demonstrated that this effect is able to improve the reaction rate.[23]

For copper-based catalyst the effect of plasmonic resonance occurs within the visible region, too. However, in hybrid catalysts where copper is combined with one or more metals, the exact position on the spectrum where plasmonic effect occurs can shift and the absorption range may even expand.[24] Having LSPR that occurs at visible and near-infrared ranged ranges open up to the possibility to utilize solar energy for photocatalytic reactions achieving significant yields at moderate conditions.[25]

Different test has been led with 523 nm light mainly with gold-based catalyst, and also with other metal-based catalyst like Pd-Cu based and Au-Si based. All the result are summarized in Figure 4.32.

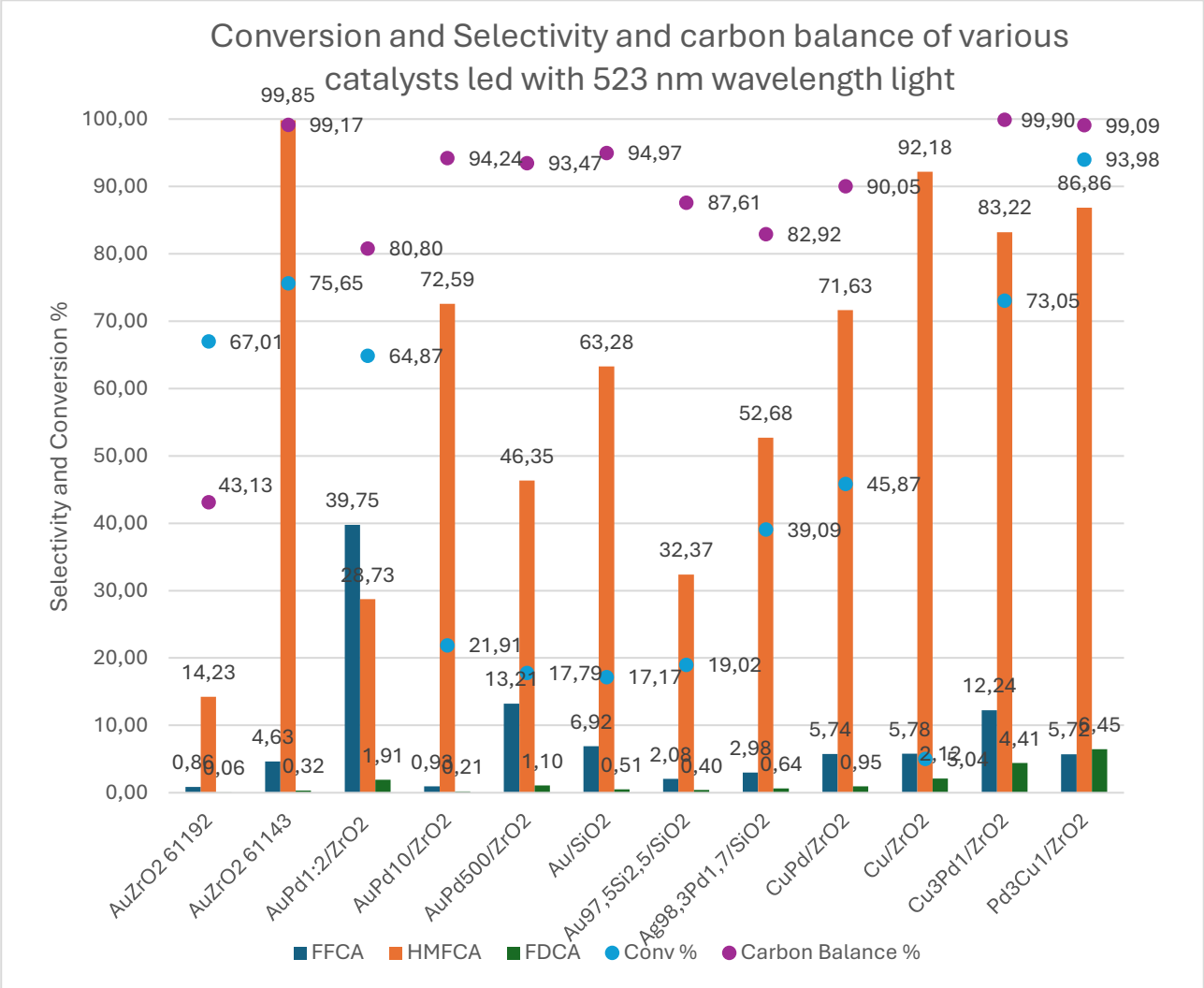

Figure 4.32: *Catalytic tests: HMF conversion, selectivity and carbon balance for different catalysts at 523 nm.*

An interesting result is obtained with $AuPd_{1:2}/ZrO_2$ catalyst; in fact, we can observe an hight selectivity in term of FFCA. To better understand if plasmonic effect occurs we must compare this catalyst with $AuPd_{500}/ZrO_2$. The comparison between the two catalysts clearly show that the alloy catalyst has better performance both in terms of conversion and selectivity with the reaction that reaches more advanced oxidation steps. The result can be explained with the core-shell structure of the Au particles that are completely covered by palladium so that the plasmonic effect on gold cannot take place in $AuPd_{500}/ZrO_2$; on the contrary with the alloy structure the gold particles are able to create the electron negative charged cloud giving rise to the plasmonic effect in $AuPd_{1:2}/ZrO_2$.

4.9 Comparison between core-shell and alloy Au-Pd/ZrO_2 catalysts

Figures 4.33 and 4.34 highlight the performance of two highly selective bimetallic AuPd catalysts supported on zirconia. These catalysts, differing in their structural configuration (core-shell vs. alloy), were evaluated under various light irradiation conditions and thermal catalysis.

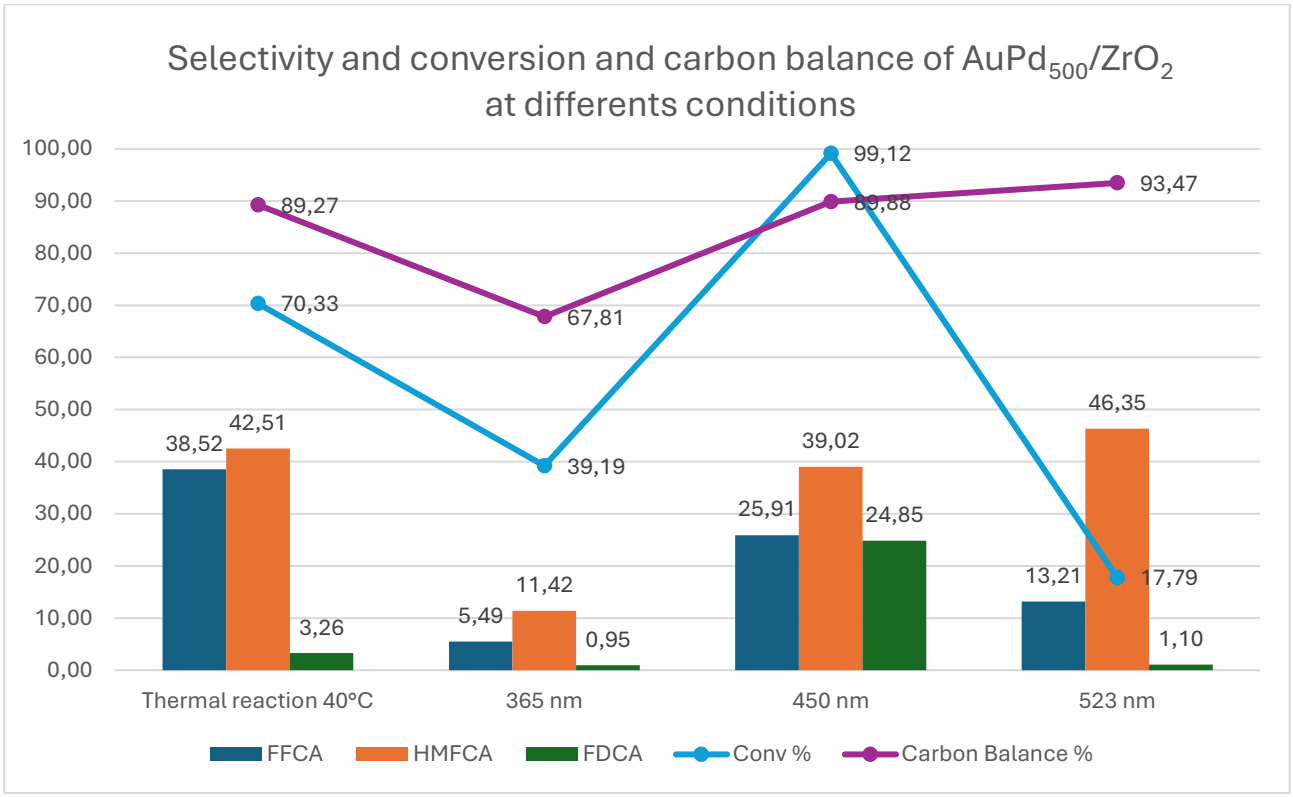

Figure 4.33: *Comparison of the performance of $AuPd_{500}/ZrO_2$ at different conditions.*

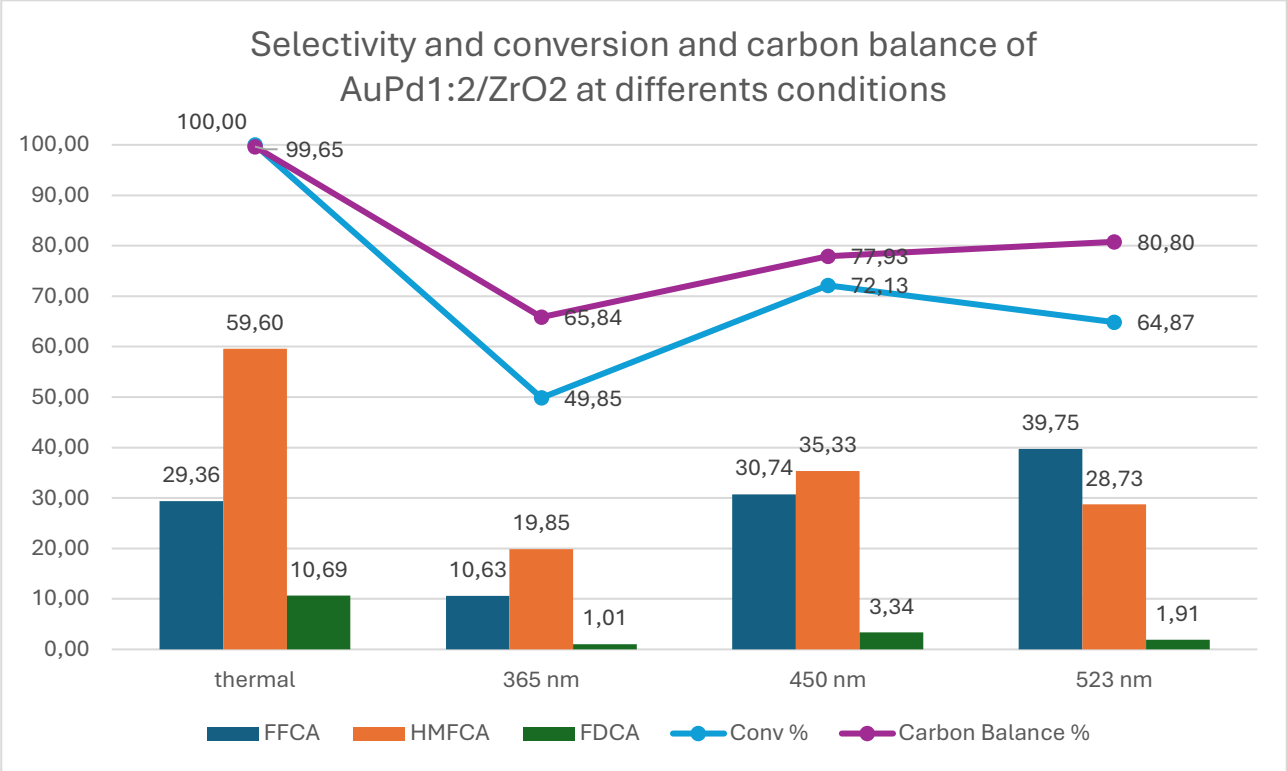

Figure 4.34: *Comparison of the performance of $AuPd_{1:2}/ZrO_2$ at different conditions.*

The structure of the catalyst, particularly the metal composition and support material, significantly impacts its catalytic performance. Bimetallic catalysts, such as $AuPd/ZrO_2$, have shown promising results in HMF oxidation. The synergistic effect between gold and palladium can enhance catalytic activity and selectivity. However, the optimal metal ratio and support material can vary depending on the specific reaction conditions and desired products.

The $AuPd500/ZrO_2$ catalyst demonstrated reasonable performance under thermal conditions, achieving a conversion of 70% and a carbon balance of 89%, but with low selectivity towards FDCA (3%). Furthermore, at 365 nm, the conversion and carbon balance were significantly lower, indicating increased degradation pathways. In contrast, at 450 nm, this catalyst exhibited excellent performance with high conversion (99%), good carbon balance (90%), and moderate selectivity towards FDCA (25%). The poor result of this catalyst at 523 nm are immediately evident when compared to those at 450 nm. This is because the 523 nm light is less energetic respect to 450 nm and as already stated there is no plasmonic effect because Pd particles cover the Au ones; which results in reduced conversion and halts the reaction to FFCA step. Conversely at 450 nm higher energy leads to a higher conversion and enables the reaction to proceed through more advanced oxidation steps, producing

FDCA. It can be concluded that this catalyst exhibits excellent performance, achieving its best results at 450 nm.

The AuPd1:2/ZrO_2 alloy catalyst, which showed the best performance among the AuPd/ZrO_2 catalysts at both 450 nm and under thermal conditions, was further investigated at 523 nm to explore the potential of plasmonic effects. As expected, the alloy catalyst exhibited higher activity at 523 nm compared to the core-shell catalyst, highlighting the role of plasmonic excitation in enhancing catalytic performance.

The wavelength of light plays a crucial role in photocatalytic reactions. Shorter wavelengths, such as 365 nm, provide higher energy photons, which can promote both desired and undesired reactions. In contrast, longer wavelengths, such as 450 nm and 535 nm, can selectively excite specific electronic transitions in the catalyst, leading to improved selectivity towards desired products. Unlike the previous core shell catalyst, the gold nanoparticles in this system are not covered by palladium, enabling plasmonic catalysis. This effect is particularly noticeable at 523 nm, where the conversion levels, although slightly lower, are comparable to those observed at 450 nm despite the lower energy of the radiation. Furthermore, at 523 nm, the selectivity toward FFCA is notably higher, showing an increase of over 9%. However, the best performances are still achieved by thermal catalysis specially in terms of conversion that achieved the maximum and also in terms of selectivity being more FDCA produced.

Comparing thermal and photocatalytic conditions provides valuable insights into the role of light in the reaction mechanism. While thermal catalysis can drive the reaction to completion, photocatalysis offers the advantage of lower reaction temperatures and potentially higher selectivity. The core-shell catalyst shows low activity at 40°C while the alloy catalyst reached 65% of HMF conversion at 40°C. This is also due to the structure and higher quantity of Pd at the surface of alloyed catalyst.

4.10 Comparison between copper-palladium/ZrO_2 catalysts at different conditions

Figures 4.35 and 4.36 summarized the results obtained with the two catalysts Cu3Pd1/ZrO_2 and Cu1Pd3/ZrO_2 at different conditions, which are both alloy catalysts that differ in copper-to-palladium ratio. These two catalysts have been selected for comparison because they exhibited interesting performance at 523 nm.

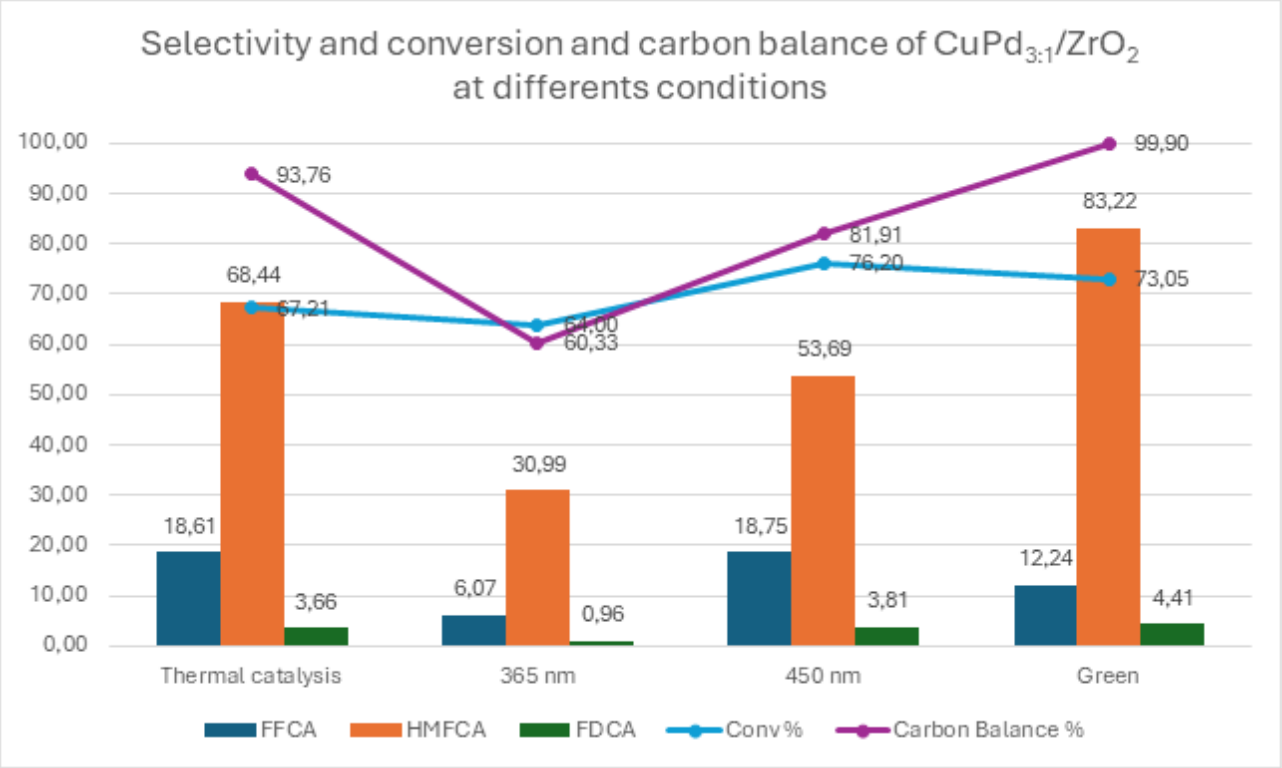

Figure 4.35: *Comparison of the performance of $CuPd_{3:1}/ZrO_2$ at different conditions.*

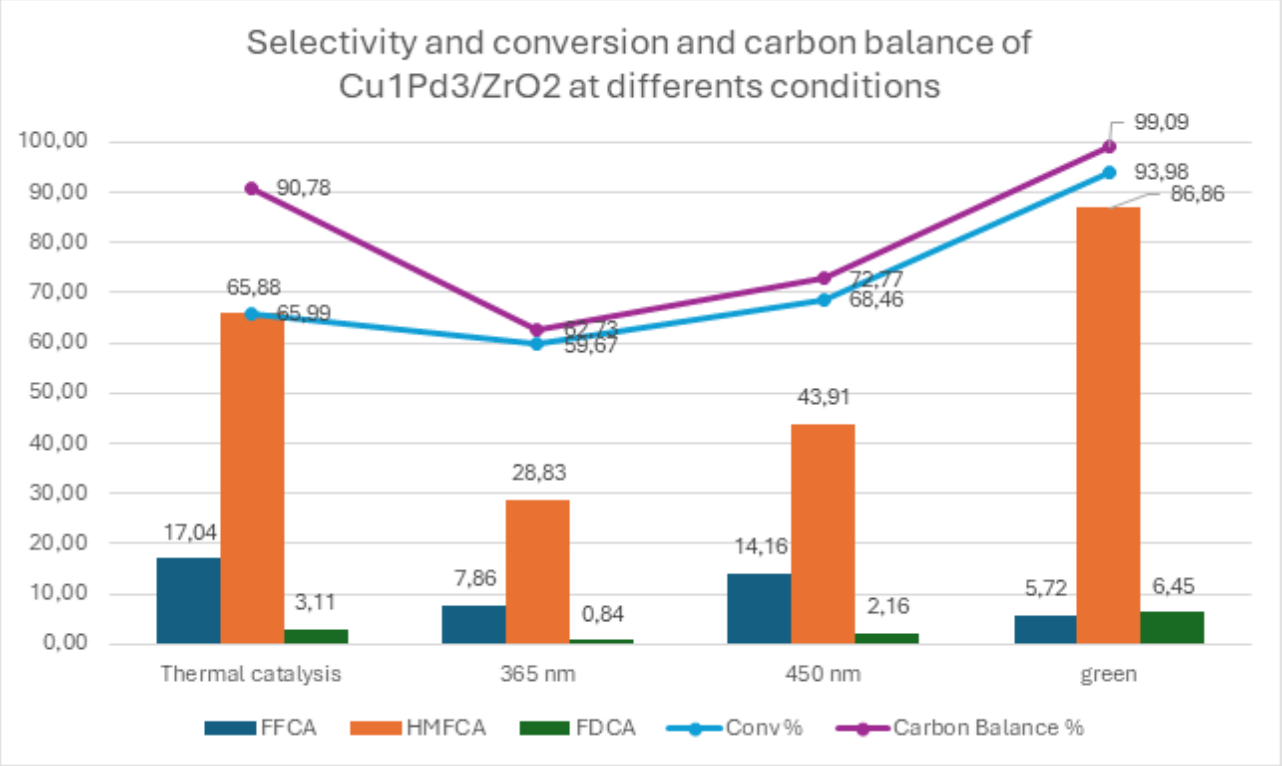

Figure 4.36: *Comparison of the performance of $CuPd_{1:3}/ZrO_2$ at different conditions.*

Both catalysts exhibited similar trend of conversion and carbon balance. In fact, conversion in thermal catalysis is around 66% for the catalysts and carbon balance is above 90%. At 365 nm a drop in carbon balance can be observed which remains just above 60%. These results are consistent with other catalysts because as already states this wavelength is more energetic and lead to degradation easily. Going to lower energetic light both conversion and carbon balance increase again and at 450 nm for both the catalyst results similar to thermal catalysis has been obtained. At 523 nm for both catalysts the best results are reached with a carbon balance of 100%, and a conversion of 73% for $Cu3Pd/ZrO_2$ and 94% for $CuPd3/ZrO_2$. High conversion with low energetic light means that plasmonic catalysis occurs at this wavelength. The main product is HMFCA, but the oxidation goes also through advanced steps obtaining a selectivity above 12% for FFCA and 4% FDCA for $CuPd3/ZrO_2$. Similar result in terms of selectivity has been obtained with $Cu3Pd/ZrO_2$ with 5,72% of FFCA and 6,45 of FDCA.

4.11 Continuous Flow Reaction

Once that all the catalysts have been tested some reactions in continuous flow have been performed utilising the fReactor. The reaction has been carried out with thermal catalysis, photocatalysis or a combination of the two processes. A sample has been collected each hour for five hours starting from the time in which the first drop fallout from the reactor. The first drops of the product have been collected, and they form the first sample that has been analysed at time zero. This first sample has been called T0R and is different from T0 that is the sample of the solution injected in the reactor at the beginning (the one utilised as initial solution for the calculus). Differently from the batch conditions it has been decided to plot the results in terms of yields instead of selectivity. In this way it is possible to better compare the quantity of product obtained at different conversion.

As a first attempt two reactors have been used with two of the most performed catalysts. Reactor 1 has been filled with 5 mg of Au/ZrO_2 and on the top has been putted the 460 nm lamp. Reactor 2 has been filled with 5 mg of Pd_3Cu/ZrO_2 and on the top has been putted the 523 nm lamp. The flow has been set at 0.2 ml/min. Since the trend of the conversion versus time curve was not well known, a sample was collected every 10 minutes for the first half hour, then a sample was collected every half hour.

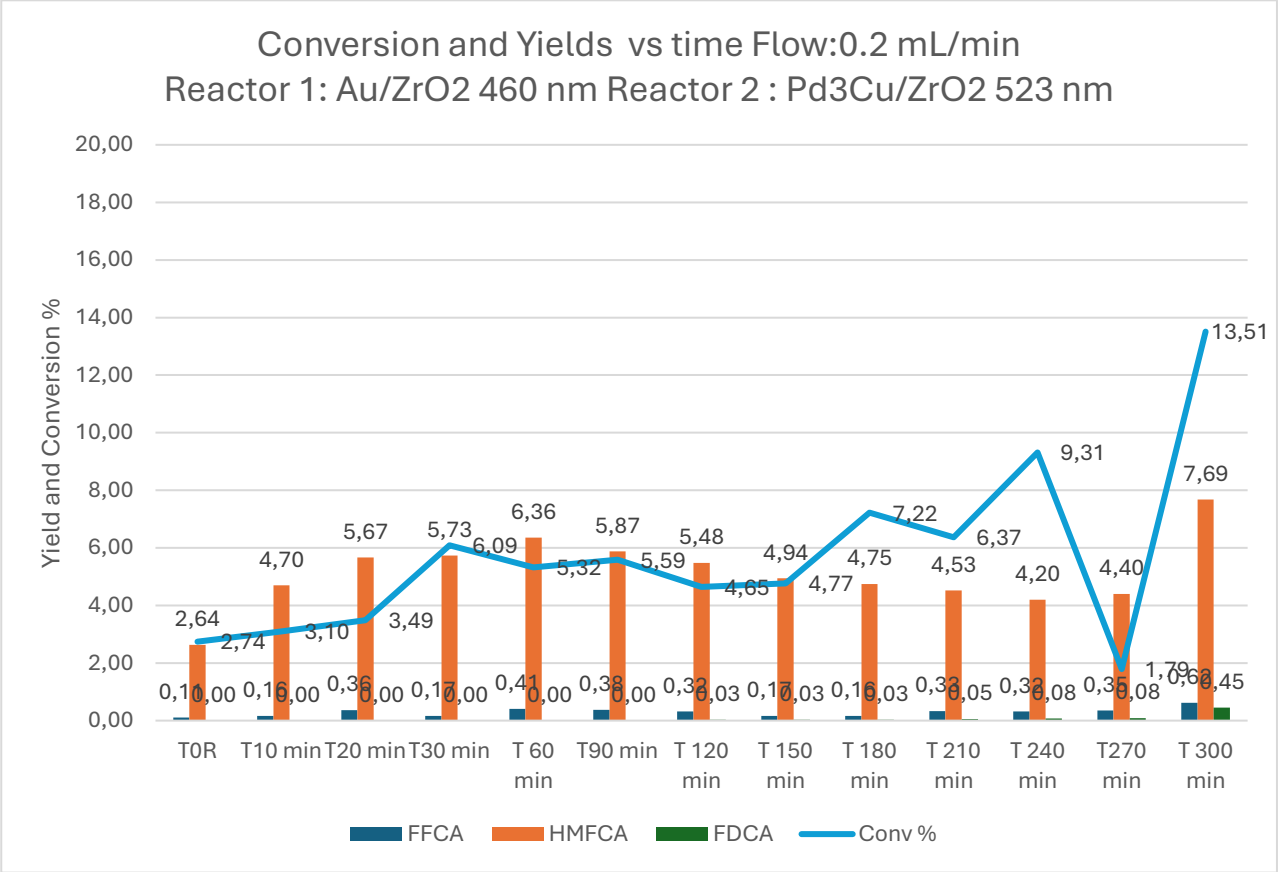

Figure 4.37 *First catalytic test on continuous reactor*

The conversion slightly increases over the time as expected and after 5 hours reach the 13,51%. The main product was HMFCA according to the yields (7,69% at 5h) and only traces of FFCA and FDCA were formed.

Given the low values of conversion obtained a second experiments have been led changing only the flow (residence time) and leaving the other parameters such as catalysts and lamps unchanged. The flow has been decreased to 0.01 ml/min (20 time lower than the first experiment) to increase the time in which the solution stays in each reaction. In this way the catalyst contact time increases and higher values of conversion are expected.

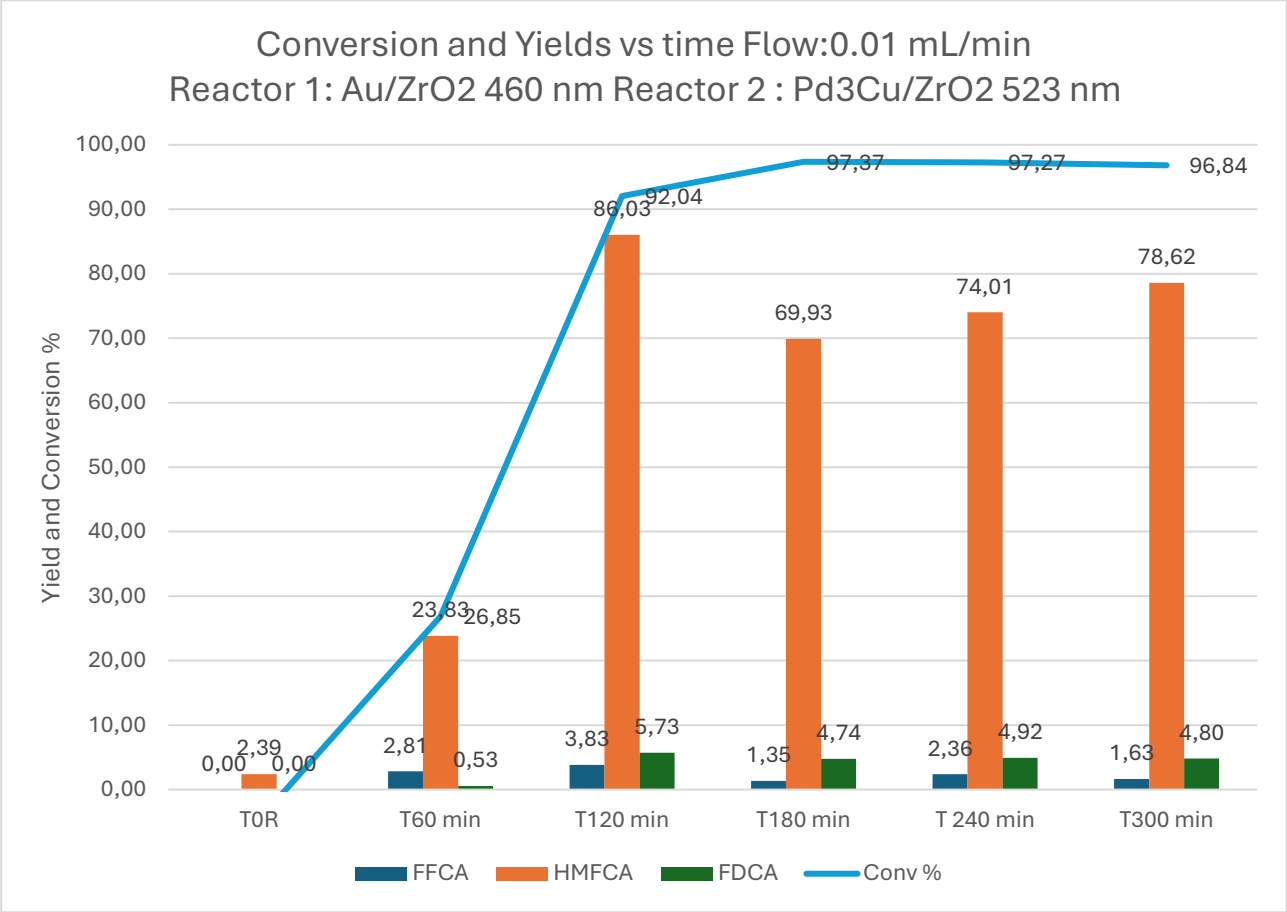

Figure 4.38: *Second catalytic test on continuous reactor*

With this flow, conversion values above 90% are reached after only two hours, after which the conversion tends to stabilize at around 97%. The main product is still HMFCA but higher quantity has been produced with the yield that had the maximum (86,03%) after one hour, then it slightly decreases. The reaction goes also through the lasts steps of oxidation producing FFCA and FDCA with respectively yields of 1.63% and 4.80% after five hours.

A third experiments has been performed changing the catalyst and keeping the same flow rate. In this third experiment in the first reactor $CuPd3/ZrO_2$ was introduced with the 523 nm wavelength lamp (the same set used before in the second reactor) while in the second reactor the core shell catalyst $AuPd500/ZrO_2$ has been used. The best performance of this catalyst in batch reactor were at 460 nm so this lamp has been chosen.

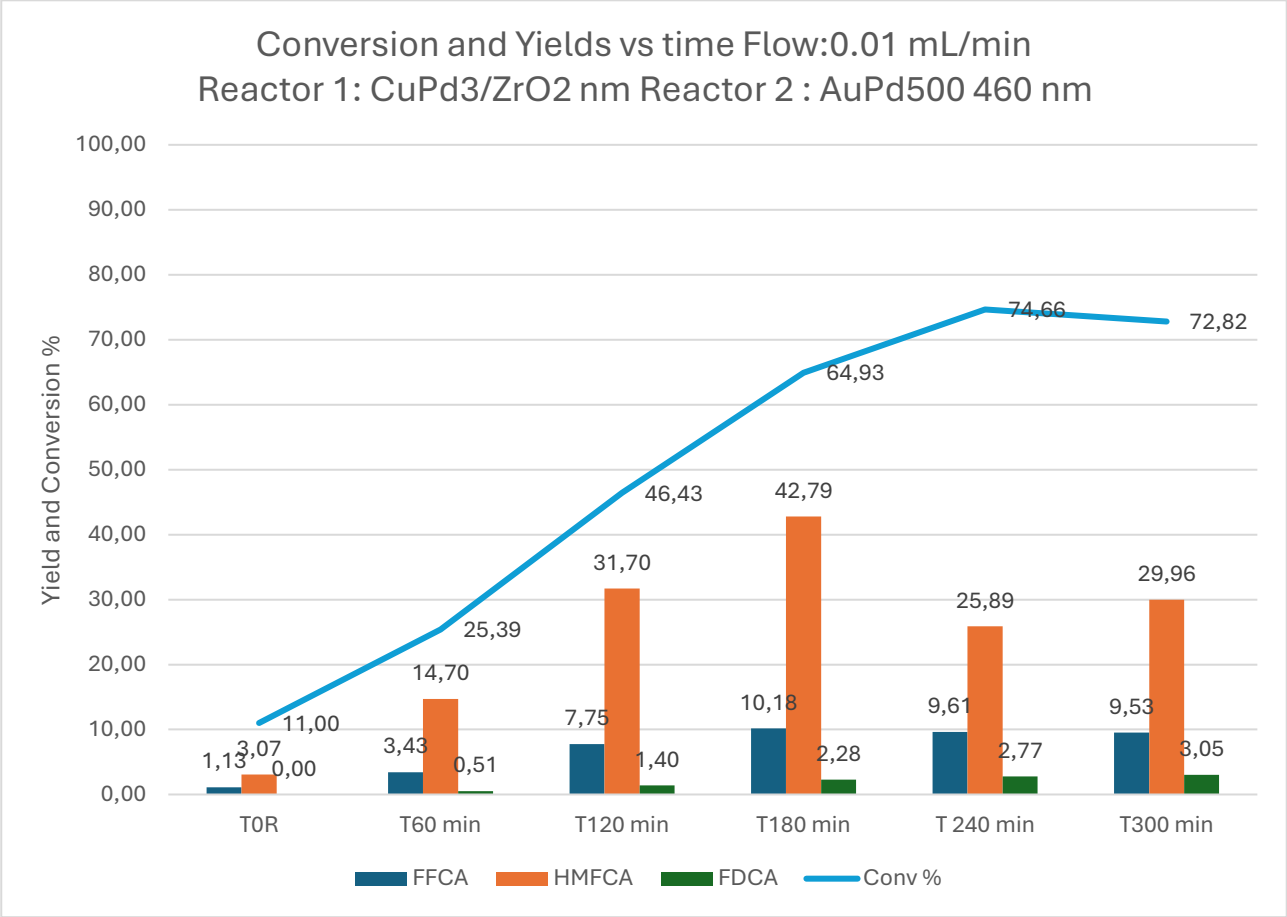

Figure 4.39: *Third catalytic test on continuous reactor*

After 5 hours the conversion reaches the value of 72,82% that is lower respect that of the previous experiments. However, it is interesting to notice how the yield of HMFCA increases until a maximum at 3 hours and then slightly decreases in favour of the next oxidation step as FFCA and FDCA. Indeed, after five hours FFCA reach a yield of 9,53% that is higher than in the previous experiments. Instead for FDCA that is the last oxidation step a yield of 3.05% has been obtained lower than the second experiment.

Another experiment has been carried out with only thermal catalysis (so without lamps). Both the reactors have been filled with 5 mg of Pd/ZrO_2, and the reactor temperature has been set to 40°C. This catalyst has been chosen because is one of the best performers in batch reactors in thermal catalysis.

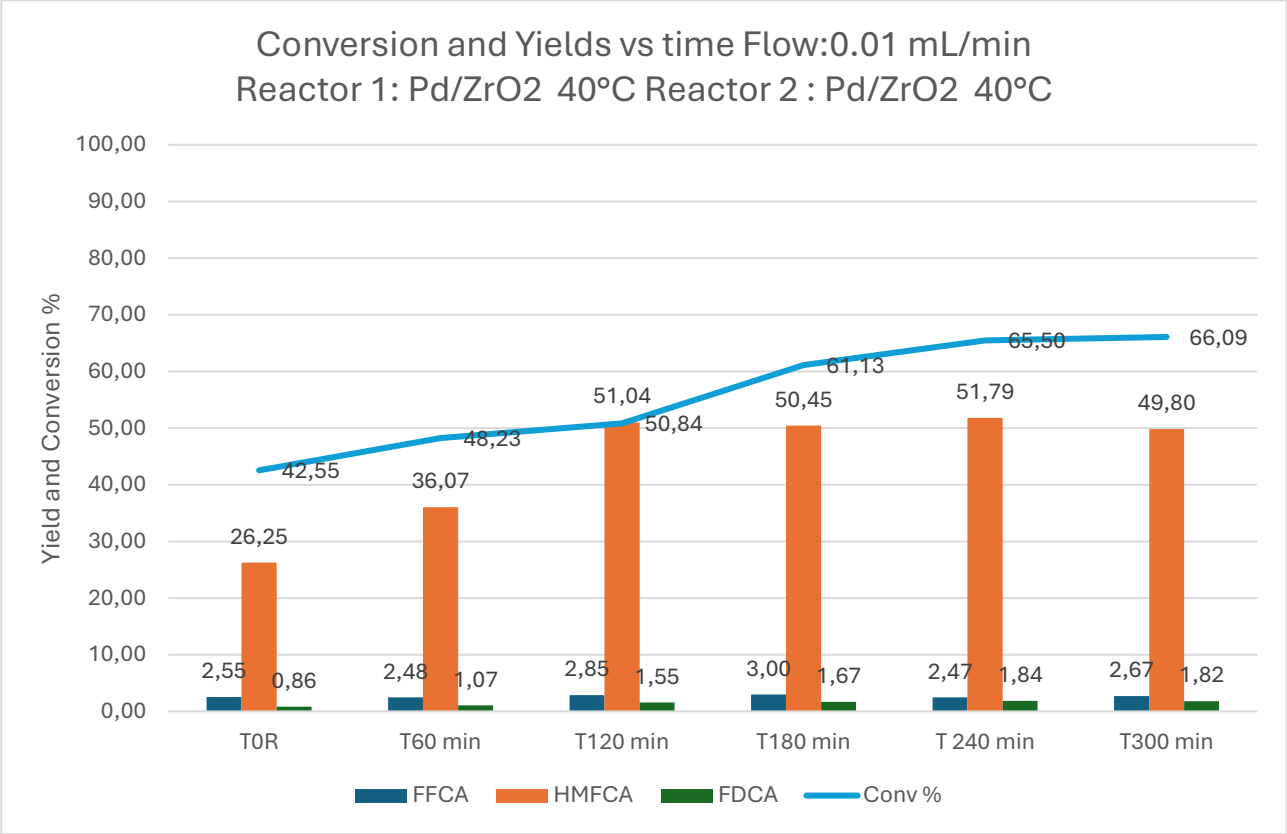

Figure 4.40: *Fourth catalytic test on continuous reactor*

Initial product collection (T0R) showed a 40% conversion, which increased to 66% after 5 hours. While HMFCA remained the primary product, trace amounts of FDCA and FFCA were also detected. This experiment yielded a lower 5-hour conversion (66%) compared to the previous one, which achieved near-total conversion. However, at shorter reaction times (under 1 hour), this experiment exhibited higher conversion than all previous trials.

Based on previous results, a further experiment was conducted using the same catalyst and flow rate, but with one thermal reactor and one photocatalytic reactor. The first reactor was equipped with a 460 nm lamp, while the second reactor was maintained at 40°C without illumination.

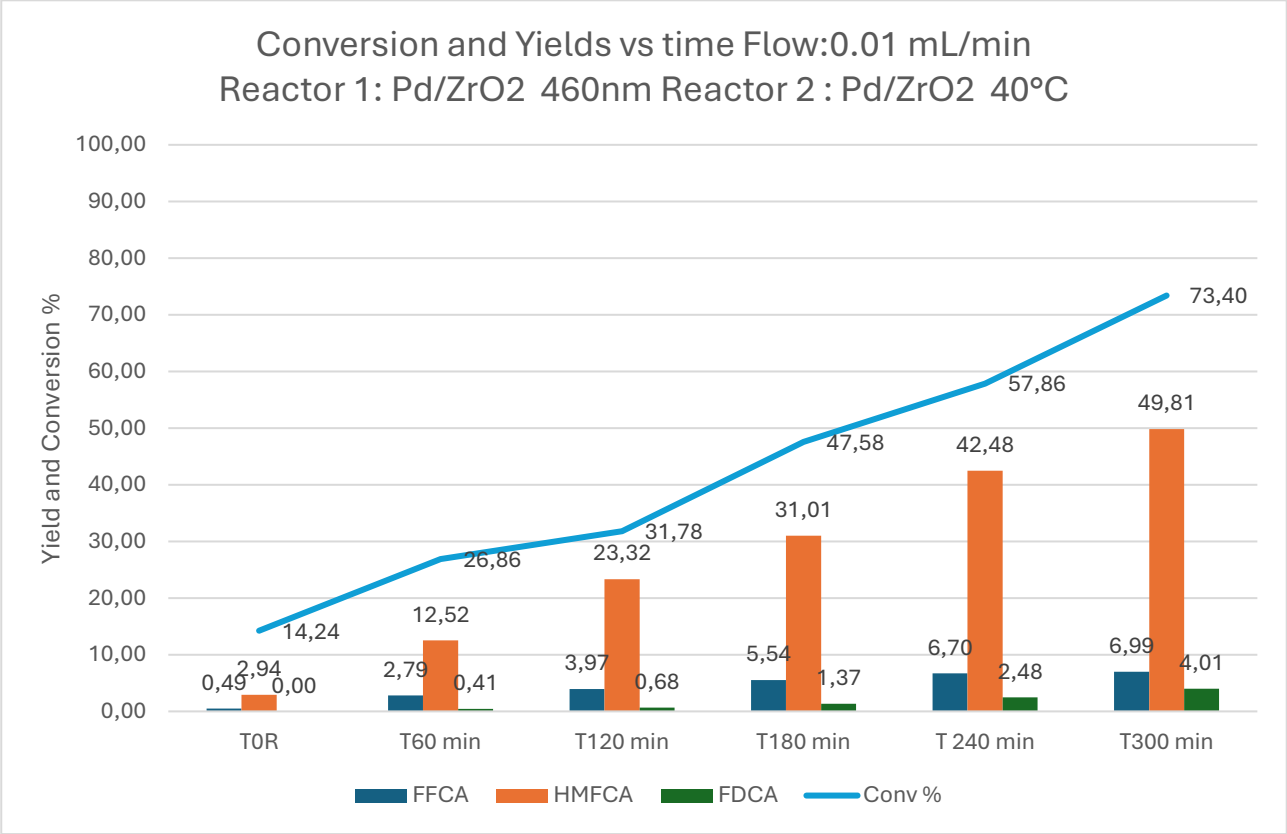

Figure 4.41: *Fifth catalytic test on continuous reactor*

The conversion increased and after 5 hours it reached 73,40% but differently from the other experiments a flattering of the conversion curve is not observed, it means that if the reaction had been held for longer time, higher values would have been reached. Compared to the previous experiment higher yield values of both FFCA and FDCA has been reached, of 6,99% and 4,01%, respectively, after the second reactor.

In conclusion, after 5 hours the best results in terms of HMF conversion have been reached with the second configuration using Au/ZrO_2 and $Pd3/Cu/ZrO_2$ catalysts, respectively with 460 nm lamp and 523 nm lamp. But with this experiment despite the higher conversion a low yield in the last oxidation products (FFCA and FDCA) has been obtained. Better results are obtained with the last experiment that combined thermal and photocatalysis but the yield even if higher does not reach competitive values.

Chapter 5

Conclusion and future prospective

In this study we aimed to identify the most effective catalyst for the selective oxidation of HMF, with the goal of reaching the final oxidation step to produce FDCA with the highest possible yield and avoiding over-oxidation of the reactant that would lead the reaction to CO_2. This process was investigated through photocatalysis using light sources of different wavelengths (365 nm, 450 nm and 523 nm). Particular attention was given to the possibility of exploiting plasmon resonance with gold and copper-based catalyst at less energetic wavelengths. Furthermore, the results obtained through photocatalysis has been compared with those achieved through thermal catalysis without light to evaluate if the presence of light enhanced yield and selectivity of the reactions. Finally using the most efficient catalysts, flow-experiments have been performed with many reactors to explore the feasibility of achieving a continuous production of FDCA.

The best results with batch reactor were achieved using zirconia as support. Among the light utilized the most effective were at 450 nm and at 523nm, while that at 365 nm was too energetic leading to low carbon balance regardless of the catalyst.

For core shell catalysts the best performance was achieved with AuPd500/ZrO_2 at 450 nm, achieving a near complete conversion with a selectivity of 24.8% of FDCA and 25.9% of FFCA.

Among the gold-palladium alloy catalysts, it was observed that at 450 nm, increasing the palladium content respect to gold, facilitated the progression of the reaction through the final oxidation steps. Best results have been reached with AuPd1:2/ZrO_2 catalyst with a conversion of 72,13% and selectivity to FFCA and FDCA of 30,7% and 3,3%, respectively. In thermal catalysis best performance has been reached with monometallic Pd/ZrO_2 where near complete conversion has been reached with very high selectivity of FFCA and FDCA (44,4% and 19,7%).

Palladium copper catalysts give excellent results at 450 nm and in thermal catalysis but perform even better at 523 nm where hight conversion are reached both with Cu3Pd1/ZrO_2 and with Cu1Pd3/ZrO_2.

Continuous tests were also carried out, aiming to achieve a continuous production of FDCA. However, only preliminary analyses have been performed. Further studied should be conducted based on these initial tests, continuing this project and aiming to maximize FDCA yield even under continuous conditions by identifying the optimal catalyst-light combination.

Optimizing the combination of catalyst and light could enhance the production of FDCA under milder conditions while utilizing visible wavelength. This kind of approach would have a significatively impact on the company reducing the production costs and the environmental impact making the process both economically and ecologically sustainable. Furthermore, having a large production of FDCA from HMF could promote the development of bioplastics as an alternative of fossil-based common plastics.

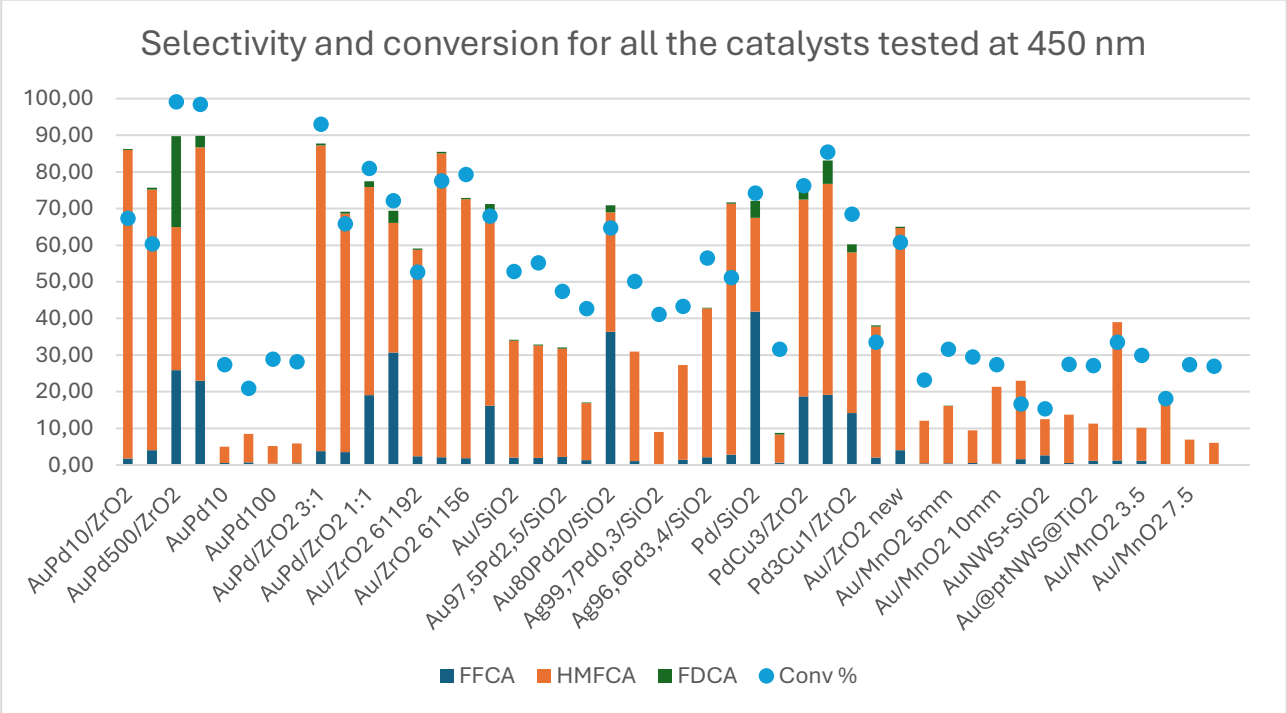

Figure 5.1: Selectivity and conversion for all the catalyst tested at 450 nm

Bibliography

1. Wang, Z. *et al.* Catalytic production of 5-hydroxymethylfurfural from lignocellulosic biomass: Recent advances, challenges and opportunities. *Renewable and Sustainable Energy Reviews* **196**, 114332 (2024).

2. Mika, L. T., Cséfalvay, E. & Németh, Á. Catalytic Conversion of Carbohydrates to Initial Platform Chemicals: Chemistry and Sustainability. *Chem. Rev.* **118**, 505–613 (2018).

3. ChemPhotoChem - 2020 - Li - Recent Advances in Photocatalytic Oxidation of 5-Hydroxymethylfurfural.pdf.

4. Davis, S. E. *et al.* Kinetics and mechanism of 5-hydroxymethylfurfural oxidation and their implications for catalyst development. *Journal of Molecular Catalysis A: Chemical* **388–389**, 123–132 (2014).

5. Advanced Science - 2022 - Guo - Advances in Selective Electrochemical Oxidation of 5-Hydroxymethylfurfural to Produce.pdf.

6. Douthwaite, M. *et al.* The controlled catalytic oxidation of furfural to furoic acid using AuPd/$Mg(OH)_2$. *Catal. Sci. Technol.* **7**, 5284–5293 (2017).

7. Oyegoke, T., Dumeignil, F., E.-Yakubu Jibril, B., Michel, C. & Wojcieszak, R. Exploring catalytic oxidation pathways of furfural and 5-hydroxymethyl furfural into carboxylic acids using Au, Pt, and Pd catalysts: a comprehensive review. *Catal. Sci. Technol.* 10.1039.D4CY00821A (2024) doi:10.1039/D4CY00821A.

8. Ferraz, C. P. *et al.* Influence of Support Basic Sites in Green Oxidation of Biobased Substrates Using Au-Promoted Catalysts. *ACS Sustainable Chem. Eng.* **6**, 16332–16340 (2018).

9. ChemSusChem - 2019 - Liguori - Continuous-Flow Oxidation of HMF to FDCA by Resin-Supported Platinum Catalysts in Neat Water.pdf.

10. Yu, H., Kim, K.-A., Kang, M. J., Hwang, S. Y. & Cha, H. G. Carbon Support with Tunable Porosity Prepared by Carbonizing Chitosan for Catalytic Oxidation of 5-Hydroxylmethylfurfural. *ACS Sustainable Chem. Eng.* **7**, 3742–3748 (2019).

11. Ke, C., Li, M., Fan, G., Yang, L. & Li, F. Pt Nanoparticles Supported on Nitrogen-Doped-Carbon-Decorated CeO_2 for Base-Free Aerobic Oxidation of 5-Hydroxymethylfurfural. *Chemistry An Asian Journal* **13**, 2714–2722 (2018).

12. Wang, Y. *et al.* Basicity-Tuned Hydrotalcite-Supported Pd Catalysts for Aerobic Oxidation of 5-Hydroxymethyl-2-furfural under Mild Conditions. *ACS Sustainable Chem. Eng.* **4**, 4752–4761 (2016).

13. Zhang, Z., Zhen, J., Liu, B., Lv, K. & Deng, K. Selective aerobic oxidation of the biomass-derived precursor 5-hydroxymethylfurfural to 2,5-furandicarboxylic acid under mild conditions over a magnetic palladium nanocatalyst. *Green Chem.* **17**, 1308–1317 (2015).

14. Siyo et al. - 2014 - Influence of support on the aerobic oxidation of H.pdf.

15. Jensen, M. H. & Riisager, A. Advances in the synthesis and application of 2,5-furandicarboxylic acid. in *Biomass, Biofuels, Biochemicals* 135–170 (Elsevier, 2020). doi:10.1016/B978-0-444-64307-0.00005-6.

16. Pandey, S., Dumont, M.-J., Orsat, V. & Rodrigue, D. Biobased 2,5-furandicarboxylic acid (FDCA) and its emerging copolyesters' properties for packaging applications. *European Polymer Journal* **160**, 110778 (2021).

17. Haas, V. *et al.* Developing future visions for bio-plastics substituting PET – A backcasting approach. *Sustainable Production and Consumption* **31**, 370–383 (2022).

18. Wojcieszak, R. & Itabaiana, I. Engineering the future: Perspectives in the 2,5-furandicarboxylic acid synthesis. *Catalysis Today* **354**, 211–217 (2020).

19. De Jong, E., Visser, H. (Roy) A., Dias, A. S., Harvey, C. & Gruter, G.-J. M. The Road to Bring FDCA and PEF to the Market. *Polymers* **14**, 943 (2022).

20. El-Brolossy et al. - 2008 - Shape and size dependence of the surface plasmon r.pdf.

21. Yi, X. *et al.* Core–shell Au@MnO2 nanoparticles for enhanced radiotherapy via improving the tumor oxygenation. *Nano Res.* **9**, 3267–3278 (2016).

22. Amendola et al. - 2017 - Surface plasmon resonance in gold nanoparticles a.pdf.

23. Dong et al. - 2023 - Plasmonic Catalysis New Opportunity for Selective.pdf.

24. Advanced Materials - 2021 - Xin - Copper-Based Plasmonic Catalysis Recent Advances and Future Perspectives.pdf.

25. Araujo et al. - 2019 - Understanding plasmonic catalysis with controlled .pdf.